Numerical Study of Nonlinear Energy Transfer From Large Generation Scale Down to Small Dissipation Scale Across the Oceanic Internal Wave Spectrum

Yoshihiro Niwa

海洋内部波スペクトル内における励起スケールから散逸スケールまでのエネルギー輸送過程に関する数値的研究

丹羽淑博

Numerical Study of Nonlinear Energy Transfer From Large Generation Scale Down to Small Dissipation Scale Across the Oceanic Internal Wave Spectrum

Thesis for a Doctorate

Yoshihiro Niwa

Division of Earth and Planetary Sciences, Graduate School of Science,
Hokkaido University

1998

Contents

Chapter 1

General Introduction

It is well known that small-scale turbulent mixing in the deep ocean plays significant roles in the dynamics of the oceanic general circulation. For example, on the basis of a simplified oceanic general circulation model, *Bryan* [1987] has demonstrated that important aspects of calculated thermohaline circulation such as the magnitude of the meridional heat transport are very sensitive to the assumed values of vertical eddy diffusivity. This clearly indicates that exact parameterization of small-scale turbulent mixing is essential for accurate modeling of the oceanic general circulation.

Various approaches have been made to investigate turbulent mixing processes in the deep ocean including microstructure measurements [*Gregg*, 1989] and tracer release experiments [*Ledwell et al.*, 1986]. Although these observations certainly enable the precise estimation of the intensity of the local turbulent mixing during the limited ship time, it is apparent that this kind of approaches is not applicable to examine the global distribution of turbulent mixing intensity including its time variability.

An approach more feasible to clarify the global distribution of turbulent mixing is to make use of the dynamics of the oceanic internal gravity wave field. Internal gravity waves are ubiquitous phenomena in the deep ocean embedded between the planetary scale and the microscale, and are supposed to provide an important link in energy cascade from large generation scale down to small dissipation scale [*Munk*, 1981; *Müller et al.*, 1986]. The energy supplied at large scales by atmospheric forcing or tide-topography interaction is considered to be transferred across the internal wave spectrum down to small dissipation scale through nonlinear wave-wave interactions causing turbulent mixing in the deep ocean. Therefore, once the energy transfer processes within the oceanic internal wave spectrum are clarified, we can expect that parameterization of small-scale turbulent mixing processes becomes possible in terms of the distribution of energy sources for large-scale

internal waves such as atmospheric disturbances which are much more easy to observe than the turbulent mixing itself.

One of the distinguished properties of the deep ocean internal wave spectrum is that it is remarkably stable in both space and time [*Wunsch and Webb*, 1979] which is *empirically* modeled as the Garrett-Munk (GM) spectrum [*Garrett and Munk*, 1972; *Munk*, 1981]. In Chapter 2, we reproduce the quasi-equilibrium internal wave field having the actually observed GM-like spectrum by calculating the nonlinear interactions among randomly phased linear internal waves, each amplitude of which is determined from the GM model. It should be noted that our numerical experiments differ from the previous ones [*Shen and Holloway*, 1982; *Lin et al.*, 1995; *Winters and D'Asaro*, 1997] in that the oceanic internal wave field ranging from large generation scale to small dissipation scale is simultaneously simulated. In particular, the vertical wavenumber spectrum thus obtained reproduces the observed feature that it starts to roll off at a vertical wavenumber of ~0.1 cycles per meter (cpm), suggesting the internal wave energy that comes from larger scales is actually removed through strongly nonlinear processes. By examining the physical processes causing the roll-off of internal wave spectrum, we propose a model for the dynamic balance between a downscale energy flux and energy dissipation within the internal wave spectrum in the deep ocean.

In Chapter 3, we examine the forcing mechanism of large-scale internal waves. Three-dimensional numerical experiments are carried out to investigate energy transfer from a traveling hurricane which is one of the major sources for large-scale internal waves. It is demonstrated that a traveling hurricane generates two distinctive kinds of internal waves, namely, near-inertial waves and superinertial waves with frequencies of 2f and 3f which are generated under nonlinear effects. Generation of near-inertial waves is

a primary oceanic response to a traveling hurricane investigated by many researchers on the basis of linear theory [*Geisler*, 1970; *Greatbatch*, 1984; *Price*, 1983]. Our special attention is then directed to the superinertial waves with frequencies of 2f and 3f whose generation mechanism is examined in detail through bispectral analysis.

In Chapter 4, we investigate energy transfer processes within the oceanic internal wave spectrum by carrying out "*Bump Experiment*" in which the quasi-equilibrium spectrum obtained in Chapter 2 is perturbed with energy bump introduced in different parts of low-wavenumber low-frequency portion of the spectrum, and thereafter time evolution of the perturbed spectrum is examined. It is found that energy of low-vertical mode double-inertial frequency (ω=2f) internal waves is transferred effectively across the internal wave spectrum down to small dissipation scales, which indicates that these superinertial waves generated by a traveling hurricane can be efficient energy sources for turbulent mixing in the deep ocean.

Despite their significant roles in turbulent mixing, no observational evidence has been obtained for the existence of low-vertical-mode double-inertial frequency internal waves. In Chapter 5, we analyze current meter data from long term moorings in the Northwest Pacific Basin together with global sea surface wind data to find that double-inertial frequency internal waves are indeed excited in the real ocean under strong atmospheric forcings.

In Chapter 6, we summarize results from the previous chapters and propose one possible scenario for the energy transfer processes from large-scale atmospheric forcing down to small-scale turbulent mixing in the deep ocean. Finally, some remaining problems to be investigated in future are briefly discussed.

References

Bryan, F., Parameter sensitivity of primitive equation ocean general circulation models, *J. Phys. Oceanogr., 17*, 970-985, 1987.

Garrett, C. J. R., and W. H. Munk, Space-time scales of internal waves, *Geophys. Fluid Dyn., 2*, 225-264, 1972.

Geisler, J. E., Linear theory of the response of a two layer ocean to a moving hurricane, *Geophys. Fluid Dyn., 1*, 249-272, 1970.

Greatbatch, R. J., On the response of the ocean to a moving storm: Parameters and scales, *J. Phys. Oceanogr., 14*, 59-77, 1984.

Gregg, M. C., Scaling turbulent dissipation in the thermocline, *J. Geophys. Res., 94*, 9686-9698, 1989.

Gregg, M. C., D. P. Winkel, and T. B. Sanford, Varieties of fully resolved spectra of vertical shear, *J. Phys. Oceanogr., 23*, 124-141, 1993.

Ledwell, J. R., A. J. Watson, and W. S. Broecker, A deliberate tracer experiment in Santa Monica Basin, *Nature, 323*, 322-324, 1986.

Lin, C.-L., J. R. Koseff, and J. H. Ferziger, On triad interactions in a linearly stratified ocean, *J. Phys. Oceanogr., 25*, 153-167, 1995.

Müller, P., G. Holloway, F. Henyey, and N. Pomphrey, Nonlinear interactions among internal gravity waves, *Rev. Geophys., 24*, 493-536, 1986.

Munk, W. H., Internal waves and small-scale processes, *in Evolution of Physical Oceanography*, edited by B. S. Warren and C. Wunsch, pp. 264-291, MIT Press, Cambridge, Mass., 1981.

Price, J. F., Internal wave wake of a moving storm Part I: Scales, energy budget and observation. *J. Phys. Oceanogr., 13*, 949-965, 1983.

Shen, C. Y., and G. Holloway, A numerical study of the frequency and energetics of nonlinear internal gravity waves, *J. Geophys. Res., 91*, 953-973, 1986.

Winters, K. B., and E. A. D'Asaro, Direct simulation of internal wave energy transfer, *J. Phys. Oceanogr., 27*, 1937-1945, 1997.

Wunsch, C., and S. Webb, The climatology of deep ocean internal waves, *J. Phys. Oceanogr., 9*, 235-243, 1979.

Chapter 2

Direct Numerical Simulation of the Roll-off Range of Internal Wave Shear Spectra in the Ocean

Abstract

Oceanic internal gravity waves play an important role in the dynamics of the ocean, providing a link in the overall energy cascade from large forcing scales to small dissipation scales. Quantifying the cascade of energy available for mixing processes in the ocean interior, for example, is essential to accurate modeling of the oceanic general circulation.

In the present study, based on an extensive numerical model that resolves most of the internal wave spectrum, the dynamics of the process by which internal waves dissipate their energy in the deep ocean are investigated. Putting all the calculated results together, we propose here a model for the dynamic balance of the internal wave spectrum wherein a downscale energy flux into the high-vertical-wavenumber near-inertial portion of the spectrum is balanced by energy dissipation at critical layers formed by high-vertical-wavenumber near-inertial flows.

2.1. Introduction

The sensitivity of the large-scale ocean circulation to subtle changes in small-scale mixing is demonstrated in oceanic general circulation models. The meridional circulation in a simple advection diffusive model of the thermohaline circulation, for example, is reversed when a constant mixing coefficient is replaced by one increasing with depth [*Gargett*, 1984]. The main energy for mixing processes in the deep ocean is considered to be originally supplied at large scales by atmospheric forcing [*Kundu*, 1993; *Rubenstein*, 1994; *Nilsson*, 1995] and tide-topography interactions [*Bell*, 1975; *Baines*, 1982; *Hibiya*, 1986; *Sjöberg and Stigebrandt*, 1992] and then transferred across the internal wave spectrum down to small dissipation scales. A full understanding of these transfer and mixing processes is thus essential to accurate modeling of the oceanic general circulation.

Observations of the internal wave spectrum in the deep ocean indicate the remarkable fact that it has much the same shape wherever it is observed, unless the observations are made close to a strong source of internal waves. On the basis of linear theory which brings together the available observational evidence, Garrett and Munk synthesized an empirical model of the complete wavenumber-frequency spectrum of the deep ocean internal wave field [*Garrett and Munk*, 1972, 1975; *Munk*, 1981] (hereafter referred to as the GM model). Except for inertial and tidal waves, this model is believed to reflect the spectral features of the internal wave climate in the deep ocean and to possess a certain global validity [*Wunsch*, 1976; *Müller et al.*, 1978; *Wunsch and Webb*, 1979].

A fundamental role in shaping the universal deep ocean spectrum could be attributed to weakly nonlinear wave-wave interactions (resonant interactions) within the internal wave field which smooth out any spectral irregularity by redistributing energy within the spectrum [*McComas*, 1977; *McComas*

and Bretherton, 1977; *McComas and Müller*, 1981; *Olbers*, 1976; *Pomphrey et al.*, 1980]. At higher wavenumbers, however, the nonlinearity of the governing equations of motion becomes stronger, violating the condition for weak interactions. Actually, although the observed vertical wavenumber spectrum of the vertical shear of horizontal velocity is nearly white at large scales (which is characteristic of the GM spectral shape), it starts to roll off at a cutoff vertical wavenumber (0.1 cycles per meter (cpm)) [*Gargett et al.*,1981; *Gregg et al.*, 1993] suggesting that the energy that comes from larger scales is removed through strongly nonlinear processes (offresonant interactions) such as wave breaking. At present, the detailed dynamics of the process by which internal waves dissipate their energy in the deep ocean remain unclarified.

In the present study, physical processes causing the roll-off of internal wave shear spectra are investigated by means of direct numerical simulation of the hydrodynamic equations of motion. Putting all the calculated results together, we propose a model for the dynamic balance between a downscale energy flux and energy dissipation within the internal wave spectrum in the deep ocean.

2.2. Description of the numerical model

We assume that the internal wave field is restricted to a vertical two-dimensional plane by requiring the variability to be independent of one horizontal coordinate. The two-dimensional Navier-Stokes equations under the Boussinesq approximation are replaced with a finite difference scheme by applying the centered difference and leapfrog scheme. In particular, the Arakawa Jacobian is used for an expression of the advective term [*Arakawa*, 1966]. The finite differenced equations are solved on a 1024×1024 grid

with resolutions of 10 m and 1.25 m in the horizontal and vertical directions respectively (Fig. 2.1), sufficient to resolve the interactions among widely disparate scales of motion. The subgrid diffusive-dissipative processes are parameterized with a Laplacian operator where eddy viscosity and diffusivity coefficients are assumed to have the same values of 1 $cm^2\ s^{-1}$ in the horizontal and 0.1 $cm^2\ s^{-1}$ in the vertical, which are the smallest possible values needed to maintain the stability of calculations. Cyclic boundary conditions are employed at the lateral sides, whereas flat perfectly reflecting bottom and surface are assumed. The initial internal wave field is assumed to be composed of a sum of randomly phased linear internal waves with horizontal wavenumbers ranging from 0 cpm to 0.025 cpm and vertical wavenumbers ranging from 3.91×10^{-4} cpm to 0.2 cpm respectively, each amplitude of which is determined from the GM model. Assuming the inertial frequency $f = 7.27 \times 10^{-5}\ s^{-1}$ (inertial period Ti =24 hours) and the constant background buoyancy frequency $N = 5.2 \times 10^{-3}\ s^{-1}$ (3 cycles per hour), the model is run during 7 inertial periods from the start of calculation with a time step of 1.5 seconds (Fig. 2.2). In order to avoid numerical instability, the Euler-backward scheme is applied every 20 time steps.

2.3. Results

With the start of nonlinear interactions among internal waves, the structure of internal wave spectrum begins to be modified. Figure 2.3 shows the time variation of the vertical wavenumber spectrum of the vertical shear of horizontal current velocity normalized by the square of buoyancy frequency (Froude spectrum). It should be noted that the spectrum is calculated from data obtained from the top down to the bottom which are averaged horizontally. After 5 inertial periods from the start of calculation, the spectrum

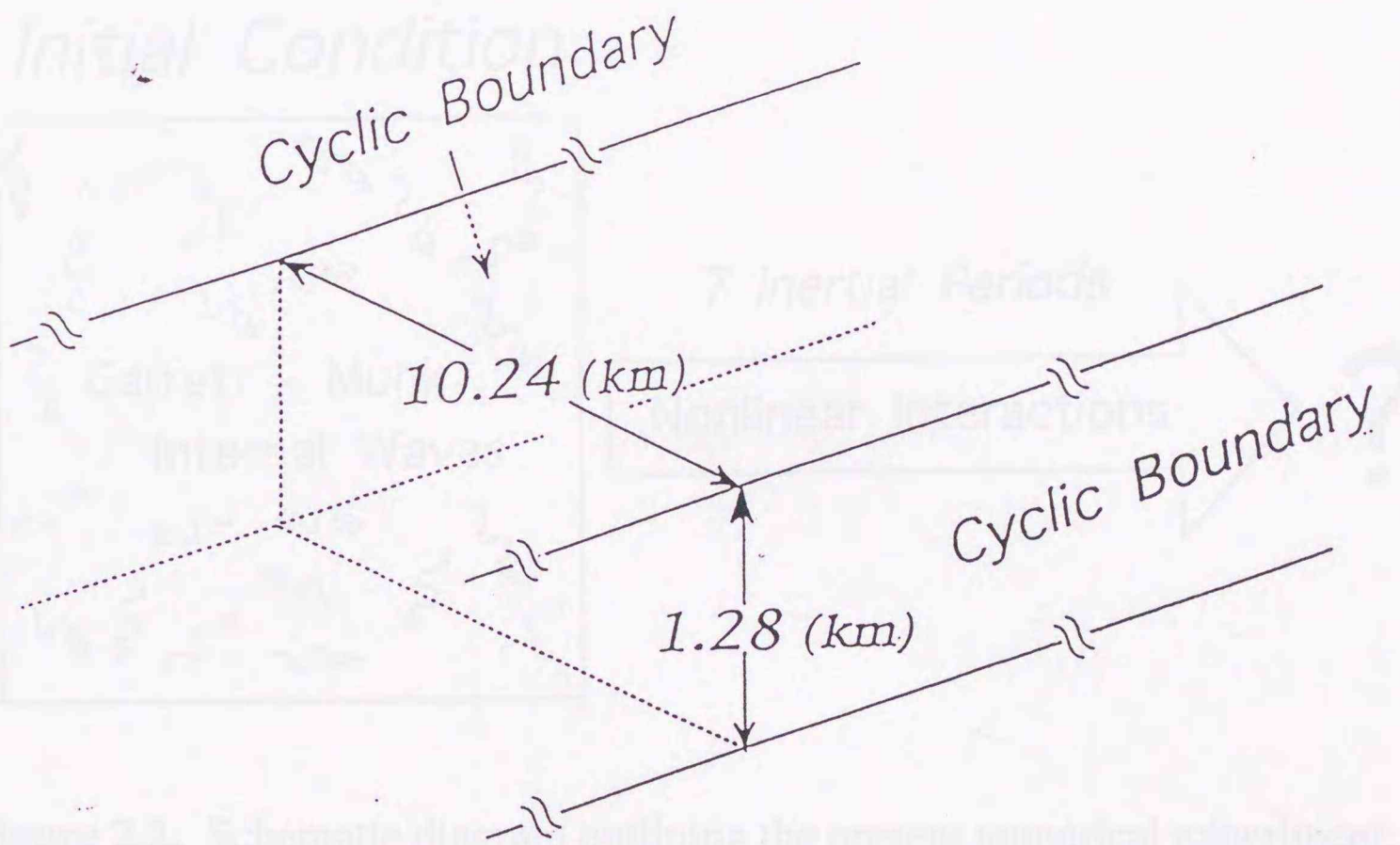

Figure 2.1. Dimensions of the model ocean.

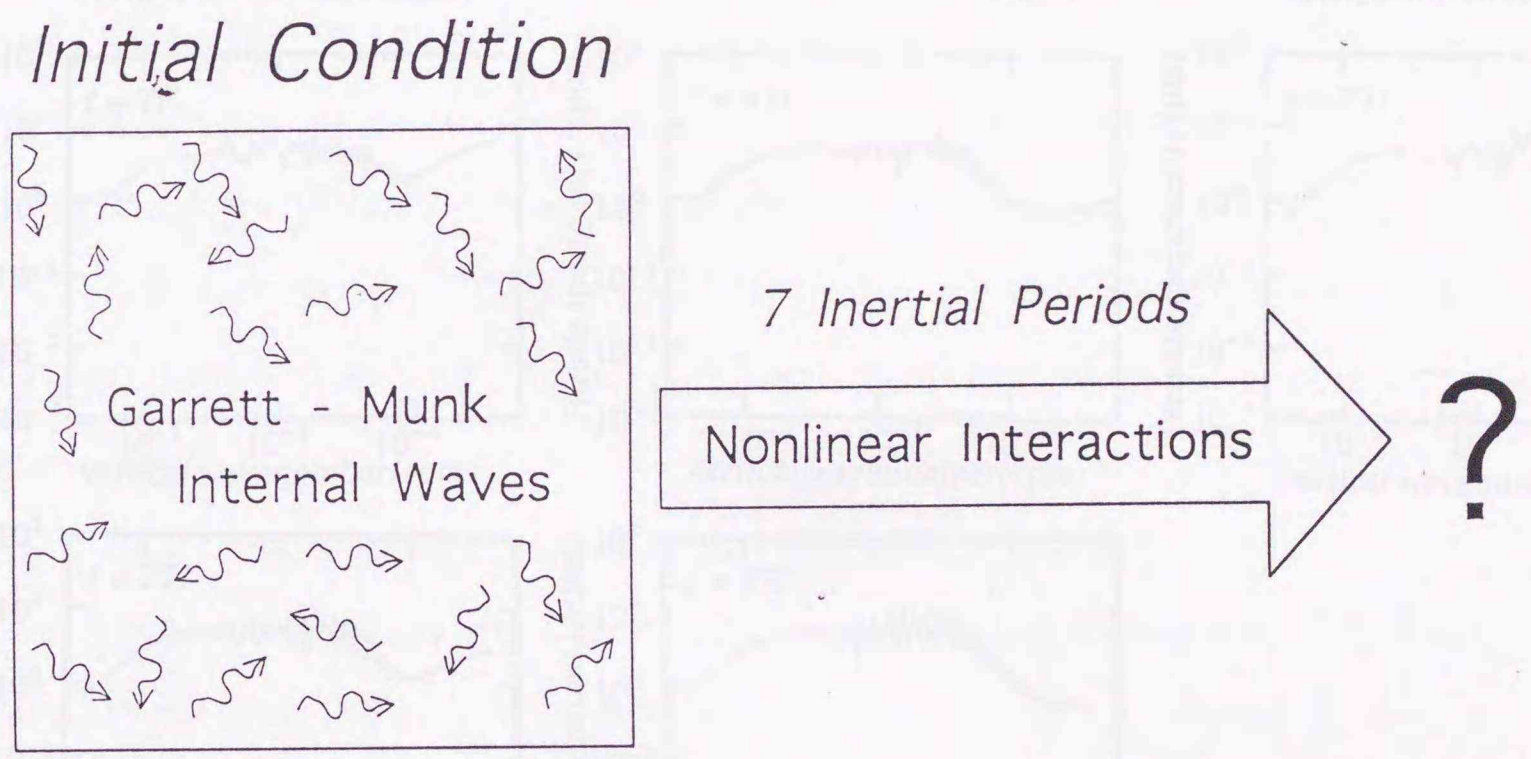

Figure 2.2. Schematic diagram outlining the present numerical experiment.

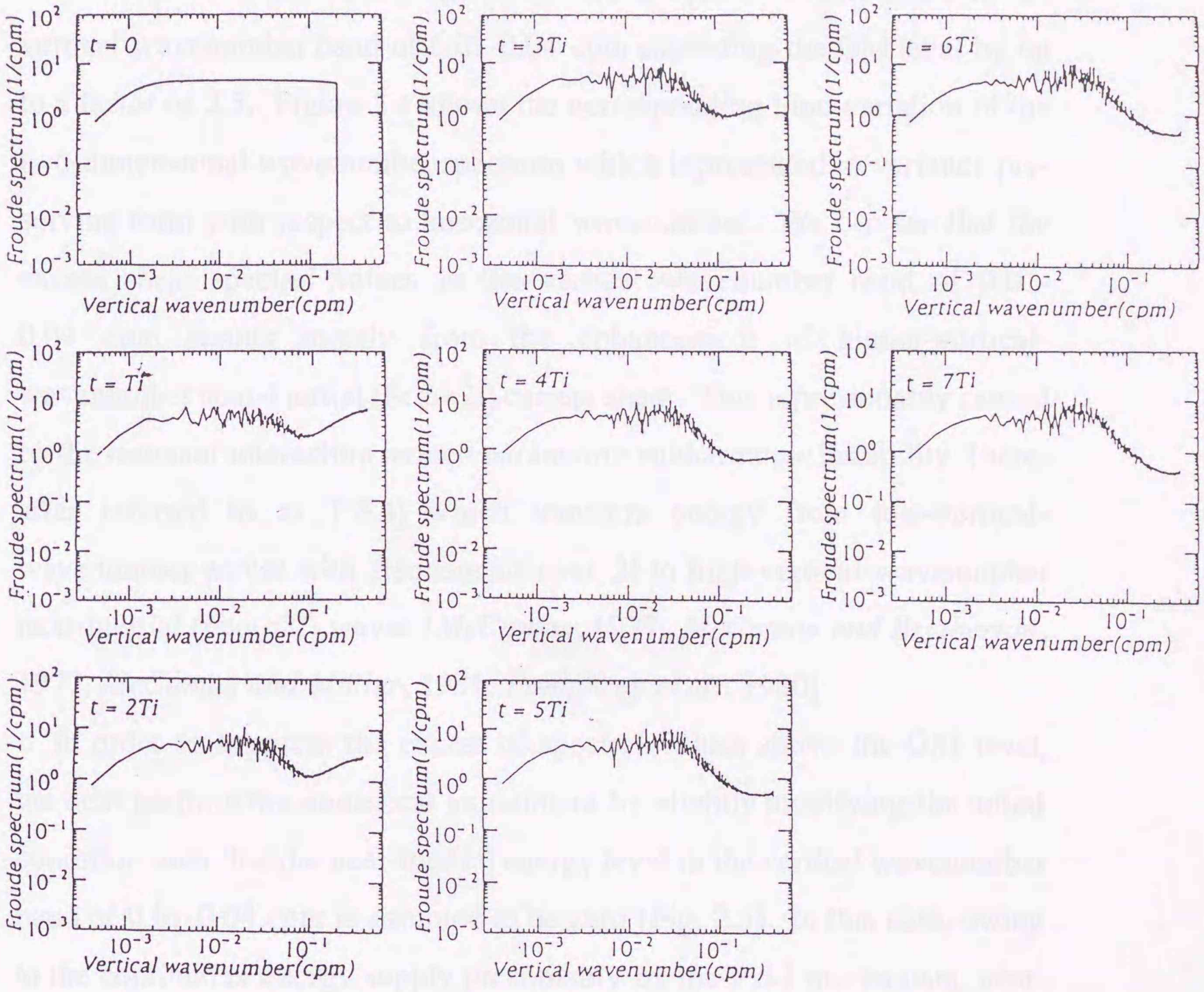

Figure 2.3. Time variations of the vertical wavenumber Froude spectrum during 7 inertial periods from the start of calculation. Note that the Garrett and Munk model spectrum is employed as an initial condition

becomes quasi-stationary where the roll-off is seen to be reproduced at vertical wavenumber 0.04 cpm which is somewhat lower than observed. At the same time, the shear spectral value is seen to be increased in the vertical wavenumber band of 0.01-0.04 cpm exceeding the GM level by up to a factor of 2.5. Figure 2.4 shows the corresponding time variation of the two-dimensional wavenumber spectrum which is presented in variance preserving form with respect to horizontal wavenumber. We can see that the excess shear spectral values in the vertical wavenumber band of 0.01-0.04 cpm results mostly from the enhancement of higher-vertical-wavenumber near-inertial ($f<\omega<2f$) current shear. This is presumably caused by the resonant interaction termed parametric subharmonic instability (hereafter referred to as P.S.I) which transfers energy from low-vertical-wavenumber waves with frequencies over 2f to high-vertical-wavenumber near-inertial ($f<\omega<2f$) waves [*McComas*, 1977; *McComas and Bretherton*, 1977; *McComas and Müller*, 1981; *Pomphrey et al.*, 1980].

In order to suppress the excess of spectral values above the GM level, we next perform the numerical experiment by slightly modifying the initial condition such that the near-inertial energy level in the vertical wavenumber band of 0.01-0.04 cpm is assumed to be zero (Fig. 2.5). In this case, owing to the continuous energy supply presumably by the P.S.I mechanism, near-inertial shear level gradually increases and thus becomes close to the GM level in the quasi-stationary state (Fig. 2.6). Of particular importance in this experiment is the fact that the roll-off shifts to higher vertical wavenumbers (0.06 cpm) in the quasi-stationary state indicating that the strength of the high-vertical-wavenumber near-inertial current shear strongly controls the roll-off wavenumber.

We also examine the spatial distributions of the inverse Richardson number ($Ri^{-1} = [(\partial u/\partial x)^2 + (\partial v/\partial x)^2] / N^2$) in the model domain as a measure of the likeli-

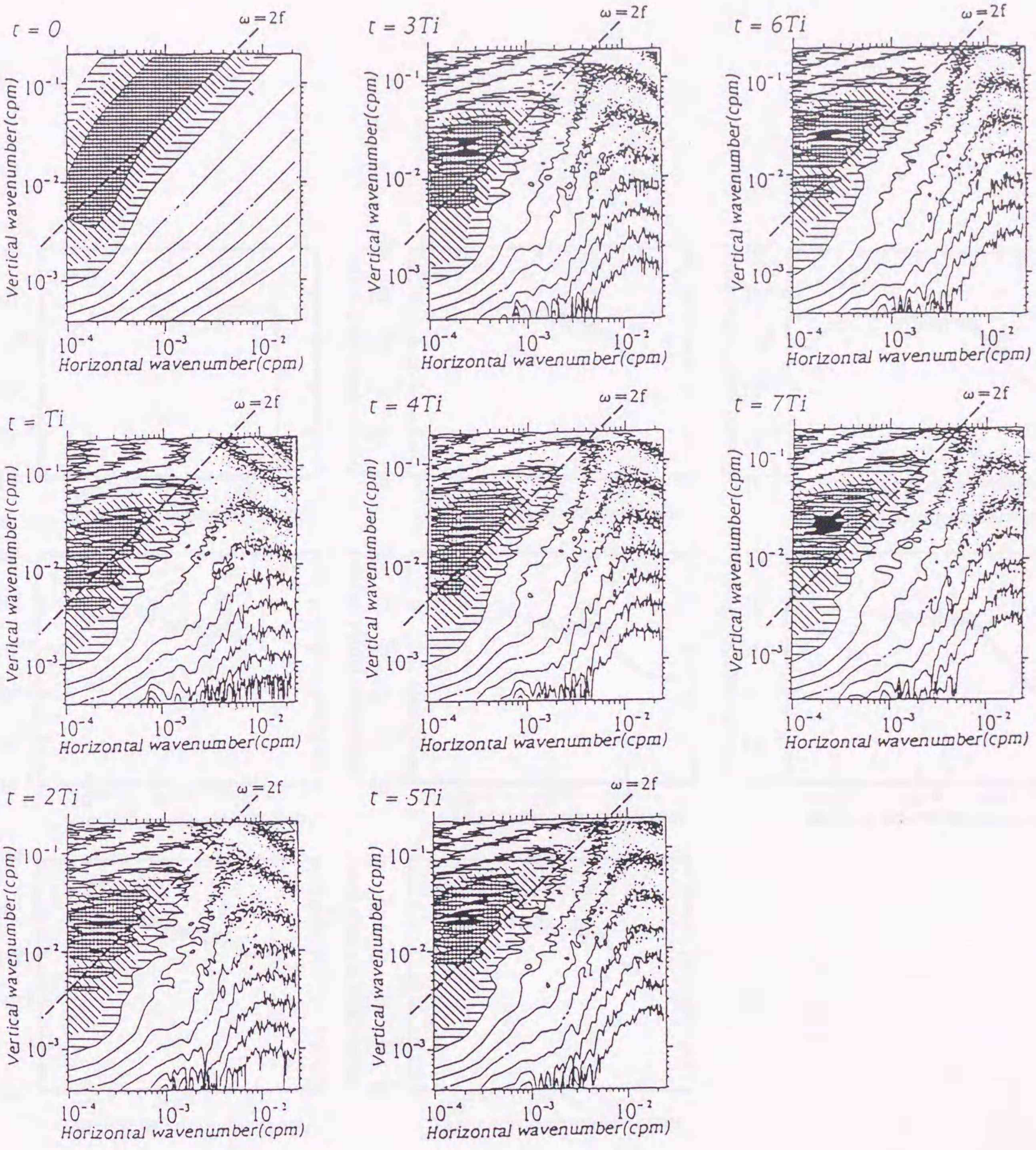

Figure 2.4. Time variations of the two-dimensional wavenumber Froude spectrum for the case corresponding to Fig. 2.3. Note that the spectrum is presented in variance preserving form with respect to horizontal wavenumber. Variations of spectral density level are represented by different intensities of shading where the darker shade indicates greater spectral density with the range of each shading being 0.25 in the logarithm. In the unshaded area, spectral density values are contoured with intervals of 0.5 in the logarithm.

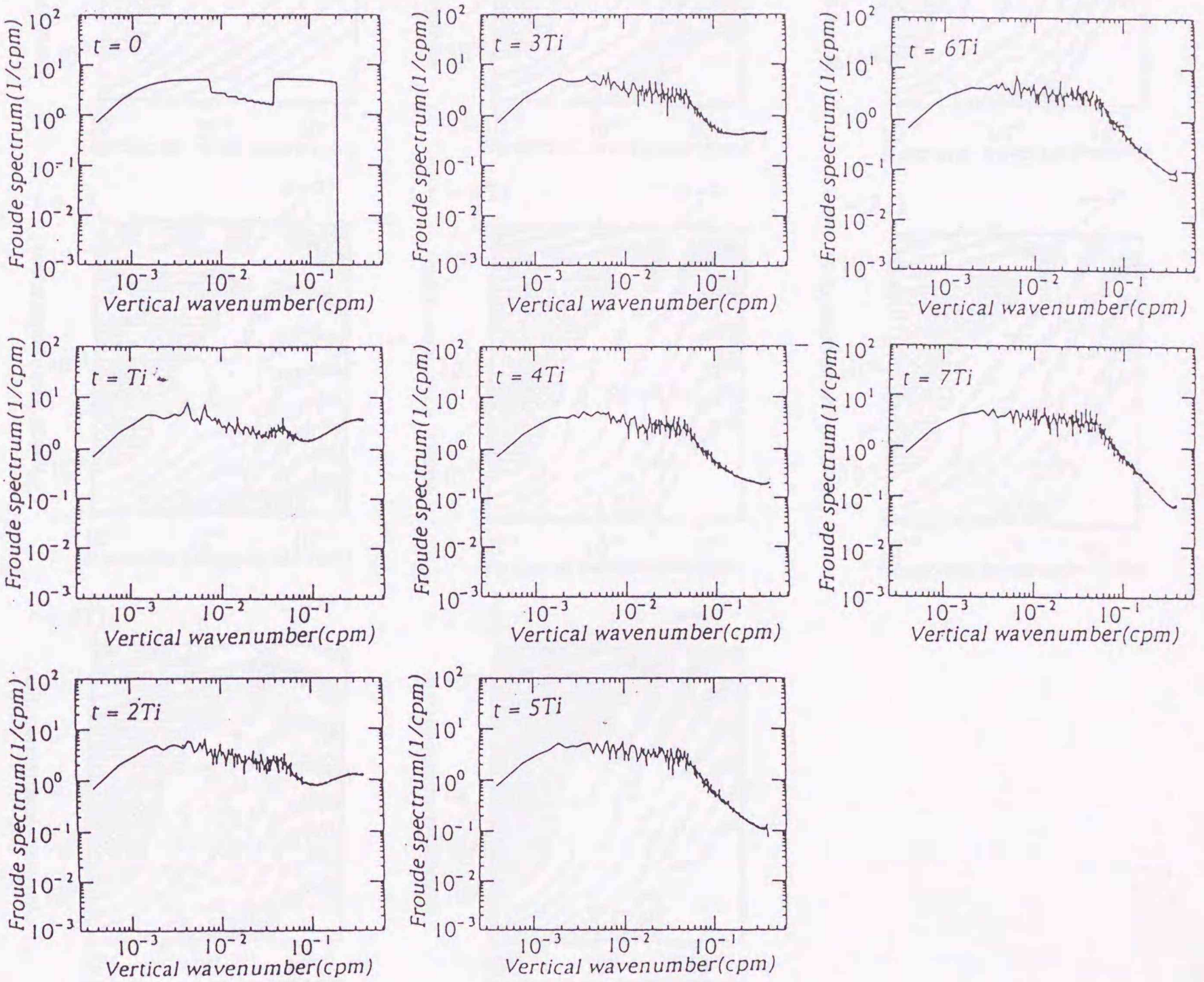

Figure 2.5. As in Fig. 2.3 but for the case where the initial condition is slightly modified such that the near-inertial energy level in the vertical wavenumber band of 0.01-0.04 cpm is assumed to be zero.

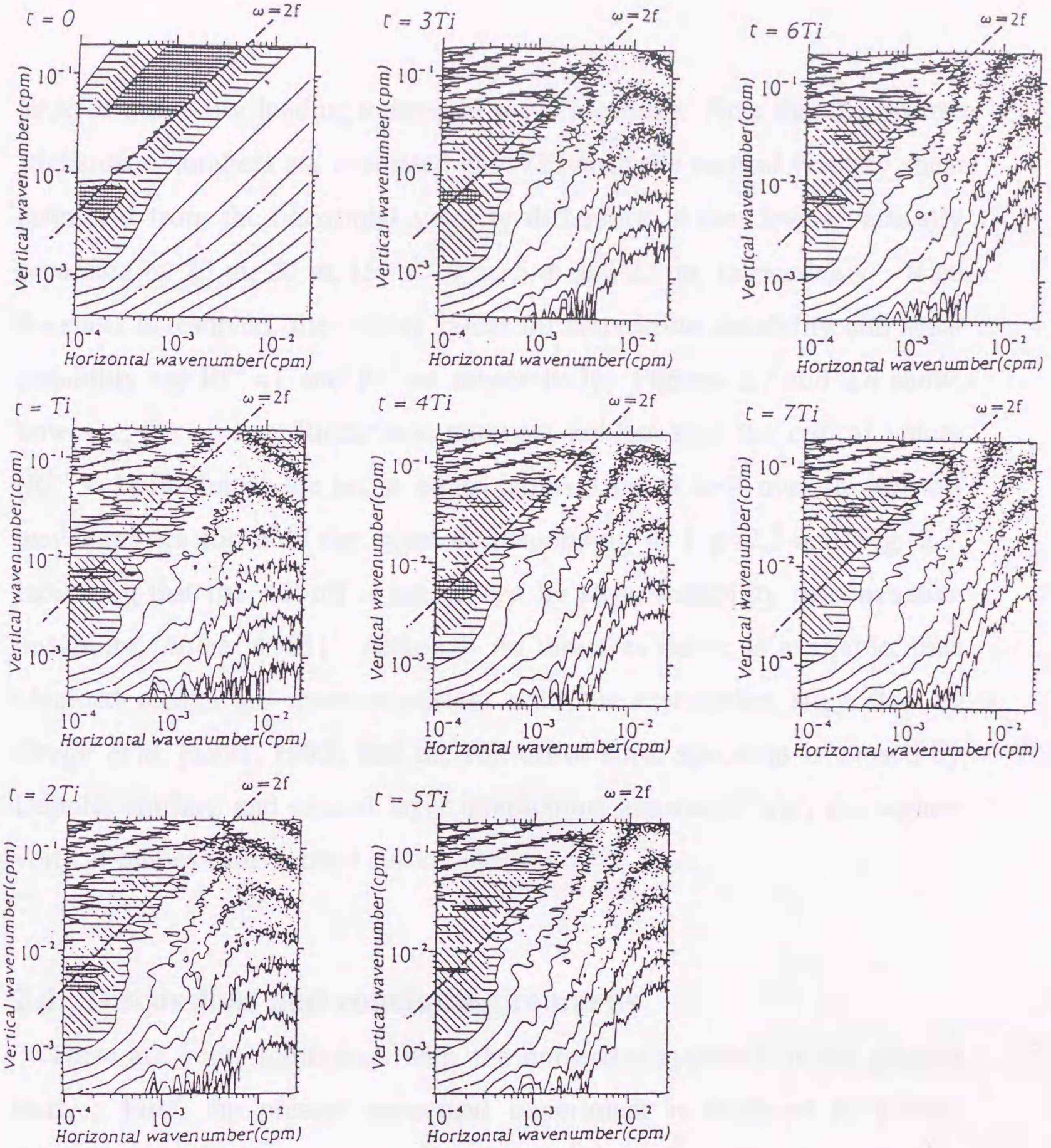

Figure 2.6. As in Fig. 2.4 but for the case corresponding to Fig. 2.5.

hood of instability leading to internal wave breaking. Note that the inverse Richardson numbers are evaluated at t=7Ti with the vertical velocity shear estimated from the horizontal velocity difference at two levels vertically separated by 25 m, 20 m, 15 m, 10 m, 5 m and 2.5 m, respectively. If all the shear is resolved, the critical values for convective instability and shear instability are Ri^{-1} =1 and Ri^{-1} =4 respectively. Figures 2.7 and 2.8 show, however, the inverse Richardson numbers are less than the critical values ($Ri^{-1} < 1$) in almost the entire model domain up to well over the roll-off wavenumbers for both the cases corresponding to Fig. 2.3 and Fig. 2.5, indicating that the roll-off is not caused by shear instability or convective instability [*Munk*, 1981]. Although no direct evidence is available, thus obtained results are more consistent with the mechanism suggested by *Gregg et al.* [1991, 1993] that the roll-off of shear spectrum is caused by Doppler shifting and critical layer interactions associated with the higher-vertical-modes near-inertial current shear.

2.4. Discussions and concluding remarks

There are some limitations with the numerical approach in the present study. First, the present numerical experiment is confined to a two-dimensional vertical plane in order to allow disparate scale wave interaction which is crucial in the internal wave dynamics. This effectively compromises the quantitative application of our results to the ocean. For example, the two-dimensional model might lack interactions found in a three-dimensional simulation because of the dynamical constrict imposed by the two-dimensionality. Nevertheless, we believe some qualitative aspects of the results summarized in the previous section are still relevant to oceanic internal waves. Second, an equilibrium state cannot be achieved in the

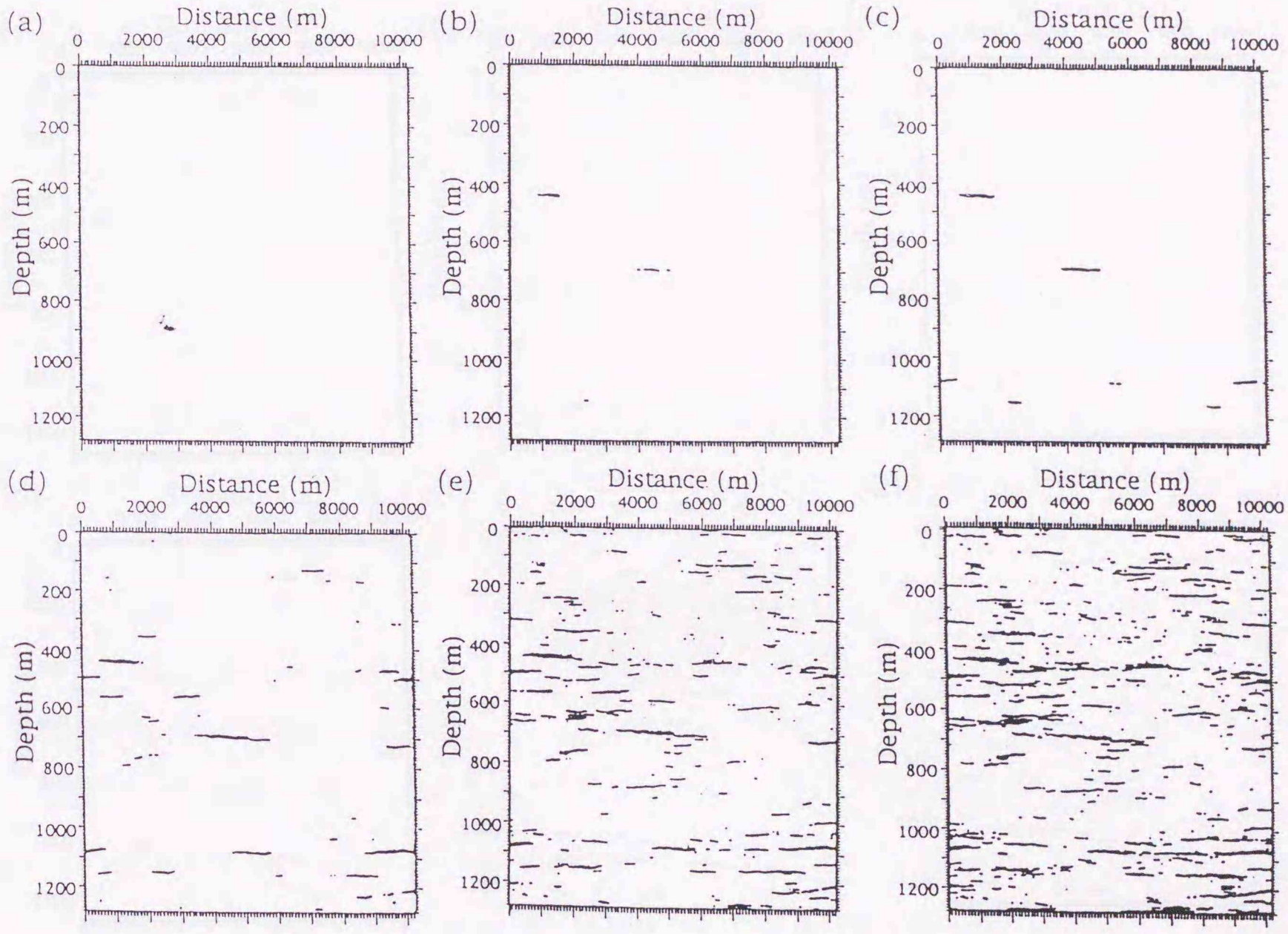

Figure 2.7. The areas where the inverse Richardson numbers become more than the critical values (Ri^{-1} >1) are shaded in the model domain for the case corresponding to Fig. 2.3. Note that the inverse Richardson numbers are evaluated at t=7Ti with the vertical velocity shear estimated from the horizontal velocity difference at two levels vertically separated by (a) 25 m, (b) 20 m, (c) 15 m, (d) 10 m, (e) 5 m and (f) 2.5 m, respectively.

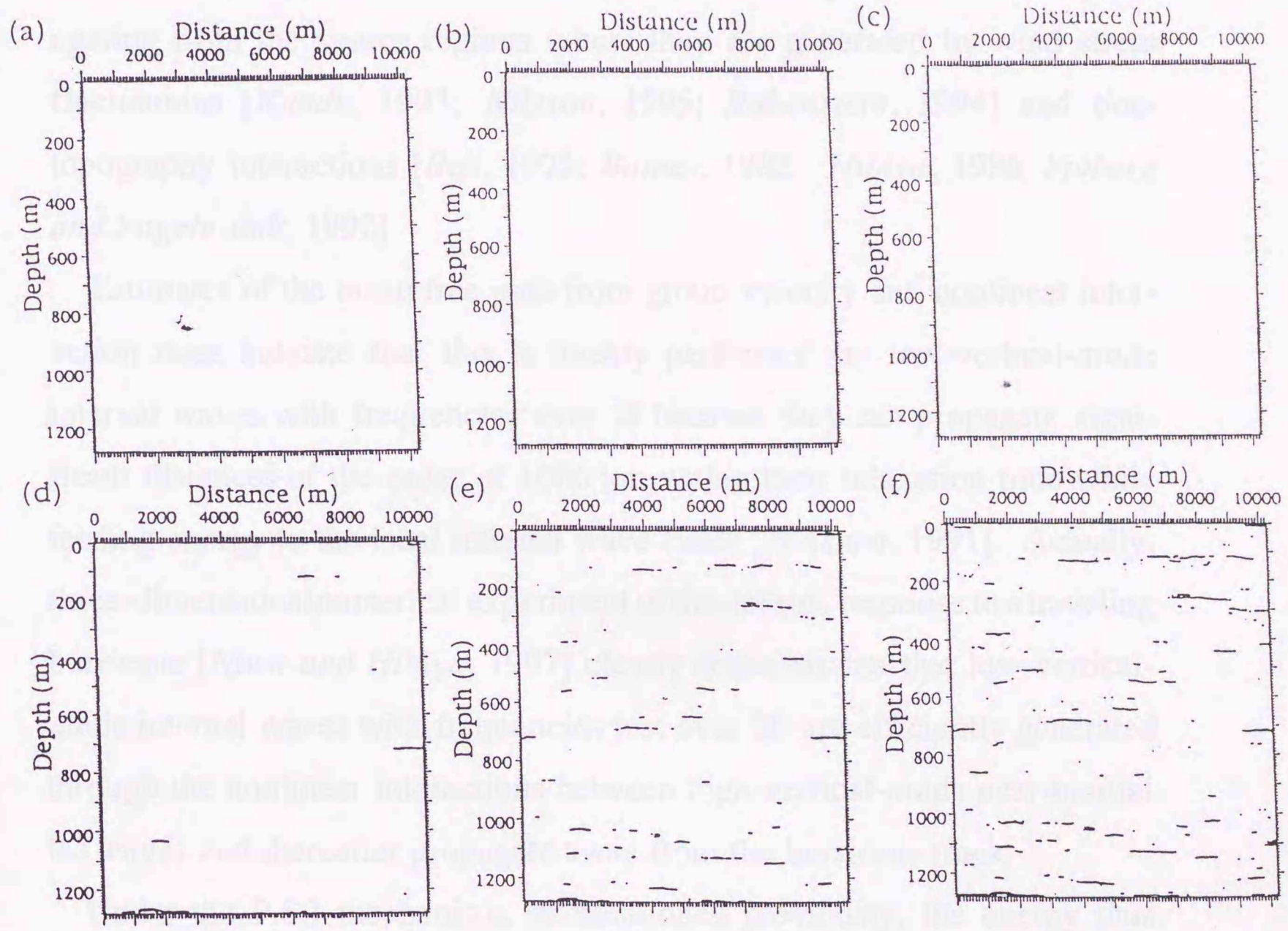

Figure 2.8. As in Fig. 2.7 but for the case corresponding to Fig. 2.5.

present numerical experiment because forcing is not applied to the internal wave spectrum. From the fact that the GM spectrum is maintained even in the regions weak in local energy sources, it is believed that energy is continuously supplied to the local wave spectrum by internal waves propagating from the source regions where they are generated by wind stress fluctuations [*Kundu*, 1993; *Nilsson*, 1995; *Rubenstein*, 1994] and tide-topography interactions [*Bell*, 1975; *Baines*, 1982; *Hibiya*, 1986; *Sjöberg and Stigebrandt*, 1992].

Estimates of the mean free path from group velocity and nonlinear interaction rates indicate that this is mostly performed by low-vertical-mode internal waves with frequencies over 2f because they can propagate significant distances of the order of 1000 km within their relaxation time while feeding energy to the local internal wave fields [*D'Asaro*, 1991]. Actually, three-dimensional numerical experiment of the oceanic response to a traveling hurricane [*Niwa and Hibiya*, 1997] clearly demonstrates that low-vertical-mode internal waves with frequencies just over 2f are efficiently generated through the nonlinear interactions between high-vertical-mode near-inertial lee waves and thereafter propagate away from the hurricane track.

Under the P.S.I mechanism, as mentioned previously, the energy thus supplied by the propagating waves is transferred to the higher-vertical-wavenumber near-inertial portion of the local internal wave spectrum. Putting all these together, we propose here a model for the dynamic balance of the internal wave spectrum such that with the increase (or decrease) of energy supply to the local internal wave spectrum, higher-vertical-modes near-inertial current shear is enhanced (or diminished) so that the roll-off shifts to lower (or higher) vertical wavenumbers leading to the increase (or decrease) in the rate of energy dissipation at critical layers.

The forcing field to the local internal wave spectrum is, therefore, needed

to clarify the distribution of available energy for mixing processes in the world ocean. Along these lines, the global internal wave field radiating from strong source regions is currently under active investigation based on three-dimensional numerical models, the results of which will be reported elsewhere.

References

Arakawa, A., Computational design for long-term numerical integration of the equations of fluid motion: two-dimensional incompressible flow, Part 1, *J. Comput. Phys., 1*, 119-143, 1966.

Baines, P. G., On internal tide generation models, *Deep Sea Res., 29*, 307-338, 1982.

Bell, T. H., Jr., Topographically generated internal waves in the open ocean, *J. Geophys. Res., 80*, 320-327, 1975.

D'Asaro, E. A., A strategy for investigating and modeling internal wave sources and sinks, in *Dynamics of Oceanic Internal Gravity Waves. Proc. Aha Huliko'a Hawaiian Winter Workshop*, pp. 451-466, edited by P. Müller and D. Henderson, Hawaii Institute of Geophysics, 1991.

Gargett, A. E., Vertical eddy diffusivity in the ocean interior, *J. Mar. Res., 42*, 359-393, 1984.

Gargett, A. E., P. E. Hendricks, T. B. Sanford, T. R. Osborn, and A. J. Williams III, A composite spectrum of vertical shear in the upper ocean, *J. Phys. Oceanogr., 11*, 1258-1271, 1981.

Garrett, C. J. R., and W. H. Munk, Space-time scales of internal waves, *Geophys. Fluid Dyn., 2*, 225-264, 1972.

Garrett, C. J. R., and W. H. Munk, Space-time scales of internal waves: A progress report, *J. Geophys. Res., 80*, 291-297, 1975.

Gregg, M. C., D. P. Winkel, and T. B. Sanford, Internal wave shear and dissipation, *in Dynamics of Oceanic Internal Gravity Waves. Proc. 'Aha Huliko'a Hawaiian Winter Workshop*, pp. 1-29, edited by P. Müller and D. Henderson, Hawaii Institute of Geophysics, 1991.

Gregg, M. C., D. P. Winkel, and T. B. Sanford, Varieties of fully resolved

spectra of vertical shear, *J. Phys. Oceanogr., 23*, 124-141, 1993.

Hibiya, T., Generation mechanism of internal waves by tidal flow over a sill, *J. Geophys. Res., 91*, 7697-7708, 1986.

Kundu, P. K., On internal waves generated by traveling wind, *J. Fluid Mech., 254*, 529-560, 1993.

McComas, C. H., Equilibrium mechanisms within the internal wave field, *J. Phys. Oceanogr., 7*, 836- 845, 1977.

McComas, C. H., and F. P. Bretherton, Resonant interaction of oceanic internal waves, *J. Geophys. Res., 83*, 1397-1412, 1977.

McComas, C. H., and P. Müller, The dynamic balance of internal waves, *J. Phys. Oceanogr., 11*, 970-986, 1981.

Müller, P., D. J. Olbers, and J. Willebrand, The IWEX spectrum, *Geophys. Res., 83*, 479-500, 1978.

Munk, W. H., Internal waves and small-scale processes, *in Evolution of Physical Oceanography*, edited by B. S. Warren and C. Wunsch, pp. 264-291, MIT Press, Cambridge, Mass., 1981.

Nilsson, J., Energy flux from traveling hurricanes to the oceanic internal wave field, *J. Phys. Oceanogr., 25*, 558-573, 1995.

Niwa, Y., and T. Hibiya, Nonlinear Processes of energy transfer from traveling hurricanes to the deep ocean internal wave field, *J. Geophys. Res., 102,* 12469-12477, 1997.

Olbers, D. J., Nonlinear energy transfer and the energy balance of the internal wave field in the deep ocean, *J. Fluid Mech., 74*, 375-399, 1976.

Pomphrey, N., J. D. Meiss, and K. M. Watson, Description of nonlinear internal wave interactions using Langevin method, *J. Geophys. Res.,*

85, 1085-1094, 1980.

Rubenstein, D., A spectral model of wind-forced internal waves. *J. Phys. Oceanogr., 24*, 819-831, 1994.

Sjöberg, B., and A. Stigebrandt, Computations of the geographical distribution of the energy flux to mixing processes via internal tides and associated vertical circulation in the ocean, *Deep Sea Res., 39*, 269-291, 1992.

Wunsch, C., Geographical variability of the internal wave field: A search for sources and sinks, *J. Phys. Oceanogr., 6*, 471-485, 1976.

Wunsch, C., and S. Webb, The climatology of deep ocean internal waves, *J. Phys. Oceanogr., 9*, 235-243, 1979.

Chapter 3

Nonlinear Processes of Energy Transfer From Traveling Hurricanes to the Deep Ocean Internal Wave Field

Abstract

Generation of large-scale internal waves by a hurricane traveling over the ocean with a uniform velocity is investigated by using three-dimensional multilevel numerical model. It is found that two distinctive kinds of internal waves are excited in the wake of the hurricane, namely, near-inertial waves which can be explained based on the linear theory and superinertial waves with frequencies $2f_0$ and $3f_0$ (f_0 is the inertial frequency at the latitude of the hurricane track) which are generated through nonlinear effects. Our special attention is directed to the superinertial waves with frequencies $2f_0$ and $3f_0$ because these internal waves are considered to be efficient energy sources for small-scale mixing in the deep ocean. These superinertial waves predominantly have low-vertical-mode structures and satisfy the dispersion relation for lee waves. In areas away from the hurricane track, in particular, the double-inertial frequency waves become larger than the near-inertial waves. The nonlinear resonant triads causing the generation of such superinertial waves are examined by calculating the bispectrum, which clearly shows that the lowest-vertical-mode double-inertial frequency wave is generated efficiently through the nonlinear interaction between the high-vertical-mode near-inertial waves.

3.1. Introduction

Internal waves are ubiquitous phenomena in the deep ocean, with the scales ranging from the planetary scales to the microscales. The most important characteristic of the deep ocean internal wave field is that its spectrum is remarkably stable in both space and time [*Müller et al.*, 1978; *Wunsch and Webb*, 1979] which is empirically modeled as the Garrett and Munk spectrum (hereafter referred to as the GM spectrum) [*Garrett and Munk*, 1972, 1975; *Munk*, 1981]. Although the exact physical processes establishing the GM spectrum have not been clarified yet, the existence of universal level of the GM spectrum indicates that energy is continuously supplied to the internal wave field by atmospheric forcing [*Rubenstein*, 1994; *Nilsson*, 1995] and tide-topography interactions [*Sjöberg and Stigebrandt*, 1992].

Understanding the energy transfer processes to the internal wave field is also crucial in larger oceanographic context. The energy supplied at large generation scales is considered to be transferred across the GM spectrum to small dissipation scales through nonlinear wave-wave interactions causing diapycnal mixing in the deep ocean [*Hibiya et al.*, 1996; *McComas and Müller*, 1981]. This small-scale diapycnal mixing is believed to affect the oceanic general circulation strongly, as is actually demonstrated in oceanic general circulation model results where strength of the circulation is very sensitive to the magnitude of vertical eddy diffusivity [*Bryan*, 1987]. Therefore, accurate modeling of the oceanic general circulation requires adequate parameterization of the diapycnal mixing in the deep ocean, which might become possible through the investigation of physical processes of energy transfer from large generation scales down to small dissipation scales.

As a first step toward the adequate parameterization of the diapycnal mixing, we examine here the energy transfer processes to the deep ocean

internal wave field from atmospheric disturbances traveling over the ocean by using three-dimensional multilevel numerical model. As an atmospheric disturbance, we consider a hurricane with an intense windstress field, which is believed to be one of the major sources of large-scale internal waves.

Spectral characteristics of the wave fields obtained from this numerical experiment show that two distinctive kinds of internal waves are generated in the wake of the hurricane, namely, near-inertial waves with frequencies close to f_0 (f_0 is the inertial frequency at the latitude of the hurricane track) and superinertial waves with frequencies $2f_0$ and $3f_0$. The generation of near-inertial waves is first studied by *Geisler* [1970] on the basis of linear theory. Geisler showed that if the speed of the hurricane greatly exceeds eigenspeeds of the internal waves, near-inertial waves are excited in the mixed layer after the passage of the hurricane. *Gill* [1984] discussed the dispersion of near-inertial energy which is initially confined in the mixed layer in terms of the low-vertical-mode near-inertial waves propagating away from the forcing region. Most of the other previous works are mainly concerned with the generation of near-inertial waves in response to a moving hurricane [*Price*, 1983; *Price et al.*, 1994; *Greatbatch*, 1983, 1984].

In this article, we focus on the generation of superinertial waves with frequencies $2f_0$ and $3f_0$. *Price* [1983] pointed out that the superinertial waves were reproduced in his three-dimensional multilayer model, but he did not discuss the generation mechanism of these waves in detail. The main reason focusing on the generation of these superinertial waves is that they are believed to supply energy to the local internal wave field which is far away from the source region; the energy thus supplied is considered to be transferred across the local internal wave spectrum down to small dissipation scales inducing the diapycnal mixing in the deep ocean. These issues are discussed more in detail in section 3.5.

3.2. Numerical model

We assume a hurricane propagating over the model ocean as is schematically shown in Fig. 3.1. The model ocean consists of a simple box with east-west and north-south dimensions of 9000 km and 5000 km, respectively, and a uniform depth of 4000 m. The hurricane is assumed to have an intense steady wind stress field and propagate eastward with a uniform velocity from a center of the western boundary of the model ocean.

The steady wind stress field of the hurricane is the same as that used by *Price* [1983] and is an axisymmetric wind stress field with a tangential component τ_θ and a radial component τ_r. The dependence of τ_θ and τ_r on the radial distance r from the center of the hurricane is assumed such that

$$\begin{aligned} \tau_\theta &= \tau_{max}\left(\frac{r}{R}\right) && r < R \\ &= \tau_{max}\left(1.2 - 0.2\frac{r}{R}\right) && R \le r \le 6R \\ &= 0 && r > 6R \end{aligned} \qquad (3.1)$$

$$\tau_r = -0.3\tau_\theta \qquad (3.2)$$

where we set τ_{max}=2.5 N m^{-2} and R=40 km.

The governing equations are the three-dimensional Navier-Stokes equations on the β-plane under the hydrostatic, Boussinesq approximations given by

$$\bar{\rho}\left(\frac{\partial u}{\partial t} + u\frac{\partial u}{\partial x} + v\frac{\partial u}{\partial y} + w\frac{\partial u}{\partial z}\right) = -\frac{\partial P}{\partial x} + (f_0 + \beta y)v + A_H\nabla_H^2 u + A_V\frac{\partial^2 u}{\partial z^2} + F_x \qquad (3.3)$$

$$\bar{\rho}\left(\frac{\partial v}{\partial t} + u\frac{\partial v}{\partial x} + v\frac{\partial v}{\partial y} + w\frac{\partial v}{\partial z}\right) = -\frac{\partial P}{\partial y} - (f_0 + \beta y)u + A_H\nabla_H^2 v + A_V\frac{\partial^2 v}{\partial z^2} + F_y \qquad (3.4)$$

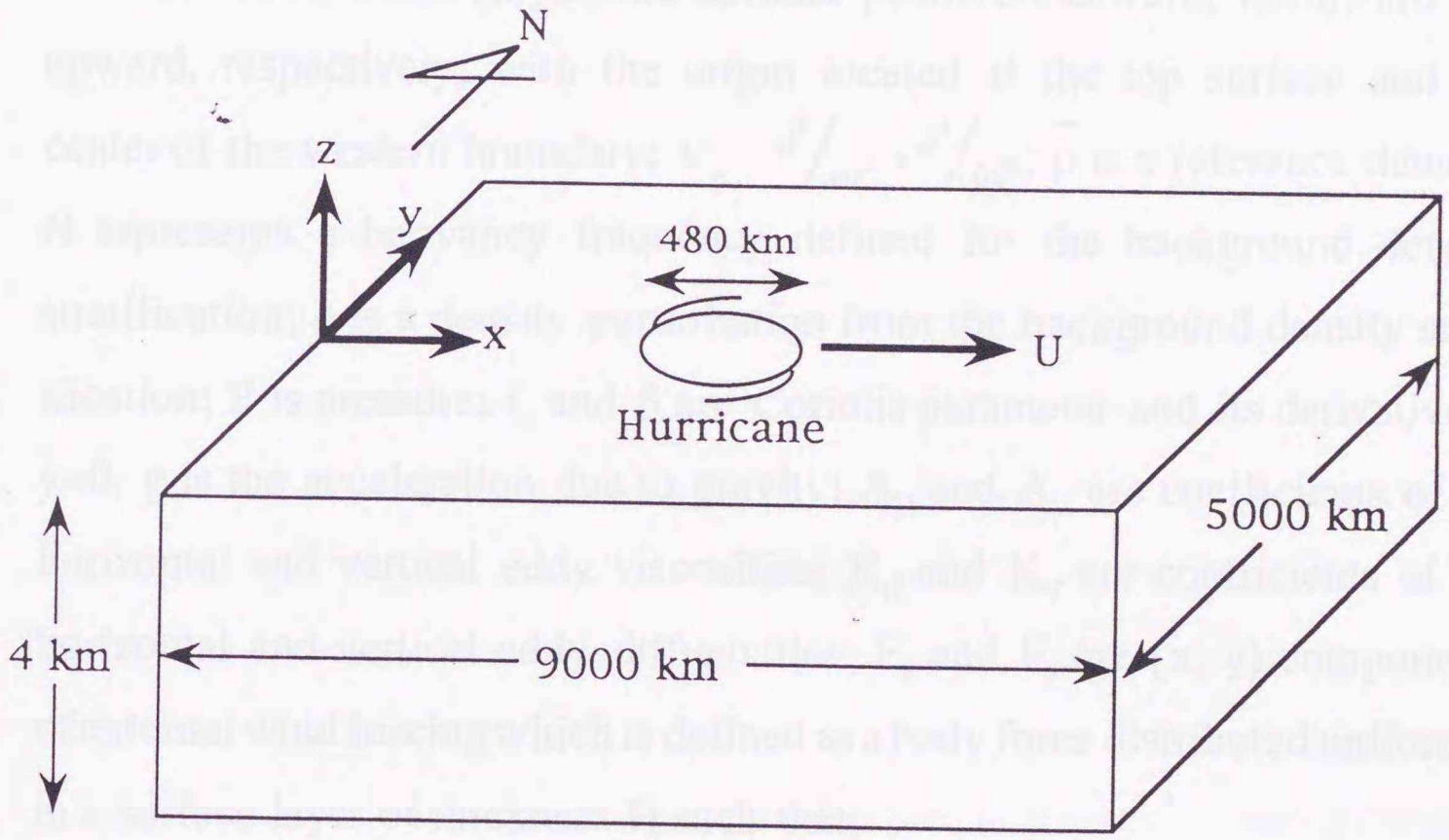

Figure 3.1. Schematic view of the numerical model used in this study.

$$\frac{\partial P}{\partial z} = -g\,\rho \tag{3.5}$$

$$\frac{\partial u}{\partial x} + \frac{\partial v}{\partial y} + \frac{\partial w}{\partial z} = 0 \tag{3.6}$$

$$\frac{\partial \rho}{\partial t} + u\frac{\partial \rho}{\partial x} + v\frac{\partial \rho}{\partial y} + w\frac{\partial \rho}{\partial z} = \frac{\bar{\rho}}{g}N^2 w + K_H \nabla_H^2 \rho + K_V \frac{\partial^2 \rho}{\partial z^2} \tag{3.7}$$

Here the coordinates (x,y,z) are defined positive eastward, northward and upward, respectively, with the origin located at the top surface and the center of the western boundary; $\nabla_H^2 = \partial^2/\partial x^2 + \partial^2/\partial y^2$; $\bar{\rho}$ is a reference density; N represents a buoyancy frequency defined for the background density stratification; ρ is a density perturbation from the background density stratification; P is pressure; f_0 and β are Coriolis parameter and its derivative at y=0; g is the acceleration due to gravity; A_H and A_V are coefficients of the horizontal and vertical eddy viscosities; K_H and K_V are coefficients of the horizontal and vertical eddy diffusivities; F_x and F_y are (x, y) components of external wind forcing which is defined as a body force distributed uniformly in a surface layer of thickness H such that;

$$(F_x, F_y) = \frac{1}{H}(\tau_x(x - U\,t, y), \tau_y(x - U\,t, y)) \tag{3.8}$$

where τ_x and τ_y denote the wind stress defined by (3.1) and (3.2), and U denotes the propagation speed of the hurricane. The typical speed of the hurricane is statistically shown to range from approximately 5 m s^{-1} to 10m s^{-1} [*Rubenstein,* 1994]. Taking account of this, the responses of stratified ocean for two extreme cases are examined in this study, namely, for the case when the hurricane propagates with a speed of 5 m s^{-1} and for the case when the hurricane propagates with a speed of 10 m s^{-1}.

We assume a uniform vertical stratification with a buoyancy frequency

$N=5.0\times10^{-3}\,s^{-1}$. Although it seems unrealistic to apply such a large density stratification over the full ocean depth, the assumption of a uniform stratification significantly simplifies the analysis to clarify the basic mechanism for internal wave generation by a traveling hurricane, which is the primary objective of this study. Actually, when a nonuniform density stratification is employed, the procedure for calculating the bispectrum,which will be discussed in section 3.4, becomes much more complicated.

The parameters f_0 and β are evaluated at 30°N so that $f_0= 7.0\times10^{-5}\,s^{-1}$ and $\beta=1.9\times10^{-11}\,s^{-1}\,m^{-1}$. The surface layer thickness H is set to be 100 m. The coefficients A_H and K_H are both assumed to be $10^2\,m^2\,s^{-1}$, and A_v and K_v are both assumed to be $10^{-3}\,m^2\,s^{-1}$.

The governing equations are solved numerically by using a finite difference method. The model ocean is divided into 900×500 horizontal grid points ($\Delta x=\Delta y=10^4$ m) and 40 vertical grid points ($\Delta z=100$ m). The sidewalls and the ocean bottom are assumed to be rigid. At the top boundary a free surface condition is used, though surface gravity waves are filtered out by employing the semi-implicit scheme. A time step (Δt) is assumed to be 1200 s which is small enough to resolve the lowest-vertical-mode of internal gravity waves. To suppress the computational mode, the Euler backward scheme is applied every 30 time steps.

3.3. Space-time scales of the generated internal waves

3.3.1. Temporal scales

Figure 3.2 shows the timeseries of the eastward velocity (u) at various locations for the case when the hurricane moves at U=5 m s^{-1}. It should be noted that the scale of the vertical axis for the velocity at z=0 m is different from the others by a factor of 10. In the timeseries at z=0 m, we can see

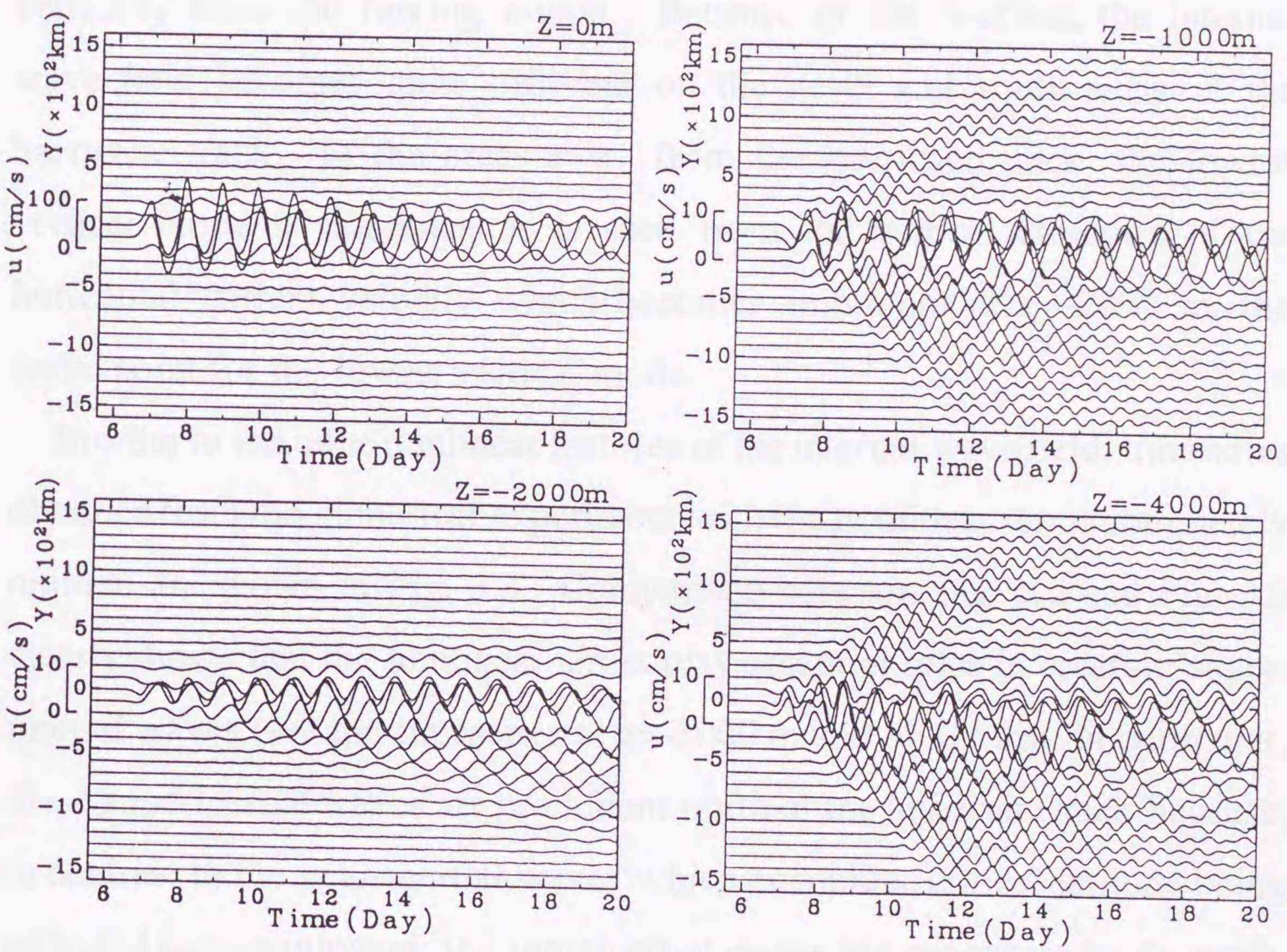

Figure 3.2. Timeseries of the eastward velocity u at x=3000 km and various positions of y ranging from -1500 km to 1500 km for each depth (z=0 m, -1000 m, -2000 m, -4000 m) when the hurricane travels at $U=5ms^{-1}$. Note that the scale of the vertical axis for u at z=0 m is different from the others by a factor of 10.

that strong near-inertial currents with a period close to one day (inertial period at the latitude of the hurricane track) are excited in the forcing region (in the top layer for $|y| < 240$ km (radius of the hurricane)) with the maximum amplitude approaching about 1.0 m s^{-1} after the passage of the hurricane [*Price*, 1983; *Price et al.*, 1994; *Greatbatch*, 1983, 1984]. Below the top layer, internal waves are seen to propagate horizontally and vertically from the forcing region. Because of the β-effect, the internal wave field becomes quite different on the north and south sides of the hurricane track. In the areas away from the hurricane track, the lowest vertical mode is dominant as is seen from the vertical structure of the horizontal current velocity which becomes minimum at z=-2000 m, the nodal point for the lowest vertical mode.

In order to examine nonlinear features of the internal wave field, timeseries obtained from the numerical experiment with the nonlinear terms completely omitted are shown in Fig. 3.3. Comparison between Fig. 3.2 and Fig. 3.3 clearly shows that the nonlinear terms play essential roles in creating super-inertial waves (see the timeseries at z=-1000 m and -4000 m). In particular, these superinertial waves are prominent north of the hurricane track because, in contrast to the near-inertial waves which encounter critical latitude being reflected back southward, the superinertial waves can propagate freely north-ward.

To examine the temporal features of the internal wave field more in detail, frequency spectra of horizontal kinetic energy are calculated at several locations for the case of U=5 m s^{-1} (Fig. 3.4). Several distinct peaks are found in these frequency spectra. Near-inertial peaks are found at $\omega \simeq f_0$ (inertial frequency at the latitude of the hurricane track) in the spectra south of the hurricane track, and at $\omega \simeq f_0 + \beta y$ (local inertial frequency) in the spectra northward of the hurricane track. Other spectral peaks are found at

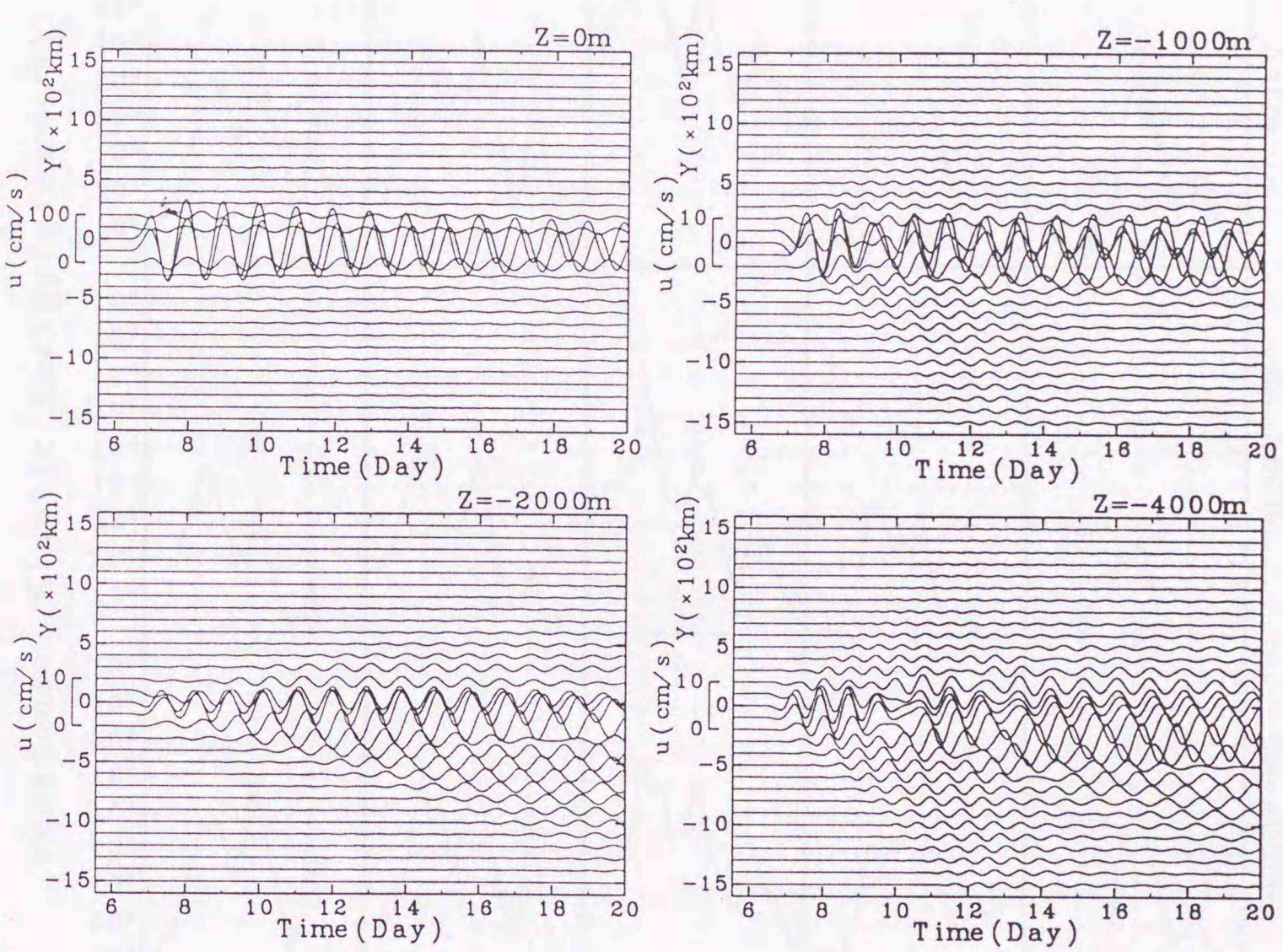

Figure 3.3. As in Fig. 3.2 but for the timeseries of the eastward velocity u obtained from the numerical model where the nonlinear terms completely omitted.

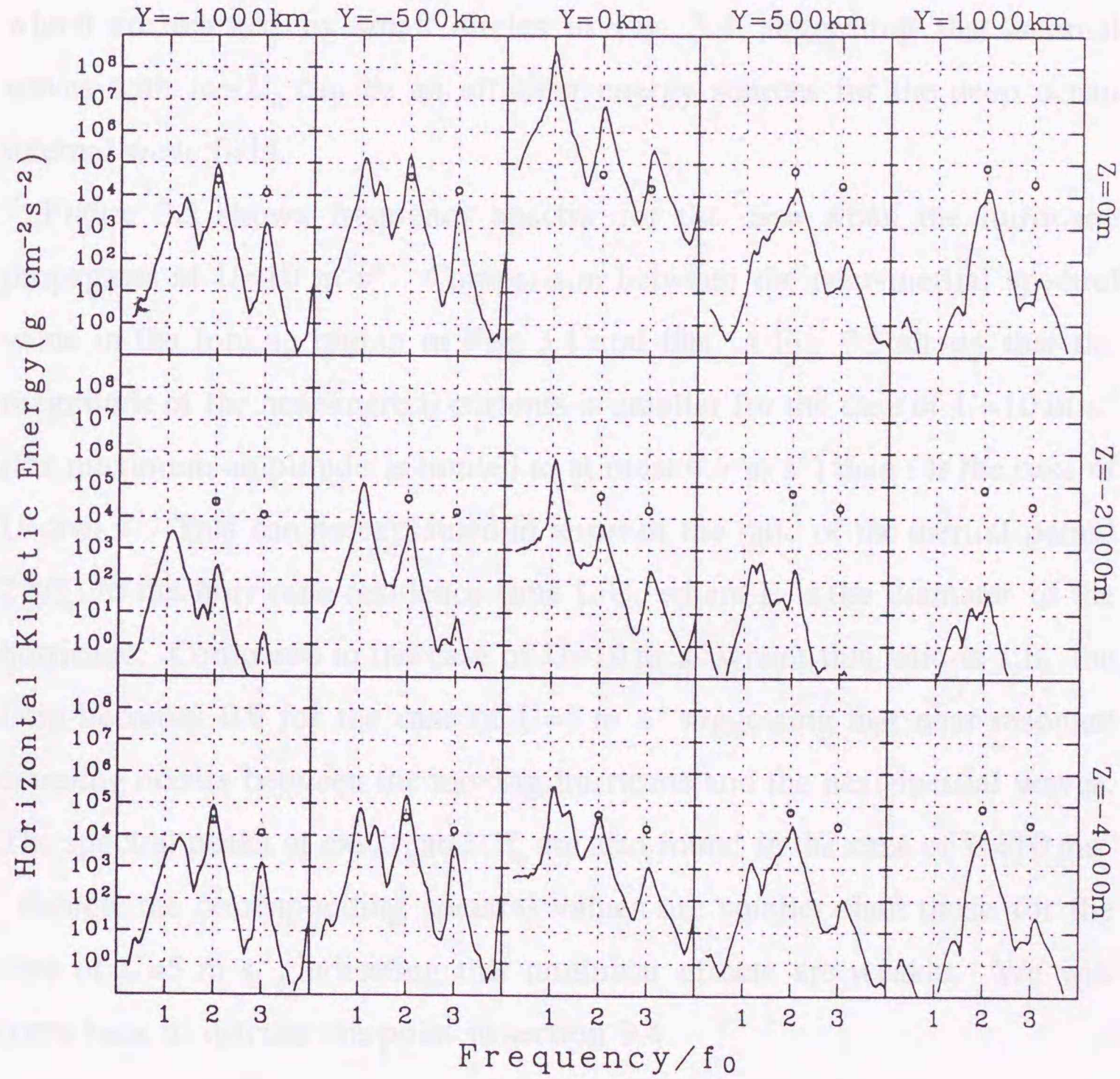

Figure 3.4. Frequency spectra of horizontal kinetic energy for the case of U=5 m s^{-1} calculated from the timeseries at x=3000 km and -1000 km≦y≦ 1000 km for the surface layer (z=0 m), mid-depth (z=-2000 m) and bottom layer (z=-4000 m). Note that frequency is normalized by the inertial frequency at the latitude of the hurricane track f_0. Small circles in each spectrum show the GM spectrum values at $\omega=2f_0$ and $3f_0$.

$\omega \simeq 2f_0$ and $3f_0$ and are not reproduced in the frequency spectra from the linear numerical model (not shown here). In the areas away from the hurricane track, in particular, the spectral values at $\omega \simeq 2f_0$ become larger than those of the near-inertial waves and the GM spectrum values at $\omega \simeq 2f_0$, which are marked by small circles in Fig. 3.4, suggesting that internal waves with $\omega \simeq 2f_0$ can be an efficient energy sources for the deep ocean internal wave field.

Figure 3.5 shows frequency spectra for the case when the hurricane propagates at U=10 m s^{-1}. Comparison between the near-inertial spectral value in the forcing region in Fig. 3.4 and that in Fig. 3.5 shows that the magnitude of the near-inertial currents is smaller for the case of U=10 m s^{-1} (the maximum amplitude is limited to at most 0.5 m s^{-1}) than for the case of U=5 m s^{-1}. This can be explained in terms of the ratio of the inertial period $2\pi/f_0$ to the hurricane residence time L/U, where L is the diameter of the hurricane. Compared to the case of U=10 m s^{-1} where this ratio is 1.8, the ratio becomes 0.9 for the case of U=5 m s^{-1} suggesting that near resonant coupling occurs between the moving hurricane and the near-inertial waves. The spectral peaks at $\omega \simeq 2f_0$ and $3f_0$ are also found in the case of U=10 ms^{-1} , though the corresponding spectral values are smaller than those for the case of U=5 m s^{-1}, indicating that nonlinear effects are weaker. We will come back to discuss this point in section 3.4.

3.3.2. Spatial scales

The spatial features of internal waves generated by the hurricane are examined by calculating two-dimensional horizontal wavenumber spectra of horizontal kinetic energy. The spectra for the lowest six vertical modes are shown in Fig. 3.6 for the case of U=5 m s^{-1} and in Fig. 3.7 for the case of U=10 m s^{-1}. The spectra for much higher vertical modes are not shown

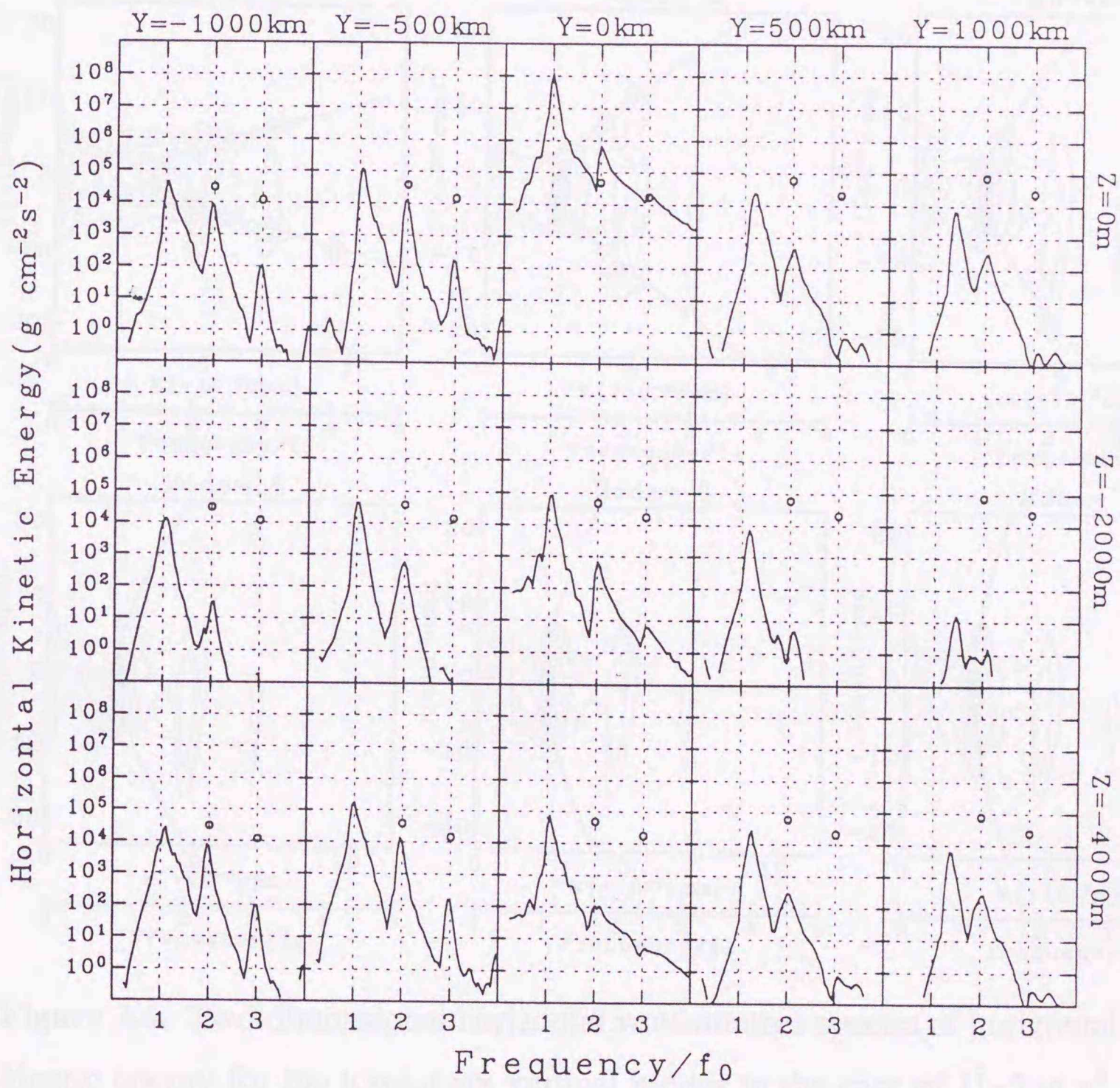

Figure 3.5. As in Fig. 3.4 but for the case of U=10 m s^{-1}.

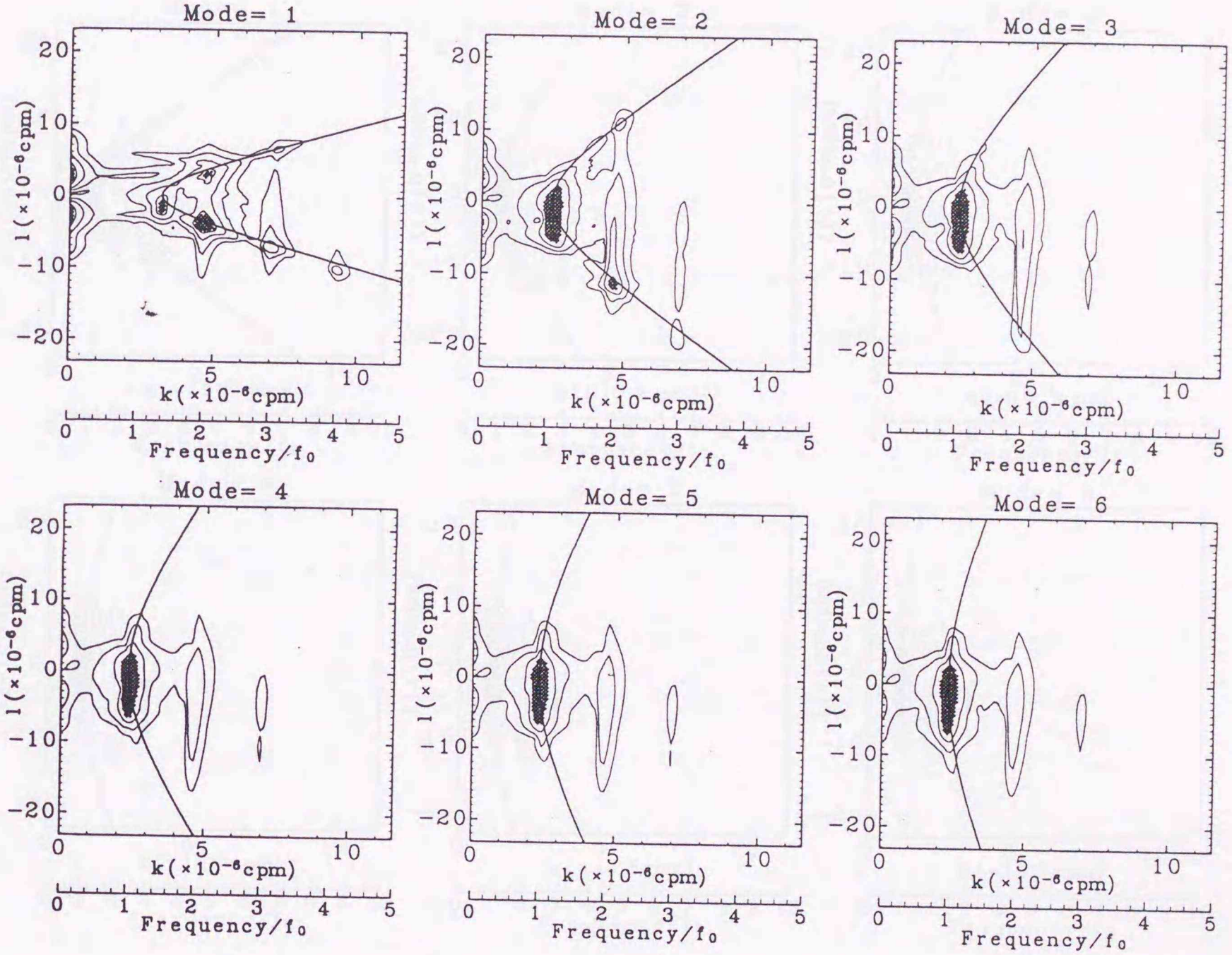

Figure 3.6. Two-dimensional horizontal wavenumber spectra of horizontal kinetic energy for the lowest six vertical modes in the case of U=5 m s^{-1}. Spectral values are contoured with a interval of 1.0 in the logarithm. Areas where spectral values are greater than 4% of the maximum are shaded. Superposed on each spectrum is the dispersion curve of the lee waves with the frequency given by $\omega = Uk$.

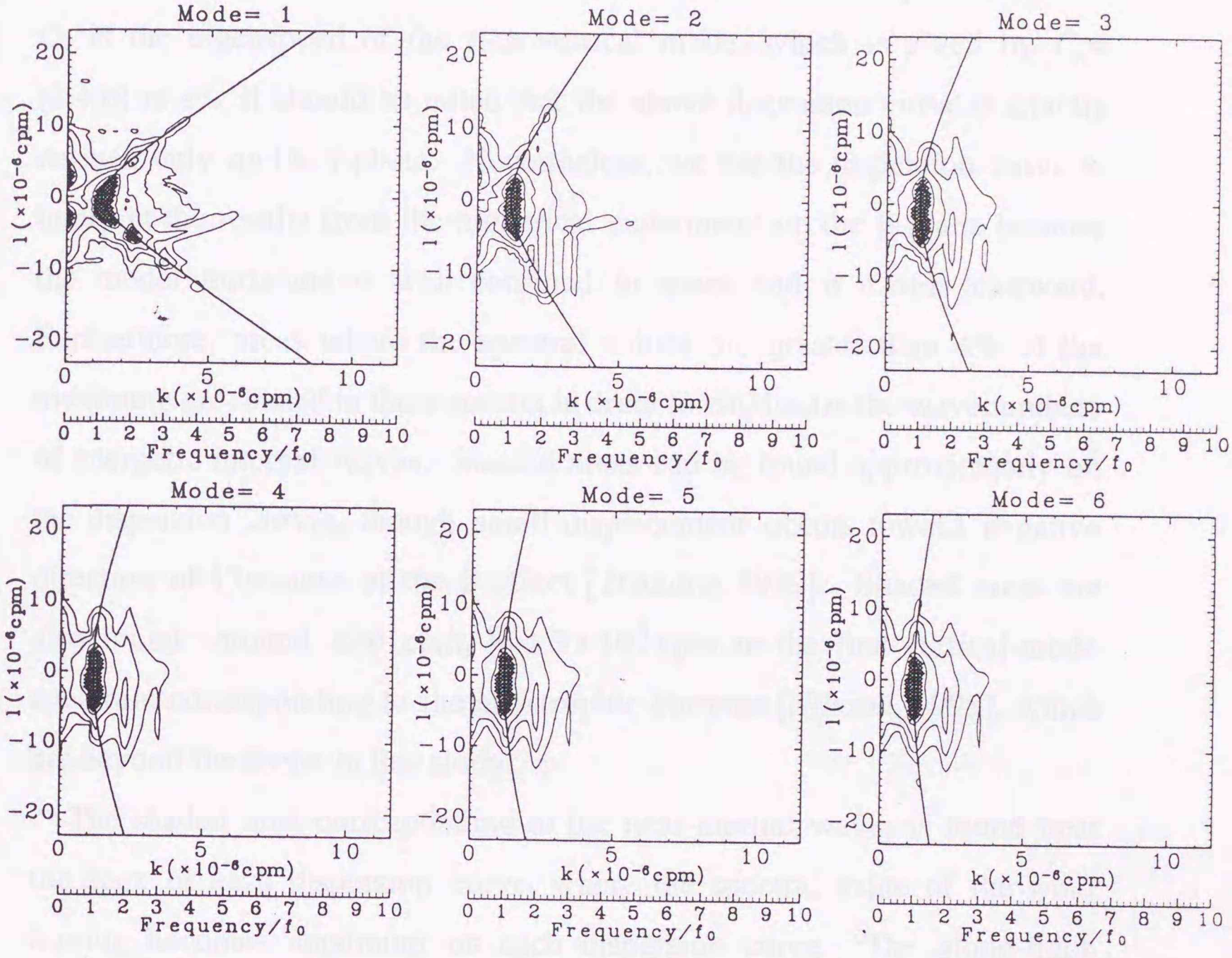

Figure 3.7. As in Fig. 3.6 but for the case of U=10 m s^{-1}.

here because they are essentially the same as the spectrum for the sixth vertical mode. Superimposed on these spectra are dispersion curves for the lee waves defined by $(Uk)^2 = f_0^2 + C_n^2\left(k^2 + l^2\right)$ where k and l are along-track and cross-track components of horizontal wavenumber, respectively; and C_n is the eigenspeed of the n-th vertical mode, which is given by C_n= (3.4/n) m s^{-1}. It should be noted that the above dispersion curve is exactly defined only on the f-plane. Nevertheless, we use the dispersion curve to interpret the results from the numerical experiment on the β-plane because the model hurricane is well confined in space and it travels eastward. Furthermore, areas where the spectral values are greater than 4% of the maximum are shaded in these spectra in order to emphasize the wavenumbers of energetic internal waves. Shaded areas can be found approximately on the dispersion curves, though small displacement occurs toward negative direction of l because of the β-effect [*D'Asaro*, 1989]. Shaded areas are also found around k=0 cpm, l= $\pm 3\times 10^{-6}$ cpm in the first-vertical-mode spectrum corresponding to the geostrophic currents [*Nilsson*, 1995], which are beyond the scope in this study.

The shaded area corresponding to the near-inertial waves is found near the apex of each dispersion curve, where the spectral value of the wind forcing becomes maximum on each dispersion curve. The along-track wavenumbers of these shaded areas are given by $k_i = f_0\left(U^2 - C_n^2\right)^{-\frac{1}{2}}$, which can be reduced to $k_i = f_0/U$ when U>>C_n. It follows that the along-track wavenumber of near-inertial waves for the case of U=5 m s^{-1} becomes about 3.0×10^{-6} cpm for the first vertical mode and about 2.2×10^{-6} cpm for the higher vertical modes, whereas the along-track wavenumber of near-inertial waves for the case of U=10 m s^{-1} becomes about 1.1×10^{-6}cpm for all the vertical modes.

The shaded areas corresponding to the double-inertial frequency waves

can be found in the first- and second-vertical-mode spectra for the case of U=5 m s^{-1} (Fig. 3.6) and in the first-vertical-mode spectrum for the case of U=10 m s^{-1} (Fig. 3.7). It should be noted that these shaded areas exist on the dispersion curves of lee waves, indicating that the double-inertial frequency waves are not transient waves but stationary waves relative to the traveling hurricane. The along-track wavenumbers of these shaded areas are given by $k_{2i} = 2f_0 / U$, and the cross-track wavenumbers of these shaded areas are given by $l_{2i} = \pm k_{2i}\left[\frac{3}{4}U^2 C_n^{-2} - 1\right]^{1/2}$, though the spectral value at positive l_{2i} becomes smaller than that at negative l_{2i} because of the β-effect. Figures 3.6 and 3.7 show that the most energetic double-inertial frequency wave has the first-vertical-mode structure with k_{2i}=4.6×10^{-6} cpm and l_{2i}=-4.0×10^{-6} cpm for the case of U=5 m s^{-1} and with k_{2i}=2.3×10^{-6} cpm and l_{2i}=-5.6-×10^{-6} cpm for U=10 m s^{-1}.

Significant superinertial energies are also found to be generated off the dispersion curve for each spectrum. However, these energies correspond to the evanescent-type motions trapped near the traveling hurricane, so that they cannot participate in the energy cascade in the deep ocean internal wave field.

3.4. Generation mechanism of the double-inertial frequency wave

In this section we examine nonlinear resonant triads causing the generation of low-vertical-mode double-inertial frequency waves through bispectral analysis [*Lin et al.*, 1995]. The internal wave with horizontal wavenumber vector $\mathbf{k}_1$ and vertical mode n_1 is generated through the nonlinear interaction between an internal wave with $\mathbf{k}_2$ and n_2 and one with $\mathbf{k}_3$ and n_3 satisfying the conditions,

$$\mathbf{k}_1 = \mathbf{k}_2 + \mathbf{k}_3,\ n_1 = |\, n_2 \pm n_3 \,|\ \ (n_1, n_2, n_3 \geqq 0)$$

The bispectral value at $(\mathbf{k}_2, n_2)$ indicates the nonlinear kinetic energy transfer rate to the internal wave with $\mathbf{k}_1$ and n_1 caused by the interaction between an internal wave with $\mathbf{k}_2$ and n_2 and one with $\mathbf{k}_3$ and n_3. It should be noted that the present bispectral analysis is carried out with the assumption that internal wave fields are stationary because, as was mentioned in section 3.3, all energetic internal waves can be considered as lee waves.

To examine the generation mechanism of the southward propagating first-vertical-mode (n_1=1) double-inertial frequency wave for U=5 m s^{-1} with horizontal wavenumbers $k_1 = 4.6 \times 10^{-6}$ cpm and $l_1 = -4.0 \times 10^{-6}$ cpm (see the first-vertical-mode spectrum in Fig. 3.6), two-dimensional horizontal wavenumber bispectra are calculated for typical pairs of interaction between the internal waves of vertical mode n_2 and n_3 (Fig. 3.8). The bispectral values in the areas from which energy is transferred to the first-vertical-mode double-inertial frequency wave (marked by small cross in each bispectrum) are contoured by solid lines, whereas those in the areas to which energy is transferred from the first-vertical-mode double-inertial frequency wave are contoured by dashed lines. We can see that near-inertial waves strongly interact with the first-vertical-mode double-inertial frequency wave. The interaction between the near-inertial waves with n_2= 9 and n_3=10 transfers energy to the first-vertical-mode double-inertial frequency wave, whereas the interaction between the near-inertial waves with n_2=3 and n_3= 4 subtracts energy from the first-vertical-mode double-inertial frequency wave. In contrast, the interactions are weak between the near-inertial waves with n_2=1 and n_3=2 and between the near-inertial waves with n_2=19 and n_3=20.

To examine the dependence of the kinetic energy transfer rate to the first-vertical-mode double-inertial frequency wave on the vertical-mode pair n_2 and n_3, the bispectral amplitude is calculated for each vertical-mode pair

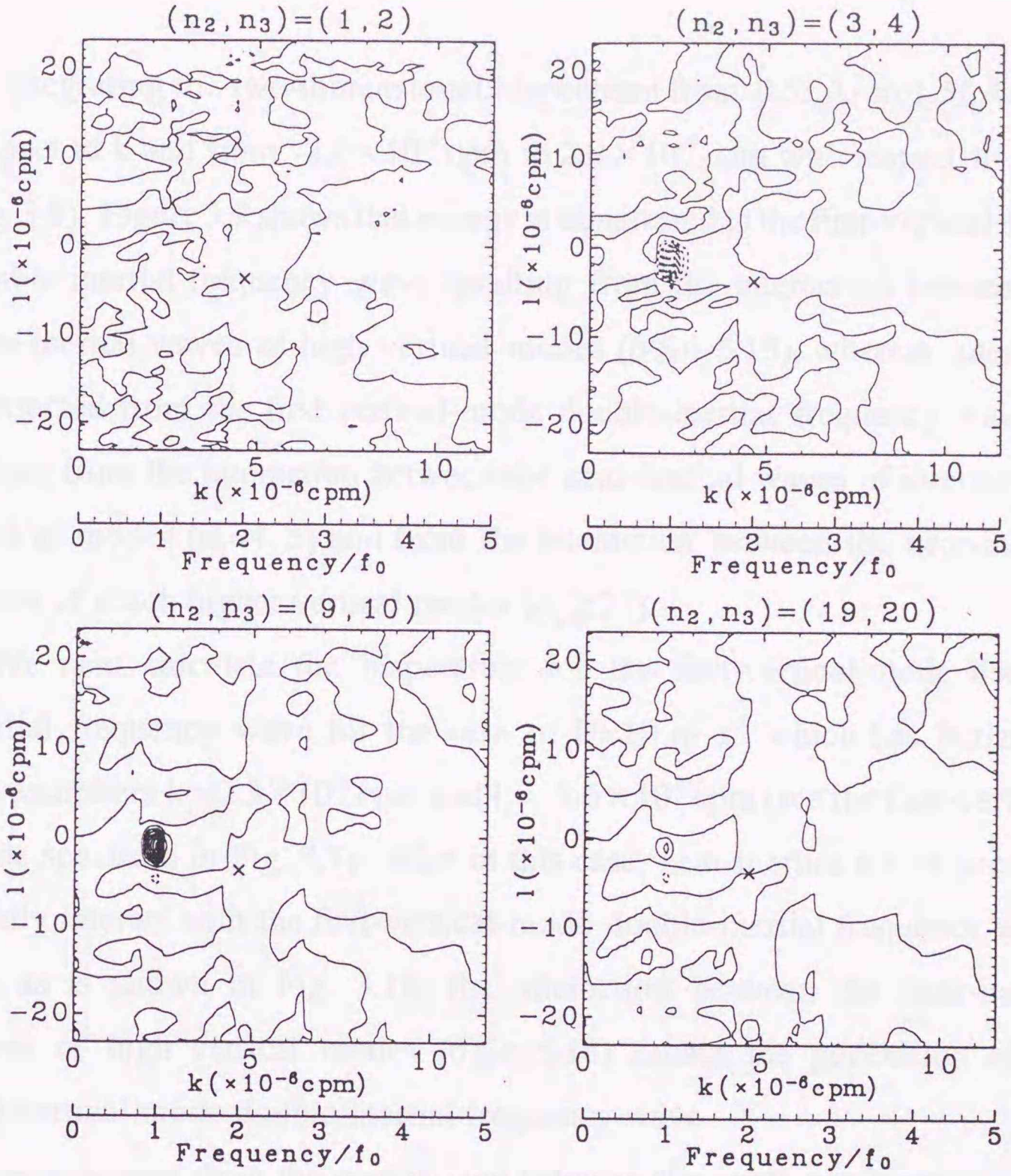

Figure 3.8. Two-dimensional wavenumber bispectrum for the case of U=5 m s^{-1} which indicates the rate of kinetic energy transfer to the first vertical mode double-inertial frequency wave with k =4.6×10^{-6} cpm an l = -4.0×10^{-6}cpm (marked by small cross in each bispectrum; see also the first vertical mode spectrum in Fig. 3.6) caused by the nonlinear interaction between the internal waves of vertical mode n_2 and n_3. For more details, see text. Bispectral values in the areas from which energy is transferred to the first vertical mode double-inertial frequency wave are contoured by solid lines, whereas those in the areas to which energy is transferred from the first vertical mode double-inertial frequency wave are contoured by dashed lines. The contour interval is 3×10^2 J m^{-3} s^{-1} cpm^{-2}.

by integrating the two-dimensional bispectrum from $0.5f_0/U$ to $1.5f_0/U$ with respect to k and from -2.0×10^{-5} cpm to 2.0×10^{-5} cpm with respect to l (see Fig. 3.8). Figure 3.9 shows that energy is transferred to the first-vertical-mode double-inertial frequency wave resulting from the interaction between the near-inertial waves of high vertical modes ($6\leqq n_2\leqq15$), whereas energy is subtracted from the first-vertical-mode double-inertial frequency wave resulting from the interaction between the near-inertial waves of intermediate vertical modes (n_2=4, 5) and from the interaction between the near-inertial waves of much higher vertical modes ($n_2\geqq21$).

We next calculate the bispectrum for the first-vertical-mode double-inertial frequency wave for the case of U=10 m s^{-1} which has horizontal wavenumbers $k_1=2.3\times10^{-6}$ cpm and $l_1=-5.6\times10^{-6}$ cpm (see the first-vertical-mode spectrum in Fig. 3.7). Also in this case, near-inertial waves predominantly interact with the first-vertical-mode double-inertial frequency wave, and as is shown in Fig. 3.10, the interaction between the near-inertial waves of high vertical modes ($6\leqq n_2\leqq18$) causes the generation of the first-vertical-mode double-inertial frequency wave.

As is evident from the comparison between the nonlinear kinetic energy transfer rates shown in Fig. 3.9 and Fig. 3.10, the first-vertical-mode double-inertial frequency wave is generated more efficiently for the case of U= 5 m s^{-1} compared to the case of U=10 m s^{-1}. This is considered to be caused by the different features of the high-vertical-mode near-inertial waves in that, compared to the case of U=10 m s^{-1}, along-track wavenumbers and amplitudes are both larger for U= 5 m s^{-1} (section 3.3), so that nonlinear effects become much stronger.

3.5. Summary and discussion

In the present study, generation processes of large-scale internal waves

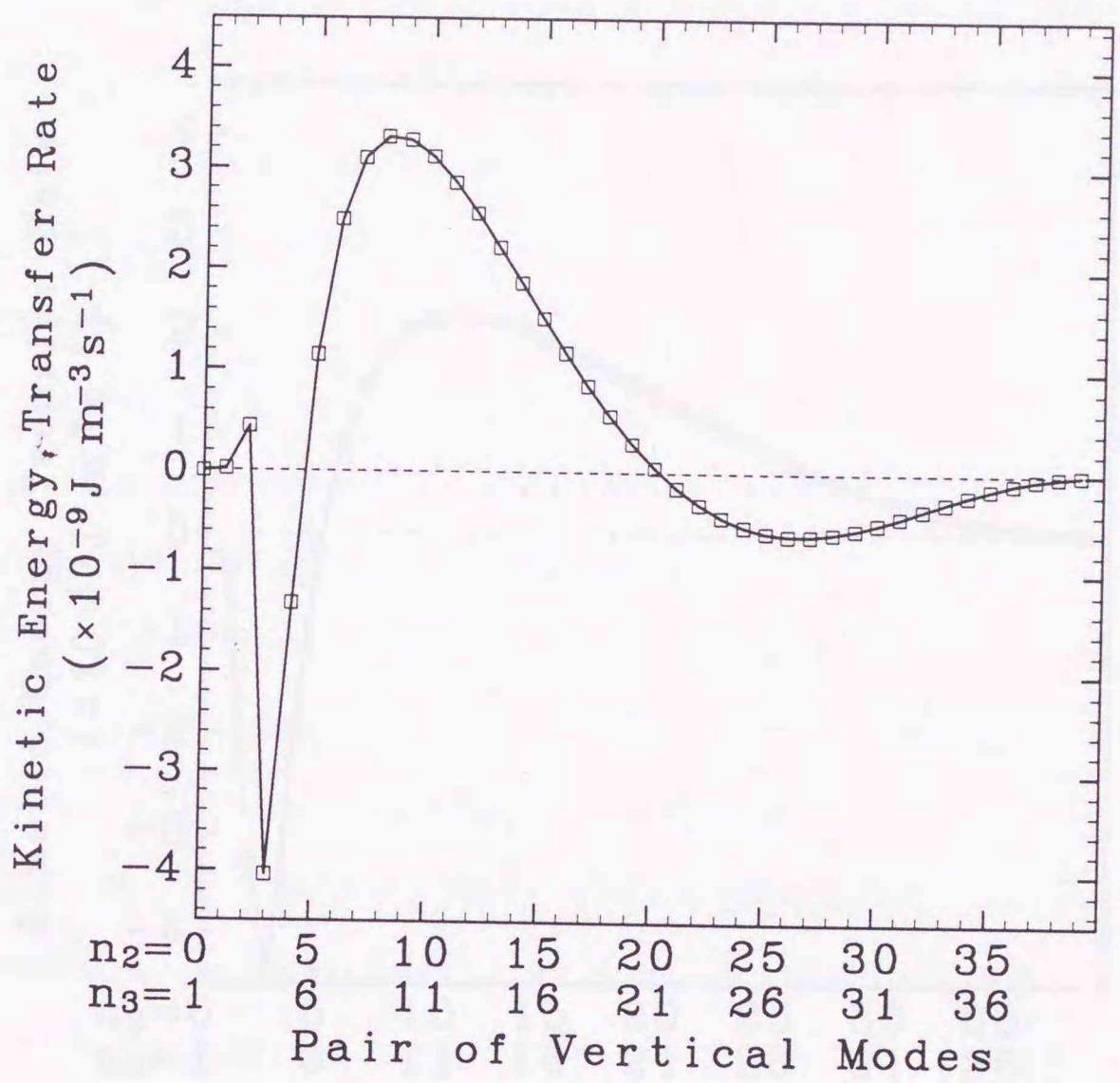

Figure 3.9. The rate of kinetic energy transfer to the first vertical mode double-inertial frequency wave caused by the interaction between the near-inertial waves of vertical mode n_2 and n_3 for the case of U=5 m s^{-1}. This is obtained by integrating two-dimensional horizontal wavenumber bispectrum for each mode pair (see Fig. 3.8) from $0.5f_0/U$ to $1.5f_0/U$ with respect to k and from -2.0×10^{-5} cpm to 2.0×10^{-5} cpm with respect to l.

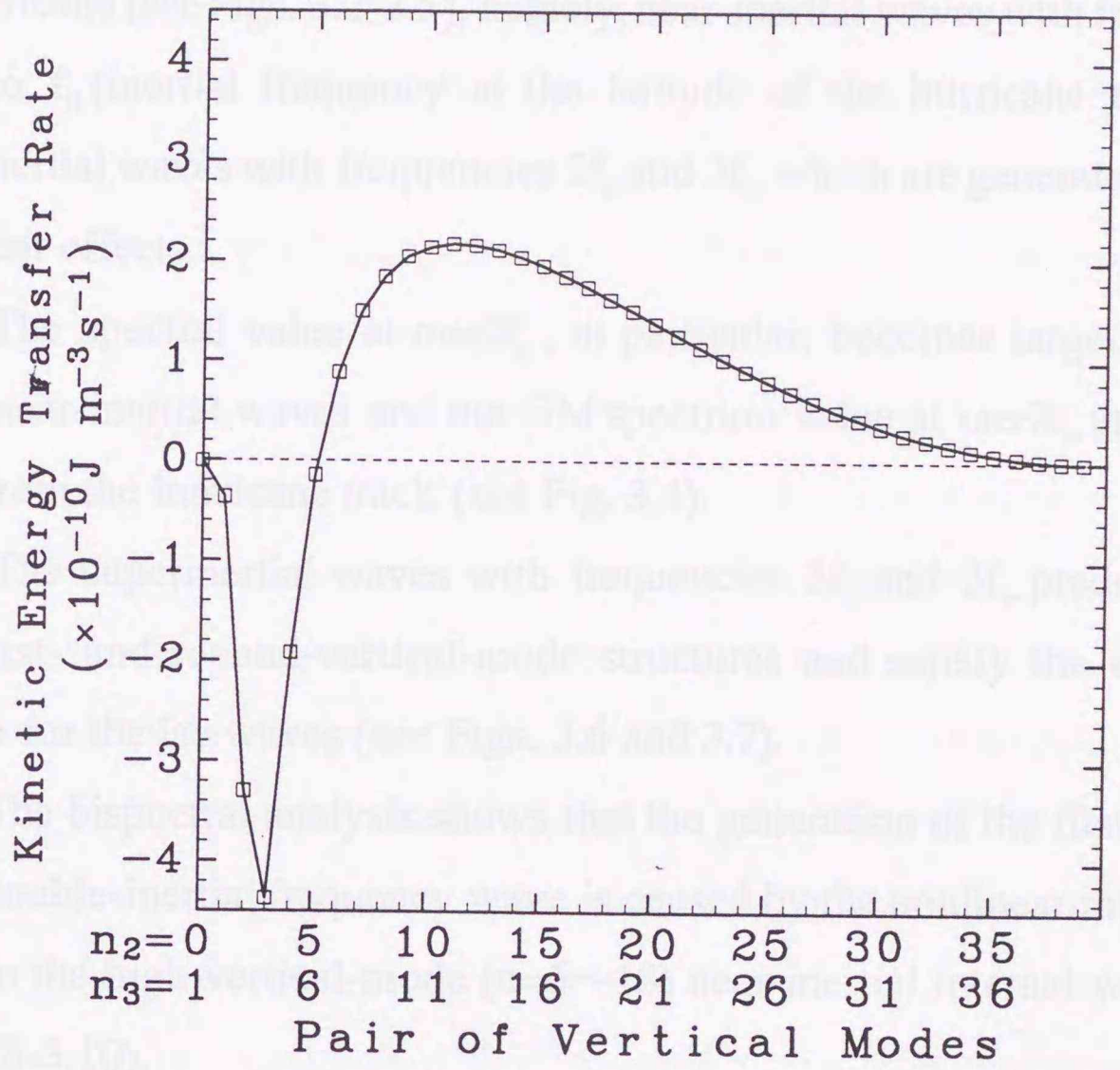

Figure 3.10. As in Fig. 3.9 but for the case of U=10 m s^{-1}.

by a hurricane which propagates eastward with a uniform speed on the β-plane have been investigated by using a three-dimensional multilevel numerical model. The major conclusions can be summarized as follows.

(1) Two distinctive kinds of internal waves are excited in the wake of the hurricane (see Figs. 3.2-3.5), namely, near-inertial waves with frequencies close to f_0 (inertial frequency at the latitude of the hurricane track) and superinertial waves with frequencies $2f_0$ and $3f_0$, which are generated through nonlinear effects.

(2) The spectral value at $\omega \simeq 2f_0$, in particular, becomes larger than that of the near-inertial waves and the GM spectrum value at $\omega \simeq 2f_0$ in the areas away from the hurricane track (see Fig. 3.4).

(3) The superinertial waves with frequencies $2f_0$ and $3f_0$ predominantly have first- and second-vertical-mode structures and satisfy the dispersion relation for the lee waves (see Figs. 3.6 and 3.7).

(4) The bispectral analysis shows that the generation of the first-vertical-mode double-inertial frequency wave is caused by the nonlinear interactions between the high-vertical-mode (n=6～18) near-inertial internal waves (see Figs. 3.8-3.10).

The reason why we focus on these superinertial waves is that the low-vertical-mode waves with frequencies over $2f_0$ are believed to play significant roles in supplying energy to the universal internal wave field in the deep ocean. We discuss this point more in detail below.

D'Asaro [1991] estimated the mean free path of oceanic internal waves based on the magnitude of group velocity and nonlinear interaction rate. The results indicate that low-vertical-mode waves with frequencies over 2f (f is local inertial frequency) can propagate basin-wide distances ($\geqq$1000km) from their sources while supplying energy to the internal wave field where local energy sources are too weak to maintain the universal level of the

internal wave spectrum. In contrast, the propagation of near-inertial waves is considered to be limited because of their small group velocities and the β-effect [*D'Asaro*, 1991] as well as the scattering by ocean bottom topographies [*Müller and Xu*, 1992] and the interactions with mesoscale eddies [*Kunze*, 1985].

Furthermore, the energy thus supplied by these low-vertical-mode waves with $\omega \geqq 2f_0$ is considered to be transferred across the local internal wave spectrum down to small dissipation scales inducing diapycnal mixing in the deep ocean. *McComas and Müller* [1981] discussed the energy balance within the GM spectrum in terms of weak resonant interaction theory. According to their study, dominant energy flux from large generation scales down to small dissipation scales is caused by the mechanism called parametric subharmonic instability (P.S.I) which transfers energy from low-vertical-mode waves with $2f<\omega<4f$ to high-vertical-mode near-inertial ($f<\omega<2f$) waves. Under the P.S.I mechanism, energy supplied by the low-vertical-mode waves with $\omega \geqq 2f_0$ is expected to be transferred efficiently to small mixing scales.

This feature is also demonstrated in direct numerical experiment [*Hibiya et al.*, 1997]. When a spectral bump is given to the low-vertical-wavenumber region within a frequency band $2f<\omega<4f$ in a quasi-equilibrium GM-like spectrum [*Hibiya et al.*, 1996], the excess energy is eventually transferred to the high-vertical-wavenumber near-inertial region. In contrast, when a spectral bump is given to the low-vertical-wavenumber near-inertial region, no significant energy cascade to the high-wavenumber region occurs.

In summary, low-vertical-mode waves with frequencies $2f_0$ and $3f_0$ propagate basinwide distances from their sources while supplying energy to the local internal wave spectrum; energy thus supplied is transferred across the local internal wave spectrum down to small mixing scales under the P.S.I

mechanisms. Accordingly, the global distribution of these superinertial waves is crucial for the adequate parameterization of the diapycnal mixing in the deep ocean.

The double-inertial frequency waves are actually observed in the realistic ocean during the Ocean Storm Experiment (OSE) observational program [see *D'Asaro et al.*, 1995, Fig. 3]. One of the important results from the OSE is that near-inertial energy in the mixed layer decayed much more rapidly than was predicted on the basis of linear theory [*D'Asaro et al.*, 1995], though successful physical explanations for it have not been given yet [*D'Asaro*, 1995]. The present study might provide one possible explanation that the nonlinear energy transfer from the high-vertical-mode near-inertial waves to the low-vertical-mode double-inertial frequency waves might promote the energy dispersion from the mixed layer because the group velocities of the low-vertical-mode double-inertial frequency waves are much larger than those of the high-vertical-mode near-inertial waves. We can actually find out in this study that the kinetic energy decay in the forcing region is more rapid in the nonlinear model compared with the linear model. The difference between the decay rates from the nonlinear and linear models for the case of U=5 m s^{-1} is about 23% and about 14% for the case of U=10 m s^{-1}, though quantitative comparison with the results from the OSE is limited because of the unrealistic density stratification employed in this study. Such a rapid decay of near-inertial energy in the mixed layer has not been reproduced in D'Asaro's two-dimensional numerical model [*D'Asaro*, 1995]. A major reason for this might be in his assumption that the internal wave fields are independent of along-storm track coordinate since the nonlinear resonant triads causing the generation of the low-vertical-mode double-inertial frequency waves cannot be reproduced under this assumption.

References

Bryan, F., Parameter sensitivity of primitive equation ocean general circulation models, *J. Phys. Oceanogr., 17*, 970-985, 1987.

D'Asaro, E. A., The decay of wind-forced mixed layer inertial oscillations due to the β effect, *J. Geophys. Res., 94*, 2045-2056, 1989.

D'Asaro, E. A., A strategy for investigating and modeling internal wave sources and sinks, in *Dynamics of Oceanic Internal Gravity Waves. Proc. Aha Huliko'a Hawaiian Winter Workshop*, pp. 451-466, edited by P. Müller and D. Henderson, Hawaii Institute of Geophysics, 1991.

D'Asaro, E. A., Upper-ocean inertial currents forced by a strong storm. Part II: Modeling, *J. Phys. Oceanogr., 25*, 2937-2952, 1995.

D'Asaro, E. A., C. C. Eriksen, M. D. Levine, P. P. Niiler, C. A. Paulson, and P. Van Meurs, Upper-ocean inertial currents forced by a strong storm. Part I: Data and comparisons with linear theory, *J. Phys. Oceanogr., 25*, 2909-2936, 1995.

Garrett, C. J. R., and W. H. Munk, Space-time scales of internal waves, *Geophys. Fluid Dyn., 2*, 225-264, 1972.

Garrett, C. J. R., and W. H. Munk, Space-time scales of internal waves: A progress report, *J. Geophys. Res., 80*, 291-297, 1975.

Geisler, J. E., Linear theory of the response of a two layer ocean to a moving hurricane, *Geophys. Fluid Dyn., 1*, 249-272, 1970.

Gill, A. E., On the behavior of internal waves in the wake of storms, *J. Phys. Oceanogr., 14*, 1129-1151, 1984.

Greatbatch, R. J., On the response of the ocean to a moving storm: the nonlinear dynamics, *J. Phys. Oceanogr., 13*, 357-367, 1983.

Greatbatch, R. J., On the response of the ocean to a moving storm: Parameters and scales, *J. Phys. Oceanogr., 14*, 59-77, 1984.

Hibiya, T., Y. Niwa, K. Nakajima, and N. Suginohara, Direct numerical simulation of the roll-off range of internal wave shear spectra in the ocean, *J. Geophys. Res., 101*, 14123-14129, 1996.

Hibiya, T., Y. Niwa, and K. Fujiwara, Numerical experiments of nonlinear energy transfer within the oceanic internal wave spectrum, submitted to *J. Geophys. Res.,* 1997.

Kunze, E., Near-inertial wave propagation in geostrophic shear, *J. Phys. Oceanogr., 15*, 544-565, 1985.

Lin, C.-L., J. R. Koseff, and J. H. Ferziger, On triad interactions in a linearly stratified ocean, *J. Phys. Oceanogr., 25*, 153-167, 1995.

McComas, C. H., and P. Müller, The dynamic balance of internal waves, *J. Phys. Oceanogr., 11*, 970-986, 1981.

Müller, P., D. J. Olbers, and J. Willebrand, The IWEX spectrum, *Geophys. Res., 83*, 479-500, 1978.

Müller, P., and N. Xu, Scattering of oceanic internal gravity waves off random bottom topography, *J. Phys. Oceanogr., 22*, 474-488, 1992.

Munk, W. H., Internal waves and small-scale processes, *in Evolution of Physical Oceanography*, edited by B. S. Warren and C. Wunsch, pp. 264-291, MIT Press, Cambridge, Mass., 1981.

Nilsson, J., Energy flux from traveling hurricanes to the oceanic internal wave field, *J. Phys. Oceanogr., 25*, 558-573, 1995.

Price, J. F., Internal wave wake of a moving storm Part I: Scales, energy budget and observation. *J. Phys. Oceanogr., 13*, 949-965, 1983.

Price, J. F., T. B. Sanford, and G. Z. Forristall, Forced stage response to a

moving hurricane, *J. Phys. Oceanogr.*, *24*, 233-260, 1994.

Rubenstein, D., A spectral model of wind-forced internal waves. *J. Phys. Oceanogr.*, *24*, 819-831, 1994.

Sjöberg, B., and A. Stigebrandt, Computations of the geographical distribution of the energy flux to mixing processes via internal tides and associated vertical circulation in the ocean, *Deep Sea Res.*, *39*, 269-291, 1992.

Wunsch, C., and S. Webb, The climatology of deep ocean internal waves, *J. Phys. Oceanogr.*, *9*, 235-243, 1979.

Chapter 4

Numerical Experiments of Nonlinear Energy Transfer Within the Oceanic Internal Wave Spectrum

Abstract

From the fact that the Garrett-Munk (GM) internal wave spectrum is maintained even in regions of weak local energy sources, it is believed that energy is continuously supplied to the local wave spectrum by internal waves propagating from the source regions where they are generated by wind stress fluctuations and tide-topography interactions. In order to examine how the energy thus supplied by propagating waves cascades through the local wave spectrum down to small dissipation scales, we carry out three sets of numerical experiments where the quasi-equilibrium internal wave spectrum obtained by *Hibiya et al.* (1996) is perturbed as an initial condition with forcing applied to different parts of the low-frequency low-wavenumber portion of the spectrum. The evolution of the internal wave spectrum is examined over 8 inertial periods after the forcing is given. First, in Experiment I, the forcing is applied to the low-vertical-wavenumber inertial-frequency (ω=f) portion of the spectrum. In this case, however, no significant increase or decrease of spectral intensity can be seen within the corresponding two-dimensional wavenumber shear spectrum. Next, in Experiment II, the forcing is applied to the spectrum at low vertical wavenumbers and frequency range of $2f<\omega<3f$. In contrast to the result of Experiment I, high-vertical-wavenumber near-inertial spectral values are seen to increase exceeding the GM level as time progresses. Finally, in Experiment III, the forcing is applied to the spectrum at low vertical wavenumbers and frequency range of $1.6f<\omega<2f$. Although the spectral location of the forcing is very close to that assumed in Experiment II, no appreciable energy transfer to high vertical wavenumbers occurs in this case. From the results of these numerical experiments, it is shown that the energy transfers to small dissipation scales are dominated by the resonant interaction mechanism termed parametric

subharmonic instability (P.S.I) which transfers energy from low-vertical-wavenumber waves with frequencies over 2f to high-vertical-wavenumber, near-inertial ($f<\omega<2f$) waves. This supports the model for the dynamic balance of the internal wave spectrum proposed by *Hibiya et al.* (1996) that, with the increase (or decrease) of energy supply to the local internal wave spectrum, higher-vertical-modes near-inertial current shear is enhanced (or diminished) leading to an increase (or decrease) in the rate of energy dissipation at critical layers.

4.1. Introduction

The pattern and magnitude of the numerically reproduced general ocean circulation strongly depend on the value of eddy viscosity and diffusivity coefficients, which indicates that the evaluation of the intensity of turbulent vertical mixing at depth is crucial to accurate modeling of the large-scale general circulation [*Bryan*, 1987]. Mixing in the stratified ocean interior is generally considered to be associated with sporadic overturning and breaking of internal waves.

The energy available for mixing processes is originally supplied at large scales (a few tens of kilometers) and then transferred across the internal wave spectrum down to small dissipation scales (a few meters) by nonlinear interactions among internal waves. Intermediate scale internal waves, therefore, provide an important link in the overall energy cascade from large generation scale down to small dissipation scale, which are empirically described as the universal Garrett and Munk model spectrum [*Garrett and Munk*, 1972, 1975; *Munk*, 1981] (hereafter referred to as the GM model). Recently *Hibiya et al.* (1996) succeeded in reproducing the quasi-equilibrium internal wave field having the actually observed GM-like spectrum with the roll-off at about 0.06 cycles per meter (cpm) by calculating the nonlinear interactions among randomly phased linear internal waves over 7 inertial periods, each amplitude of which is determined from the GM model.

The above numerical experiment is, however, unforced so that thus reproduced internal wave spectrum must erode ultimately. From the fact that the universal GM spectrum is actually maintained even in regions of weak local energy sources, it is believed that energy is continuously supplied to the local wave spectrum by internal waves propagating from the source regions where they are generated by wind stress fluctuations [*Kundu*, 1993; *Rubenstein*, 1994; *Nilsson*, 1995] and tide-topography interactions [*Sjöberg*

and Stigebrandt, 1992]. Although it remains unknown which of the possible sources of internal wave energy is most important, *Niwa and Hibiya* (1997) have examined the stratified ocean responses to a traveling storm on the basis of three-dimensional numerical experiments. One of the important findings is that, in addition to low-vertical-mode near-inertial internal waves, low-vertical-mode internal waves with frequencies just over 2f (f is the inertial frequency) are left behind the traveling storm, which are generated through the nonlinear interactions between high-vertical-mode near-inertial waves. Estimates of the mean free path from the horizontal group velocity and nonlinear interaction time indicate that thus generated low-vertical-mode internal waves can propagate significant distances of the order of 1000 km from their source regions within their relaxation time while feeding energy to the local internal wave fields [*Olbers*, 1983; *D'Asaro*, 1991]. Although a number of theoretical studies have been made on energy transfers by nonlinear wave-wave interactions within the GM spectrum, they are restricted to weak or scale-separated interactions (resonant or eikonal wave-wave interactions) [*Olbers*, 1976; *McComas*, 1977; *McComas and Bretherton*, 1977; *Pomphrey et al.*, 1980; *McComas and Müller*, 1981; *Flatté et al.*, 1985; *Heyney et al.*, 1986]. While forcing at large scales must be balanced by dissipation at small scales, it remains unknown how the energy thus supplied by low-vertical-mode low-frequency waves cascades through the local internal wave spectrum down to small dissipation scales.

In the present study, we carry out three sets of numerical experiments where the quasi-equilibrium internal wave spectrum obtained by *Hibiya et al.* (1996) is perturbed as an initial condition with energy applied to different parts of the low-frequency low-vertical-wavenumber portion of the background spectrum. It should be noted that the physics of weak wave-wave and strong wave-wave interactions and of wavenumber local and nonlocal

interactions are all retained in this numerical experiment. The evolution of the internal wave spectrum is monitored to clarify how the energy thus supplied at large scales is transferred across the local wave spectrum down to small dissipation scales.

4.2. Numerical model

We assume that the internal wave field is restricted to a vertical two-dimensional plane by requiring the variability to be independent of one horizontal coordinate. The two-dimensional Navier-Stokes equations under the Boussinesq approximation are integrated with a finite difference scheme by applying the centered difference and leapfrog scheme. In particular, the Arakawa Jacobian is used for an expression of the advective term [Arakawa, 1966]. The finite differenced equations are solved on a 1024×1024 grid with resolutions of 10 m and 1.25 m in the horizontal and vertical directions, respectively, sufficient to resolve the disparate-scale wave interactions.

The subgrid diffusive-dissipative processes are parameterized with a Laplacian operator where eddy viscosity and diffusivity coefficients are assumed to have the same value of 1 $cm^2 s^{-1}$ in the horizontal and 0.1 $cm^2 s^{-1}$ in the vertical, which are the smallest possible values needed to maintain the stability of calculations. Cyclic boundary conditions are employed at the lateral sides, whereas flat perfectly reflecting bottom and surface are employed. We assume the inertial frequency $f=7.27 \times 10^{-5}\ s^{-1}$ (inertial period Ti=24 hours) and the constant background buoyancy frequency $N=5.2 \times 10^{-3}\ s^{-1}$ (3 cycles per hour (cph)) (linear stratification).

A background quasi-equilibrium internal wave field having the actually observed shear spectrum with the roll-off at about 0.06 cpm (see Fig. 4.1) is reproduced by calculating the nonlinear interactions among randomly

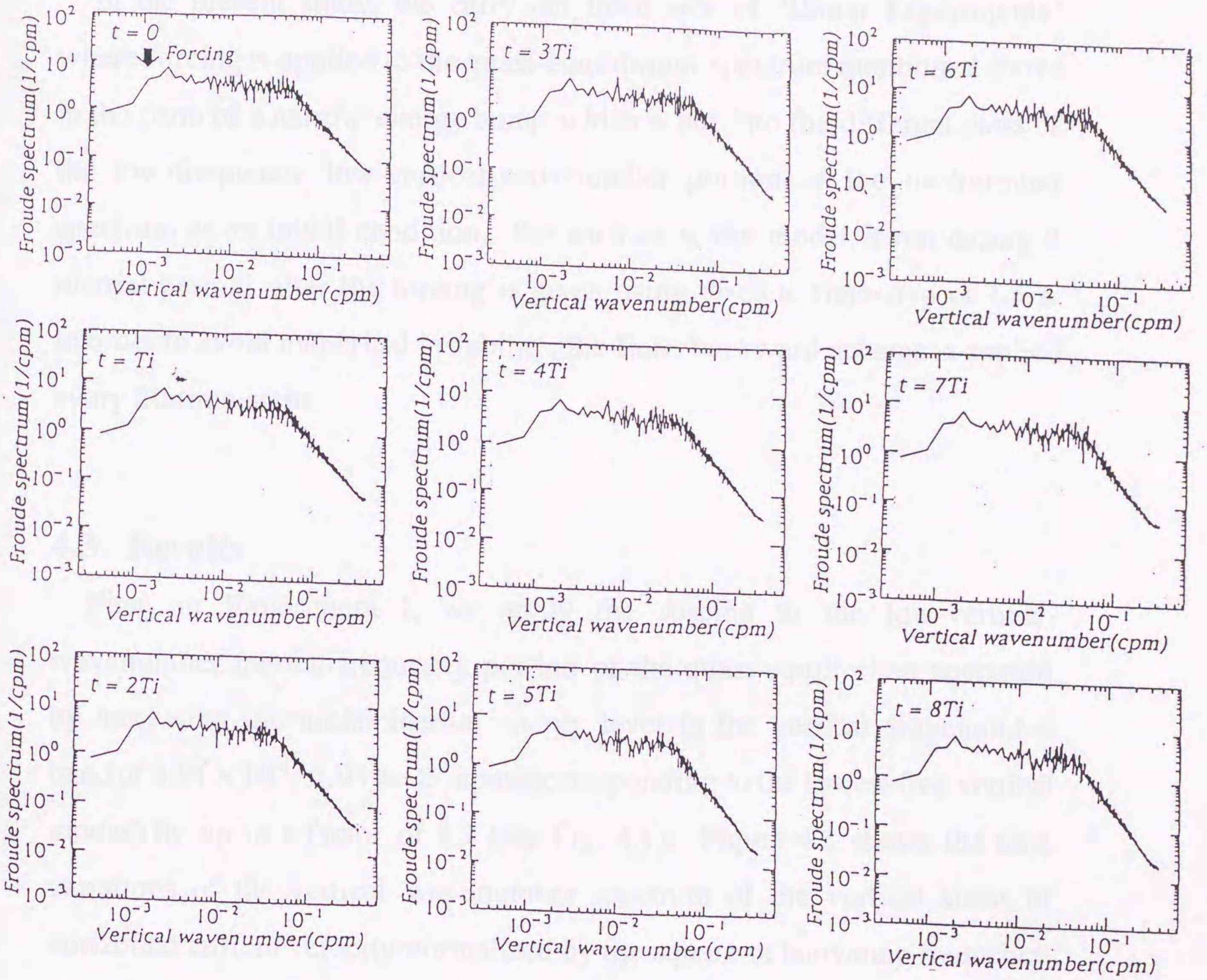

Figure 4.1. Time variations of the vertical wavenumber Froude spectrum during 8 inertial periods after the energy bump is put into the low-vertical-wavenumber inertial-frequency portion of the quasi-equilibrium spectrum obtained by Hibiya et al. (1996). The arrow in the figure at t=0 indicates the inertial energy bump which is put into the vertical wavenumber band of 3.91×10^{-4} - 1.95×10^{-3} cpm.

phased linear internal waves over 7 inertial periods, each amplitude of which is determined from the GM model [*Hibiya et al.*, 1996].

In the present study, we carry out three sets of "Bump Experiments" where forcing is applied to the quasi-equilibrium spectrum mentioned above in the form of a narrow energy bump which is put into the different parts of the low-frequency low-vertical-wavenumber portion of the background spectrum as an initial condition. For each case, the model is run during 8 inertial periods after the forcing is given using discrete time-step of 1.5 s. In order to avoid numerical instability, the Euler backward scheme is applied every 20 time-steps.

4.3. Results

First, in Experiment I, we apply the forcing to the low-vertical-wavenumber inertial-frequency portion of the quasi-equilibrium spectrum by increasing the initial inertial energy level in the vertical wavenumber band of 3.91×10^{-4} - 1.95×10^{-3} cpm (corresponding to the lowest five vertical modes) by up to a factor of 1.2 (see Fig. 4.1). Figure 4.1 shows the time variations of the vertical wavenumber spectrum of the vertical shear of horizontal current velocity normalized by the square of buoyancy frequency (Froude spectrum) over 8 inertial periods after the energy bump is given. It should be noted that the spectrum is calculated from data obtained from the top down to the bottom which are averaged horizontally. The spectrum remains quite close to the initial spectrum over this period; the energy bump stays at the wavenumbers where it is given. This is more directly confirmed in the corresponding two-dimensional wavenumber Froude spectrum which is presented in variance-preserving form with respect to horizontal wavenumber (Fig. 4.2). We can find no significant increase or

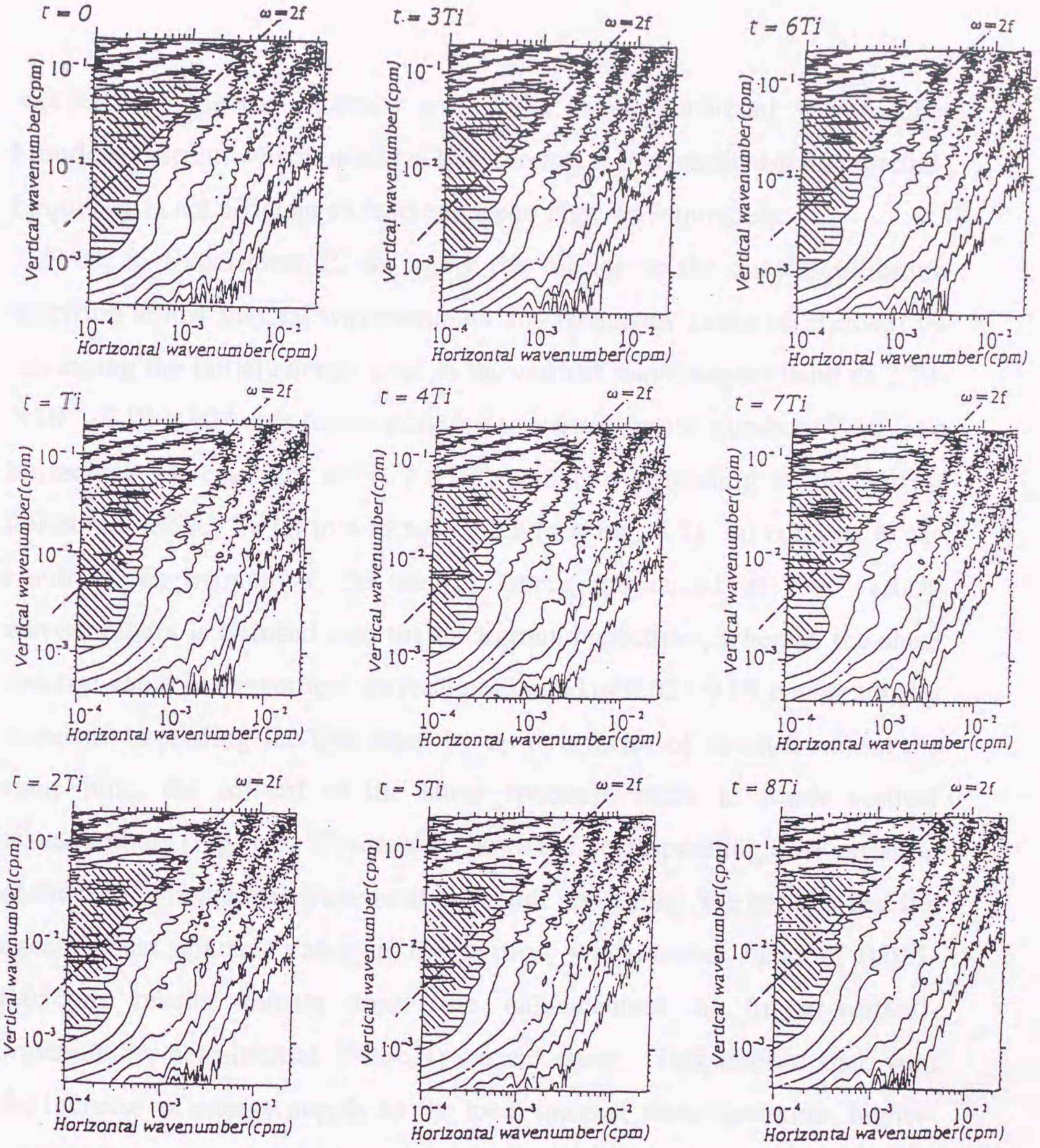

Figure 4.2. Time variations of the two-dimensional wavenumber Froude spectrum for the case corresponding to Figure 4.1 which is presented in variance-preserving form with respect to horizontal wavenumber. Variations of spectral density level are represented by different intensities of shading where the darker shade indicates greater spectral density with the range of each shading being 0.25 in the logarithm. In the unshaded area, spectral density values are contoured with intervals of 0.5 in the logarithm.

decrease of spectral intensity within the two-dimensional wavenumber Froude spectrum, which indicates that forcing at low-vertical-mode inertial-frequency is not efficient to feed energy to high wavenumbers.

Next, in Experiment II, we apply the forcing to the quasi-equilibrium spectrum at low vertical wavenumbers and frequency range of $2f<\omega<3f$ by increasing the initial energy level in the vertical wavenumber band of $2.73\text{-}\times10^{-3}$ - 3.91×10^{-3} cpm (corresponding to vertical mode numbers 7-10) at a horizontal wavenumber of 9.77×10^{-5} cpm (corresponding to the lowest horizontal mode) by up to a factor of 2.1 (see Fig. 4.3). In contrast to the result of Experiment I, the energy bump introduced at low vertical wavenumbers is diffused into the background spectrum, whereas the shear spectral value in the vertical wavenumber band of 0.025-0.05 cpm gradually increases exceeding the GM level by up to a factor of about 2 and, at the same time, the roll-off of the shear spectrum shifts to lower vertical wavenumbers (Fig. 4.3). Figure 4.4 shows the corresponding time variation of the two-dimensional wavenumber Froude spectrum. We can see that the excess shear spectral value in the vertical wavenumber band of 0.025-0.05cpm results mostly from the enhancement of higher-vertical-wavenumber near-inertial ($f<\omega<2f$) current shear. This implies that, with the increase of energy supply to the local internal wave spectrum, higher-vertical-modes near-inertial current shear is enhanced so that the roll-off shifts to lower vertical wavenumbers leading to an increase in the rate of energy dissipation.

Finally, in Experiment III, we apply the forcing to the quasi-equilibrium spectrum at low vertical wavenumbers and frequency range of $1.6f<\omega<2f$ by increasing the initial energy level in the vertical wavenumber band of 4.3×10^{-3} - 5.47×10^{-3} cpm (corresponding to vertical mode numbers 11-14) at a horizontal wavenumber of 9.77×10^{-5} cpm (corresponding to the lowest

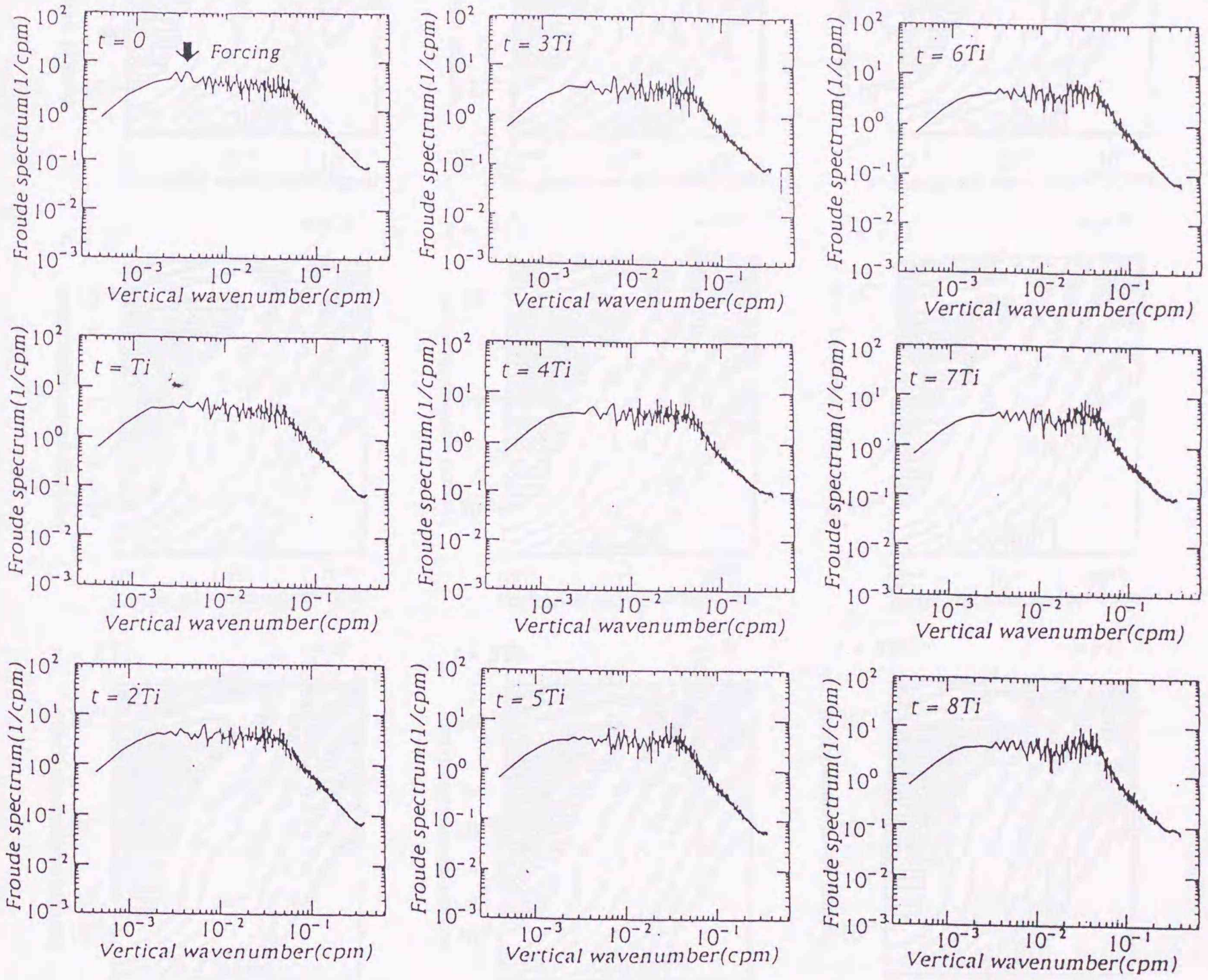

Figure 4.3. As in Figure 4.1 but for the case where the forcing is applied to the quasi-equilibrium spectrum at low vertical wavenumbers and frequency range of $2f<\omega<3f$. The arrow in the figure at t=0 indicates the energy bump which is put into the vertical wavenumber band of 2.73×10^{-3} - 3.91×10^{-3} cpm at a horizontal wavenumber of 9.77×10^{-5} cpm.

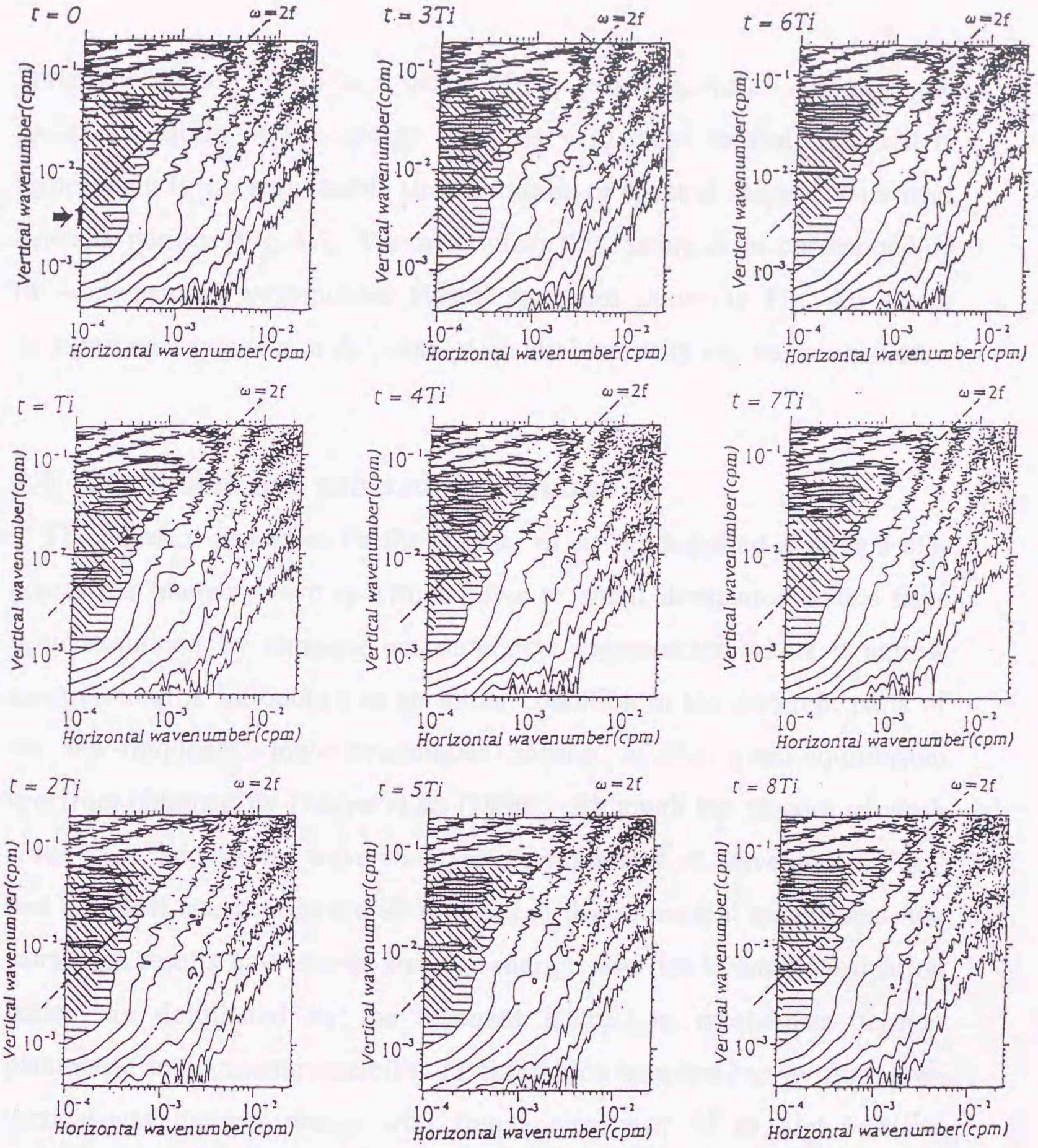

Figure 4.4. As in Figure 4.2 but for the case corresponding to Figure 4.3. The arrow in the figure at t=0 indicates the vertical wavenumber band of 2.73×10^{-3} - 3.91×10^{-3} cpm at a horizontal wavenumber of 9.77×10^{-5} cpm where the energy bump is introduced as an initial condition.

horizontal mode) by up to a factor of 3.3 (see Fig. 4.5). Although the spectral location of the energy bump is very close to that assumed in Experiment II, no appreciable time-variation of spectral shape occurs over 8 inertial periods (Fig. 4.5). We can confirm this feature in the corresponding two-dimensional wavenumber Froude spectrum shown in Fig. 4.6 where no significant increase or decrease of spectral intensity can be recognized.

4.4. Discussion and concluding remarks

The physical processes for the transfer of energy supplied at large scales across the internal wave spectrum down to small dissipation scales have been examined by carrying out numerical experiments where a narrow energy bump is introduced as an initial condition in the different parts of the low-frequency low-wavenumber portion of the quasi-equilibrium spectrum obtained by *Hibiya et al.* (1996). Although the physics of weak wave-wave and strong wave-wave interactions and of wavenumber local and nonlocal interactions are all retained in this numerical experiment, the calculated results have shown that the energy cascades to small dissipation scales are dominated by the resonant interaction mechanism termed parametric subharmonic instability (P.S.I) which transfers energy from low-vertical-wavenumber waves with frequencies over 2f to high-vertical-wavenumber near-inertial waves [*McComas*, 1977; *McComas and Bretherton*, 1977; *McComas and Müller*, 1981; *Pomphrey et al.*, 1980]. This supports the model for the dynamic balance of the internal wave spectrum proposed by *Hibiya et al.* (1996) that, with the increase (or decrease) of energy supply to the local internal wave spectrum, higher-vertical-modes near-inertial current shear is enhanced (or diminished) leading to an increase

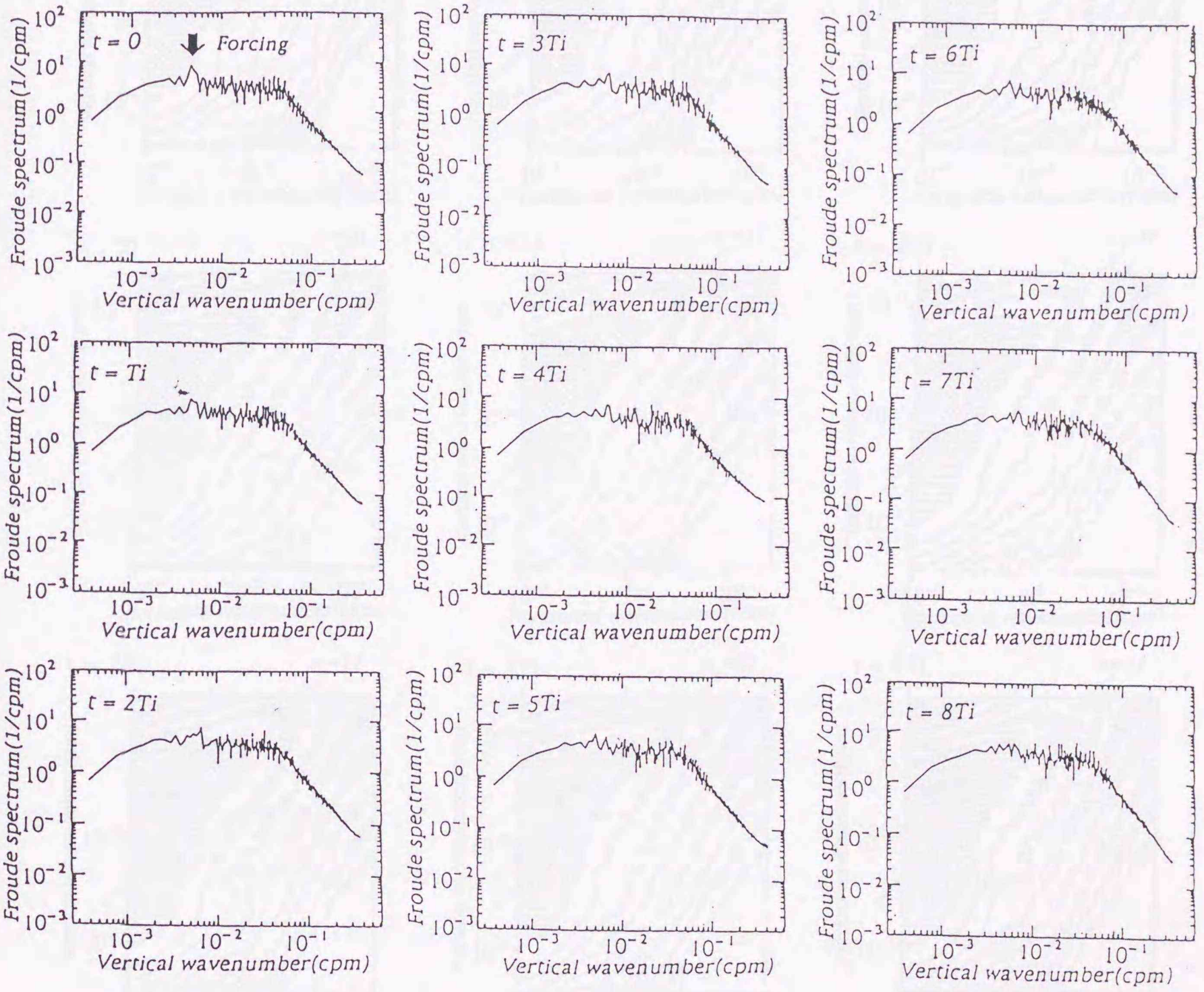

Figure 4.5. As in Figure 4.1 but for the case where the forcing is applied to the quasi-equilibrium spectrum at low vertical wavenumbers and frequency range of $1.6f<\omega<2f$. The arrow in the figure at t=0 indicates the energy bump which is put into the vertical wavenumber band of 4.3×10^{-3} - 5.47×10^{-3} cpm at a horizontal wavenumber of 9.77×10^{-5} cpm.

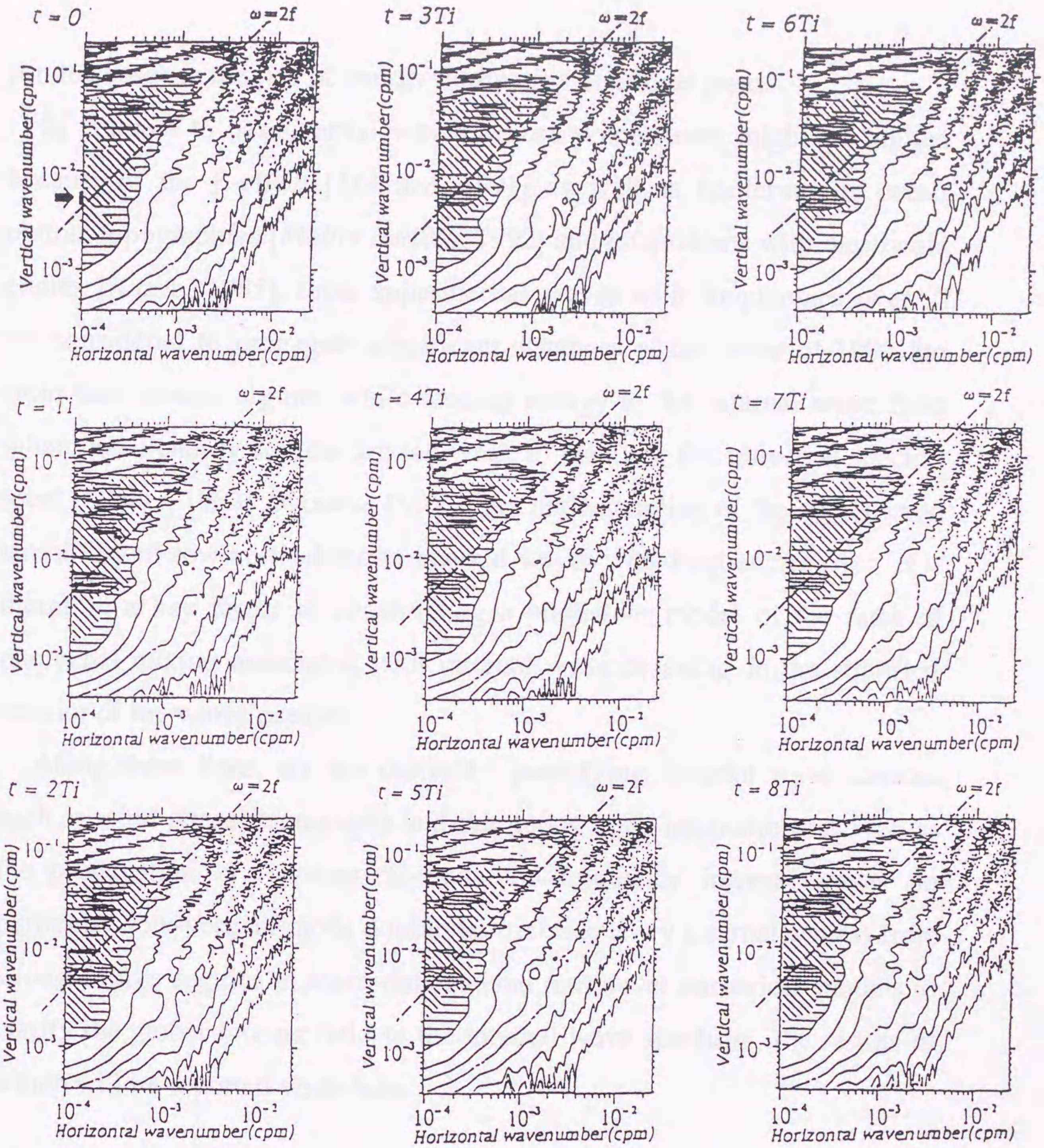

Figure 4.6. As in Figure 4.2 but for the case corresponding to Figure 4.5. The arrow in the figure at t=0 indicates the vertical wavenumber band of 4.3×10^{-3} - 5.47×10^{-3} cpm at a horizontal wavenumber of 9.77×10^{-5} cpm where the energy bump is introduced as an initial condition.

(or decrease) in the rate of energy dissipation at critical layers.

In contrast to near-inertial waves whose propagation might be limited because of the β-effect [*D'Asaro*, 1991] as well as scattering by ocean bottom topographies [*Müller and Xu*, 1992] and interactions with mesoscale eddies [*Kunze*, 1985], these superinertial waves with frequencies over 2f are considered to propagate significant distances of the order of 1000 km from their source regions while feeding energy to the internal wave field where local energy sources are too weak to maintain the universal spectral level [*Olbers*, 1983; *D'Asaro*, 1991]. An understanding of the sources and variability of low-vertical-mode internal waves with frequencies over 2f is therefore a key factor in constructing a predictive model of the rates of diapycnal mixing associated with internal wave breaking in the stratified interior of the world oceans.

Along these lines, we are currently quantifying internal wave sources such as wind stress fluctuations and tide-topography interactions as well as the propagation of low-vertical-mode low-frequency internal waves (in particular, low-vertical-mode double-inertial frequency internal waves) from strong source regions in three-dimensional multilevel numerical models to clarify the global forcing field to the internal wave spectrum, the results of which will be reported elsewhere.

References

Arakawa, A., Computational design for long-term numerical integration of the equations of fluid motion: two-dimensional incompressible flow, Part 1, *J. Comput. Phys., 1*, 119-143, 1966.

Bryan, F., Parameter sensitivity of primitive equation ocean general circulation models, *J. Phys. Oceanogr., 17*, 970-985, 1987.

D'Asaro, E. A., A strategy for investigating and modeling internal wave sources and sinks, in *Dynamics of Oceanic Internal Gravity Waves. Proc. Aha Huliko'a Hawaiian Winter Workshop*, pp. 451-466, edited by P. Müller and D. Henderson, Hawaii Institute of Geophysics, 1991.

Flatté, S. M., F. S. Heyney, and J. A. Wright, Eikonal calculations of short wavelength internal-wave spectra, *J. Geophys. Res., 90*, 7265-7272, 1985.

Garrett, C. J. R., and W. H. Munk, Space-time scales of internal waves, *Geophys. Fluid Dyn., 2*, 225-264, 1972.

Garrett, C. J. R., and W. H. Munk, Space-time scales of internal waves: A progress report, *J. Geophys. Res., 80*, 291-297, 1975.

Heyney, F. S., J. Wright, and S. M. Flatté, Energy and action flow through the internal wave field: An eikonal approach, *J. Geophys. Res., 91*, 8487-8495, 1986.

Hibiya, T., Y. Niwa, K. Nakajima, and N. Suginohara, Direct numerical simulation of the roll-off range of internal wave shear spectra in the ocean, *J. Geophys. Res., 101*, 14123-14129, 1996.

Kundu, P. K., On internal waves generated by traveling wind, *J. Fluid Mech., 254*, 529-560, 1993.

Kunze, E., Near-inertial wave propagation in geostrophic shear, *J. Phys.*

Oceanogr., 15, 544-565, 1985.

McComas, C. H., Equilibrium mechanisms within the internal wave field, *J. Phys. Oceanogr., 7*, 836- 845, 1977.

McComas, C. H., and F. P. Bretherton, Resonant interaction of oceanic internal waves, *J. Geophys. Res., 83*, 1397-1412, 1977.

McComas, C. H., and P. Müller, The dynamic balance of internal waves, *J. Phys. Oceanogr., 11*, 970-986, 1981.

Müller, P., and N. Xu, Scattering of oceanic internal gravity waves off random bottom topography, *J. Phys. Oceanogr., 22*, 474-488, 1992.

Munk, W. H., Internal waves and small-scale processes, *in Evolution of Physical Oceanography*, edited by B. S. Warren and C. Wunsch, pp. 264-291, MIT Press, Cambridge, Mass., 1981.

Nilsson, J., Energy flux from traveling hurricanes to the oceanic internal wave field, *J. Phys. Oceanogr., 25*, 558-573, 1995.

Niwa, Y., and T. Hibiya, Nonlinear Processes of energy transfer from traveling hurricanes to the deep ocean internal wave field, *J. Geophys. Res., 102,* 12469-12477, 1997.

Olbers, D. J., Nonlinear energy transfer and the energy balance of the internal wave field in the deep ocean, *J. Fluid Mech., 74*, 375-399, 1976.

Olbers, D. J., Models of the oceanic internal wave field, *Rev. Geophys., 21*, 1567-1606, 1983.

Pomphrey, N., J. D. Meiss, and K. M. Watson, Description of nonlinear internal wave interactions using Langevin method, *J. Geophys. Res., 85*, 1085-1094, 1980.

Rubenstein, D., A spectral model of wind-forced internal waves. *J. Phys.*

Oceanogr., *24*, 819-831, 1994.

Sjöberg, B., and A. Stigebrandt, Computations of the geographical distribution of the energy flux to mixing processes via internal tides and associated vertical circulation in the ocean, *Deep Sea Res.*, *39*, 269-291, 1992.

Chapter 5

Response of the Deep Ocean Internal Wave Field to Traveling Midlatitude Storms as Observed in Long Term Current Measurements

Abstract

It has been demonstrated in a recent numerical experiment that double-inertial frequency waves play a crucial role in diapycnal mixing processes in the deep ocean, with the energy effectively transferred across the internal wave spectrum down to small dissipation scales by nonlinear wave-wave interactions (*Hibiya et al.*, 1997). To examine whether or not such double-inertial frequency waves are actually generated in the real ocean, we analyze current meter data from long term moorings in the Northwest Pacific Basin together with global sea surface wind data. By incorporating the wind data into a simple damped slab model, it is found that predominant inertial currents are excited in the mixed layer by traveling midlatitude storms in the Northwest Pacific Basin during fall and winter. Composite frequency spectra for the time period during which the predominant inertial currents are excited exhibit a significant increase in the double-inertial frequency band as well as in the near-inertial frequency band. This clearly indicates that, in addition to near-inertial frequency waves, double-inertial frequency waves are excited by strong atmospheric disturbances through nonlinear effects as demonstrated in the numerical experiment by *Niwa and Hibiya* (1997). Double-inertial frequency waves thus excited are found to propagate over horizontal distances of the order of 1000 km from their source region, while feeding their energy to the local internal wave field, consistent with the theoretical prediction based on the magnitudes of group velocity and nonlinear interaction time (*D'Asaro*, 1991).

5.1. Introduction

It is well known that wind stress fluctuation is one of the major sources for internal waves in the ocean. In particular, traveling atmospheric disturbances such as hurricanes or midlatitude storms can generate energetic internal waves because of the large amplitude wind stress which changes its direction significantly over timescales less than the local inertial period.

Primary oceanic responses to atmospheric disturbances include generation of near-inertial waves in the mixed layer which has been studied by many researchers on the basis of the linear theory. Representative work is the one by *Pollard and Millard* [1970] who proposed a simple damped slab model which could reproduce many observed features of generation of near-inertial waves in the mixed layer. In general, however, the amplitude of the near-inertial waves excited by traveling hurricanes or storms becomes so large that nonlinear effects cannot be neglected. Actually, the present authors carried out numerical experiment using three-dimensional multilevel numerical model [*Niwa and Hibiya*, 1997] which demonstrated that low-vertical-mode superinertial waves with frequencies $2f_0$ and $3f_0$ (f_0 is the inertial frequency at the latitude of the hurricane track) were excited by a traveling hurricane through nonlinear interactions between high-vertical-mode near-inertial waves which were originally excited in the mixed layer. In areas away from the hurricane track, in particular, the amplitude of the double-inertial frequency waves becomes comparable to that of the near-inertial waves.

The distinguished properties of the low-vertical-mode superinertial waves with frequencies over 2f are that they are believed to propagate significant horizontal distances from their source region while feeding their energy to the local internal wave field [*D'Asaro*, 1991]; the energy thus supplied is considered to be transferred effectively across the local internal wave spec-

trum down to small dissipation scales through resonant interaction mechanism called parametric subharmonic instability (P.S.I) [*McComas and Müller*, 1981; *Hibiya et al.*, 1996, 1997]. The low-vertical-mode superinertial waves are therefore considered to play significant roles in diapycnal mixing in the deep ocean whose parameterization is essential for accurate modeling of the oceanic general circulation [*Bryan*, 1987].

The above mentioned numerical experiment, however, assumes idealized situations such as a uniform stratification, a constant translation speed of the hurricane, no background eddy field, so that the applicability of the calculated results to the real ocean remains unknown. Actually, previous observations of the double-inertial frequency waves generated by strong atmospheric disturbances have been carried out mostly in the upper ocean [*D'Asaro et al.*, 1995; *Krauss*, 1981], and there is no observational evidence for the existence of the double-inertial frequency waves in the deep ocean.

In the present study, we analyze current meter data from long term moorings in the deep ocean and atmospheric wind data to examine whether significant double-inertial frequency waves are actually generated in the real ocean by strong atmospheric disturbances. We first predict near-inertial wave field in the mixed layer by incorporating wind data into a simple damped slab model. Next, we examine the relation between estimated near-inertial wave field in the mixed layer and deep ocean internal wave field deduced from current meter data.

5.2. Data sources and analysis

Oceanic current data are obtained from four moorings located at 2° intervals between 27°N and 33°N along 165°E in the Northwest Pacific Basin (Fig. 5.1) deployed from September 1991 to May 1993 by the Ocean

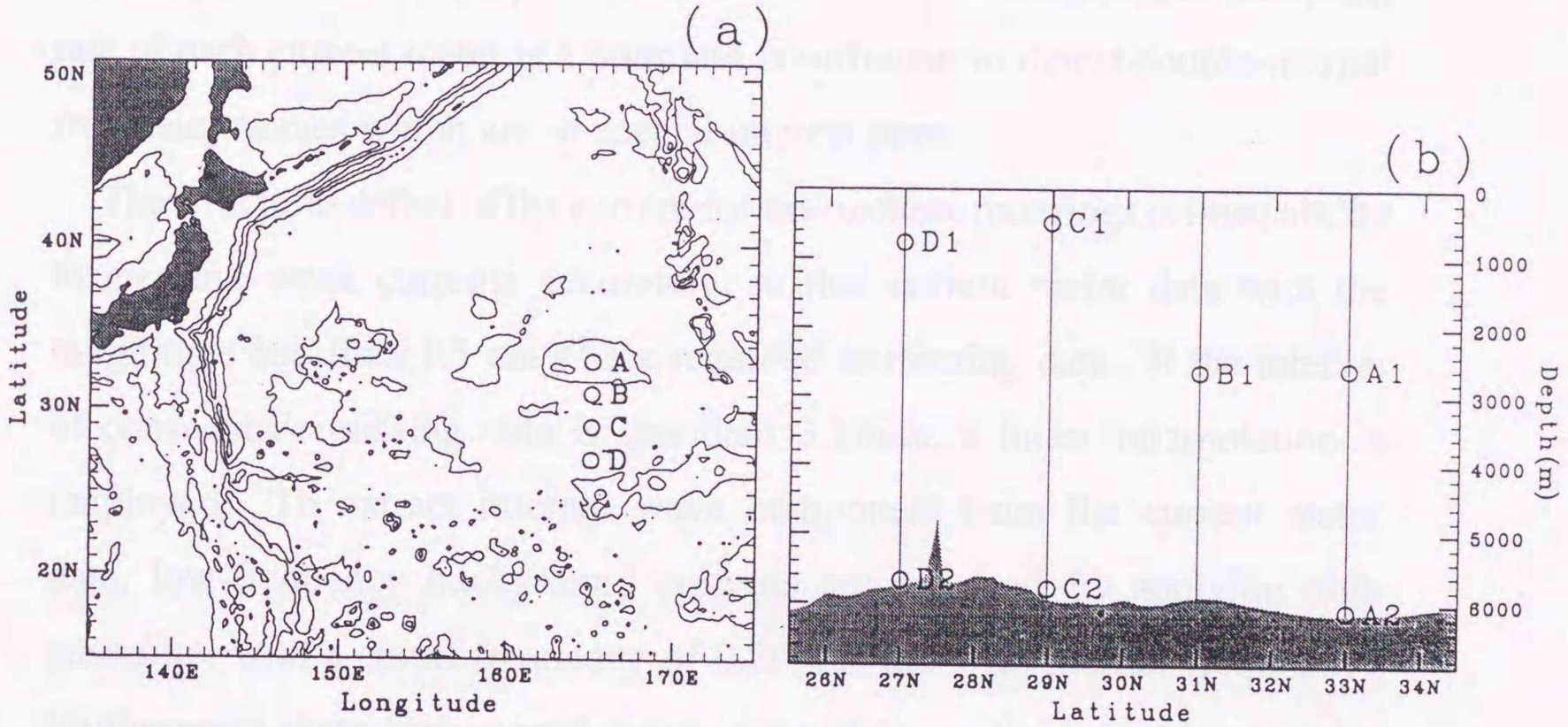

Figure 5.1. Bathymetry of the Northwest Pacific Basin (contour interval is 2000km) and the geographical locations of four mooring sites (a). Depths of the current meters are shown in the cross section along 165°E (b).

Research Institute, the University of Tokyo. The comparison between internal wave field and atmospheric forcing is limited from September 1991 to October 1992 because the current meter data obtained after this period are not of high quality. Figure 5.1 shows the geographical location and depth of each current meter as well as bathymetric configuration. The depths of the current meters range from 480 m to 6040 m, where A2, C2, D2 are, in particular, deployed within 15 m above the ocean bottom. Sampling rate of each current meter is 1 hour and is sufficient to detect double-inertial frequency waves which are of special interest here.

The structural defect of the current meters on these moorings is incapability to measure weak currents accurately, so that current meter data with the magnitude less than 1.5 cm s^{-1} are regarded as missing data. If the interval of consecutive missing data is less than 3 hours, a linear interpolation is employed. To extract internal wave component from the current meter data, low-frequency background currents are removed by applying high pass filter with a cutoff frequency of 0.2f (f is the local inertial frequency). Furthermore, these high passed current meter data are divided into successive data pieces which have length of 15 days and are overlapped by 5 days. For each data piece of good quality in which missing data are no more than 20%, we calculate frequency spectrum of horizontal kinetic energy using Blackman-Tukey method with maximum correlation lag of 5 days and examine the time variation of the internal wave field. For the comparison among the data from varied stratification, each frequency spectrum is divided by the annual mean buoyancy frequency at the location of each current meter calculated from the dataset of National Oceanographic Data Center's World Ocean Atlas [*Levitus and Boyer,* 1994; *Levitus et al.,* 1994].

Sea surface wind data are obtained from the Global Objectively Analyzed Data provided by the Japan Meteorological Agency. These data include

wind vectors at 10 m height above sea surface with longitudinal and latitudinal grid spacings of $1.875° \times 1.875°$ at time intervals of 6 hours.

The surface wind stress is calculated from the 10 m height wind vector $\boldsymbol{U}_{10}$ using the usual bulk transfer formula,

$$\boldsymbol{\tau} = \rho_a C_d U_{10} \boldsymbol{U}_{10} \tag{5.1}$$

where $\boldsymbol{\tau}$ is wind stress vector, ρ_a is air density and U_{10} is 10 m height wind speed. Following *Large and Pond* [1981], the drag coefficient C_d is determined such that;

$$\begin{aligned} C_d &= 1.14 \times 10^{-3} && \text{for } U_{10} < 10 \text{ms}^{-1} \\ &= (0.49 + 0.065 U_{10}) \times 10^{-3} && \text{for } U_{10} \geq 10 \text{ms}^{-1} \end{aligned} \tag{5.2}$$

Near-inertial wave field in the mixed layer is predicted by incorporating the wind stress data into a damped slab model [*Pollard and Millard*, 1970],

$$\frac{dV}{dt} + if\, V = T - rV \tag{5.3}$$

where $V=u+iv$ with u and v the eastward and northward components of horizontal current velocity, respectively, i the imaginary unit ($\sqrt{-1}$); f the local inertial frequency; $T = (\tau_x + i\tau_y)/\rho H$ with τ_x and τ_y the eastward and northward components of wind stress, respectively, H the mixed layer depth and ρ water density; r an empirical damping constant which parameterizes energy transfer from the mixed layer to the deeper ocean. The solution of (3) consists of Ekman transport $V_E = \frac{T}{(if+r)}$ and inertial current V_I given by

$$\frac{dV_I}{dt} + if\, V_I = \frac{1}{(if+r)} \frac{dT}{dt} - rV_I \tag{5.4}$$

We assume constant mixed layer depth of H=50 m. On the basis of mixed layer current measurements, damping time r^{-1} is considered to range from 2 to 10 days [*D'Asaro*, 1985]. Although we assume r^{-1}= 4 days somewhat arbitrarily in this study, qualitative results of this paper are not

altered even if we change the values of r within the above range. Equation (5.4) is integrated by assuming linear time variation of wind stress between successive data points and solving the equation (5.4) analytically for this time interval [*D'Asaro*, 1985].

5.3. Inertial current field in the mixed layer

Figure 5.2 shows time series of wind stress and amplitude of inertial currents in the mixed layer calculated by applying the local damped slab model to various locations from 20°N to 50°N along longitude 165°E. In particular, strong inertial currents with their amplitude exceeding 50 cm s^{-1} can be found mainly in midlatitude (35°N-45°N) during November to February, which are excited in response to the intermittent passages of the midlatitude storms.

As a typical example, time evolution of wind stress rotation field during November 29-30, 1991 is illustrated in Fig. 5.3 together with the region of strong inertial currents with the amplitude exceeding 50 cm s^{-1}. We can see that, corresponding to the traveling midlatitude storm, the wind stress rotation field shifts eastward with a speed of about 20 m s^{-1}, and after the passage of the midlatitude storm, strong inertial currents are excited in the area of 160°E-170°E and 35°N-40°N.

To examine spatial distribution of atmospheric disturbances which excite inertial currents in the mixed layer, annual mean field of the inertial current amplitude in the mixed layer is shown in Fig. 5.4 where the contour of the horizontal distance from the center of the four mooring locations, namely, 165°E and 30°N is superimposed. The large amplitude of inertial currents is found in the midlatitude band (30°N-50°N) corresponding to the passages of midlatitude storms such as shown in Fig. 5.3. In particular, the largest

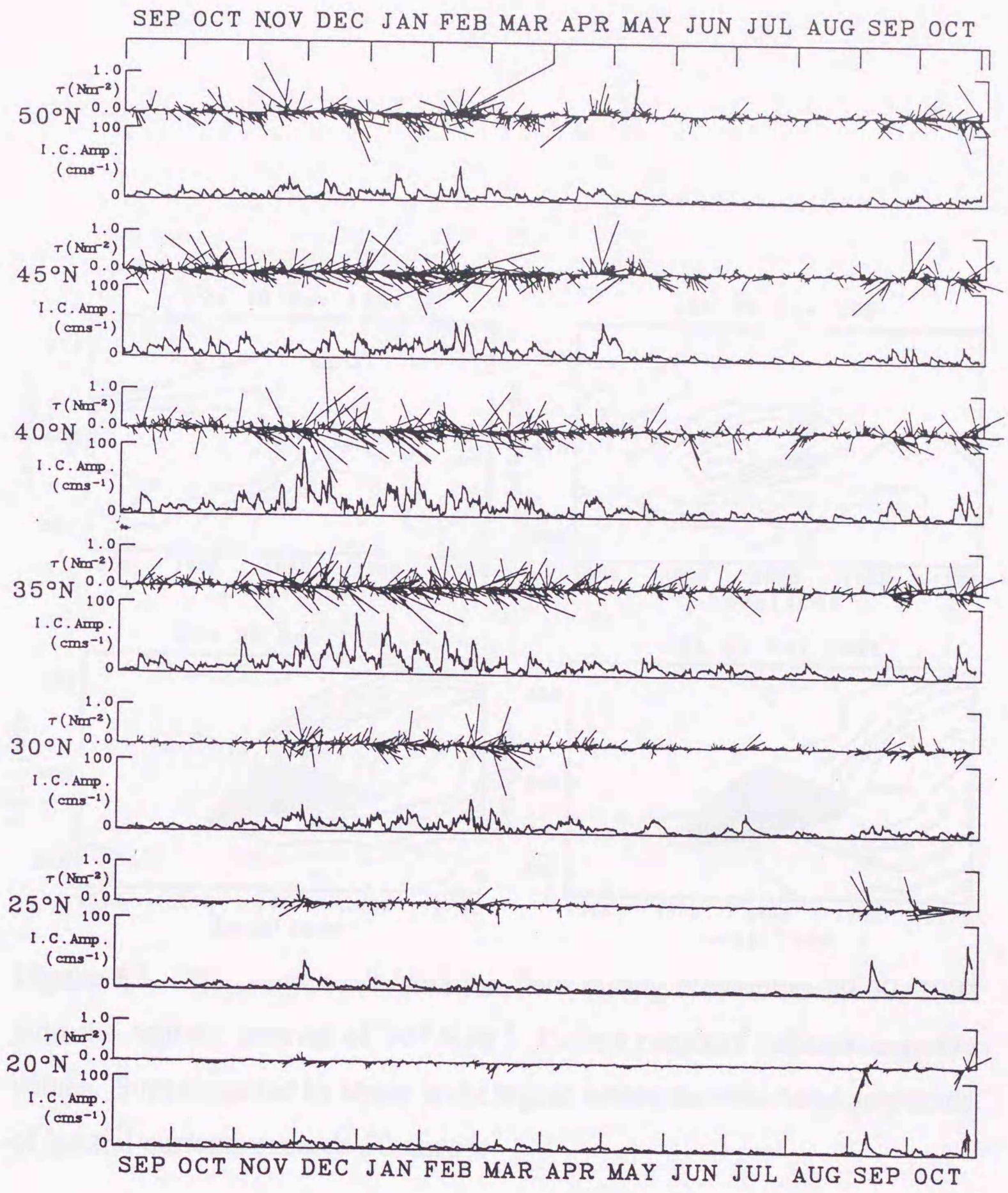

Figure 5.2. The time series of wind stress vector and calculated amplitude of inertial currents in the mixed layer at various latitudes from 20°N to 50°N along 165°E. The wind stress is plotted as a vector with northern direction being vertical upward and the base of the vector giving its time. The amplitudes of inertial currents are calculated by incorporating wind stress data into a simple damped slab model (Pollard and Millard, 1970).

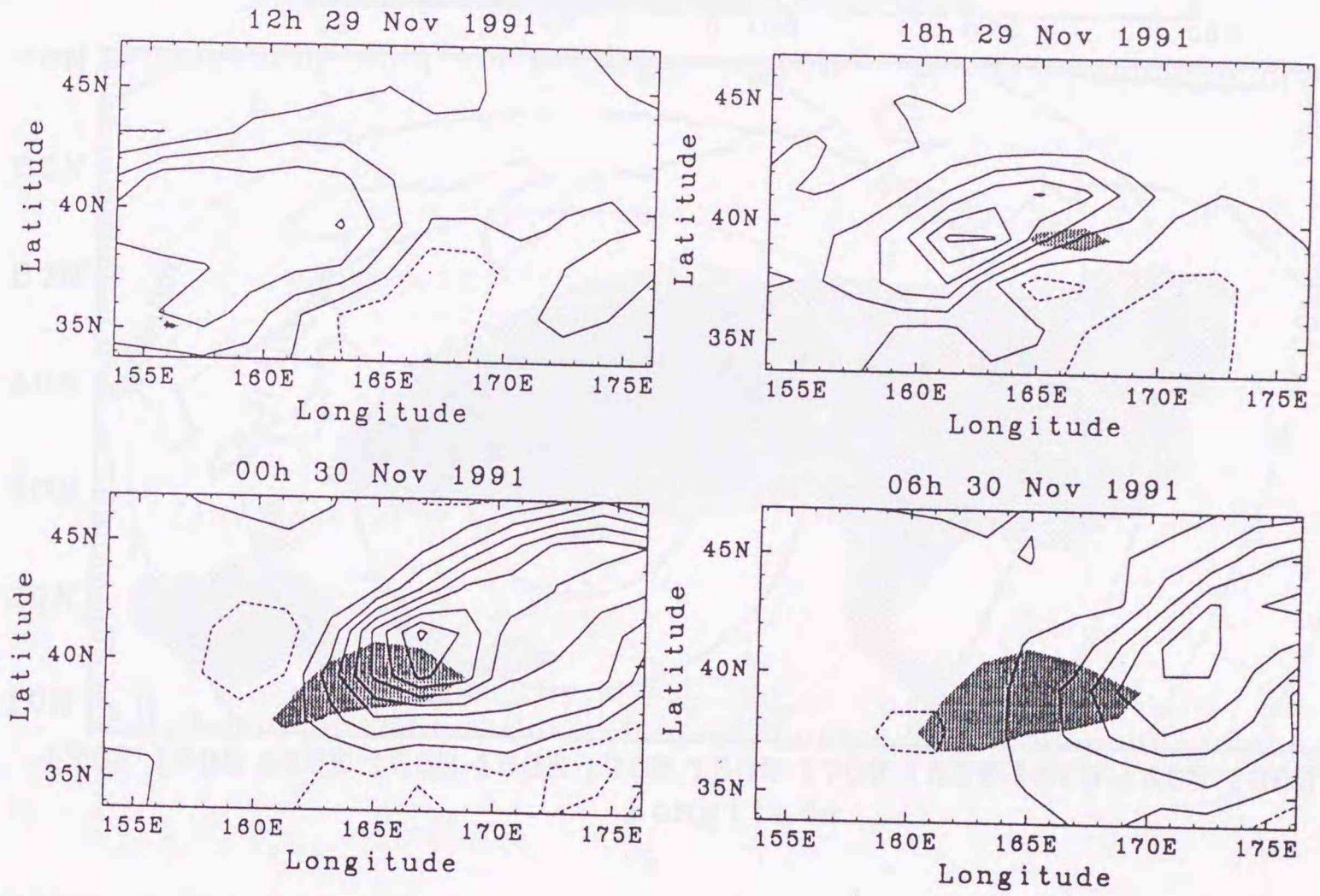

Figure 5.3. The wind stress rotation field during November 29-30, 1991 with the contour interval of 10^{-6} N m^{-3}. Dotted contours indicate negative values. Superimposed by shade is the region where the calculated amplitude of inertial currents exceeds 50 cm s^{-1}.

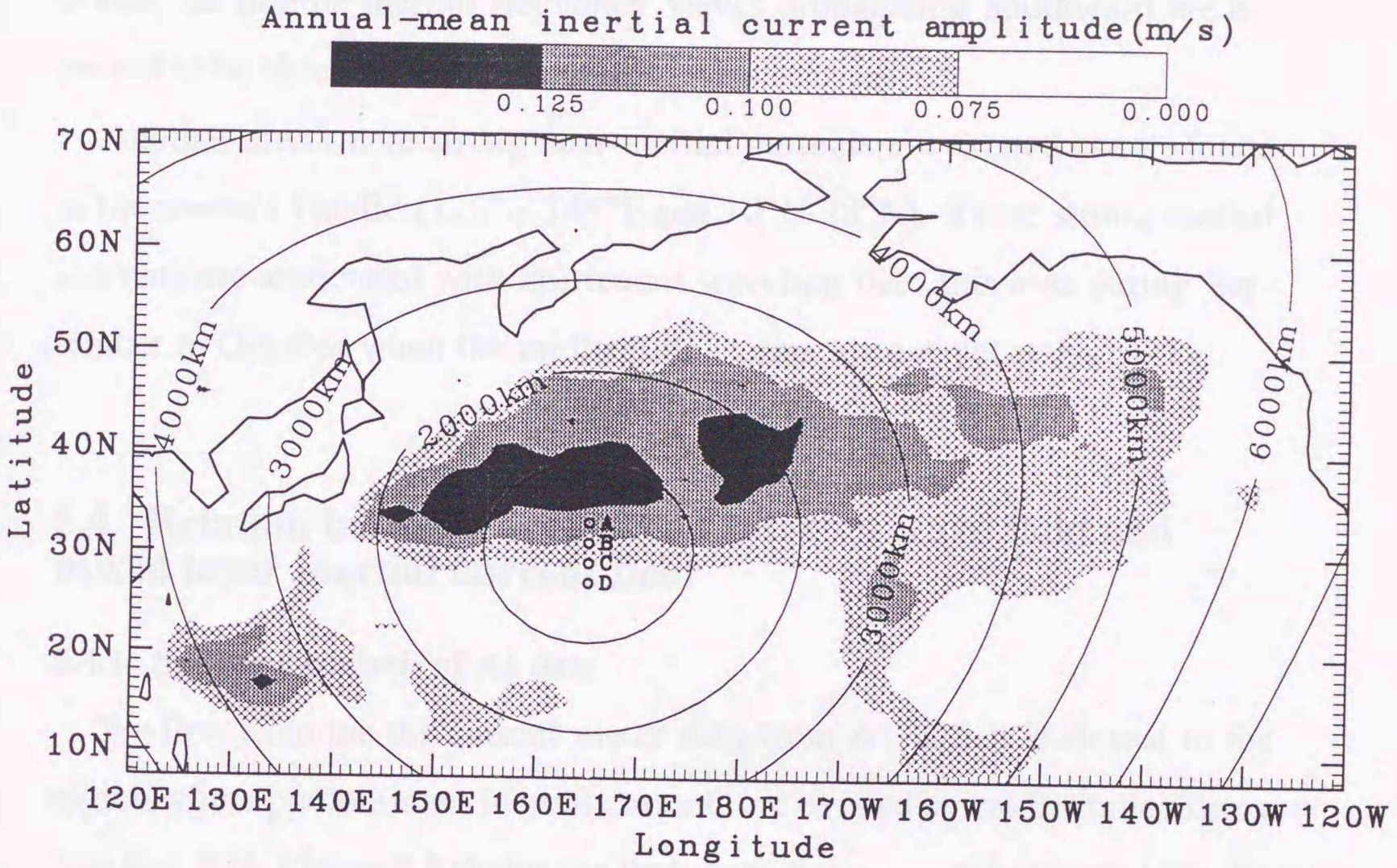

Figure 5.4. The spatial distribution of the annual mean inertial current amplitudes in the mixed layer. Superimposed are the contours showing the horizontal distance from 165°E and 30°N, the center of the four mooring locations.

inertial currents are found to occur 500-1000 km to the north of the moorings sites. If the generation mechanism of the double-inertial frequency waves proposed by *Niwa and Hibiya* [1997] is actually working in the real ocean, the double-inertial frequency waves propagating southward are expected to be detected at these mooring sites.

Another area where strong near-inertial currents are excited can be found in the western Pacific (125°E-145°E and 10°N-20°N). These strong inertial currents are associated with hurricanes traveling over this area during September to October when the midlatitude storms are not yet active.

5.4. Relation between deep ocean internal wave field and mixed layer inertial current field

5.4.1. Spectral analysis of A1 data

We first examine the current meter data from A1 which is closest to the region where predominant inertial currents are excited by midlatitude storms (see Fig. 5.4). Figure 5.5 shows the frequency spectrum of horizontal kinetic energy obtained by taking an average of all the frequency spectra for the divided data pieces. This average frequency spectrum shows familiar features of the deep ocean internal wave spectrum with prominent peaks at the inertial and semidiurnal tidal frequencies and spectral decay over frequencies higher than semidiurnal tidal frequency. It can be seen that, except for the inertial and tidal peaks, the level and form of the average spectrum are well approximated by those of the canonical Garrett and Munk internal wave spectrum [*Munk*, 1981].

Figure 5.6 shows all the frequency spectra of horizontal kinetic energy for the data pieces during fall, winter, spring and summer, respectively. We can notice large diversity among the frequency spectra, which is pre-

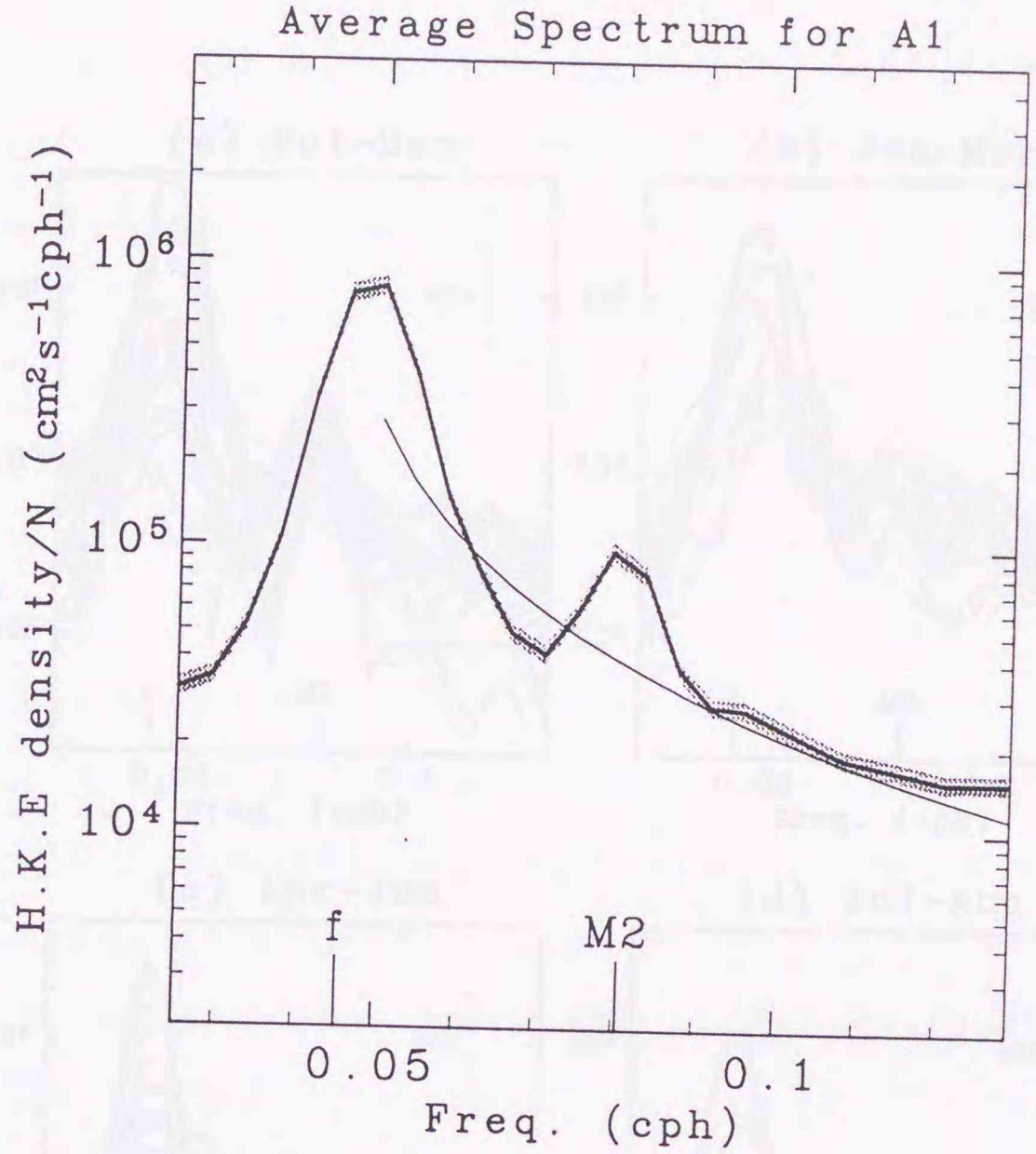

Figure 5.5. The frequency spectrum of horizontal kinetic energy for A1 which is obtained by taking an average of all the frequency spectra for the divided data pieces. For comparison, the canonical Garrett and Munk internal wave spectrum is shown by thin solid line. Note that the spectra are divided by the annual mean buoyancy frequency. The local inertial frequency and the semidiurnal tidal frequency are both marked. Shading denotes the 90% confidence range of spectral estimate.

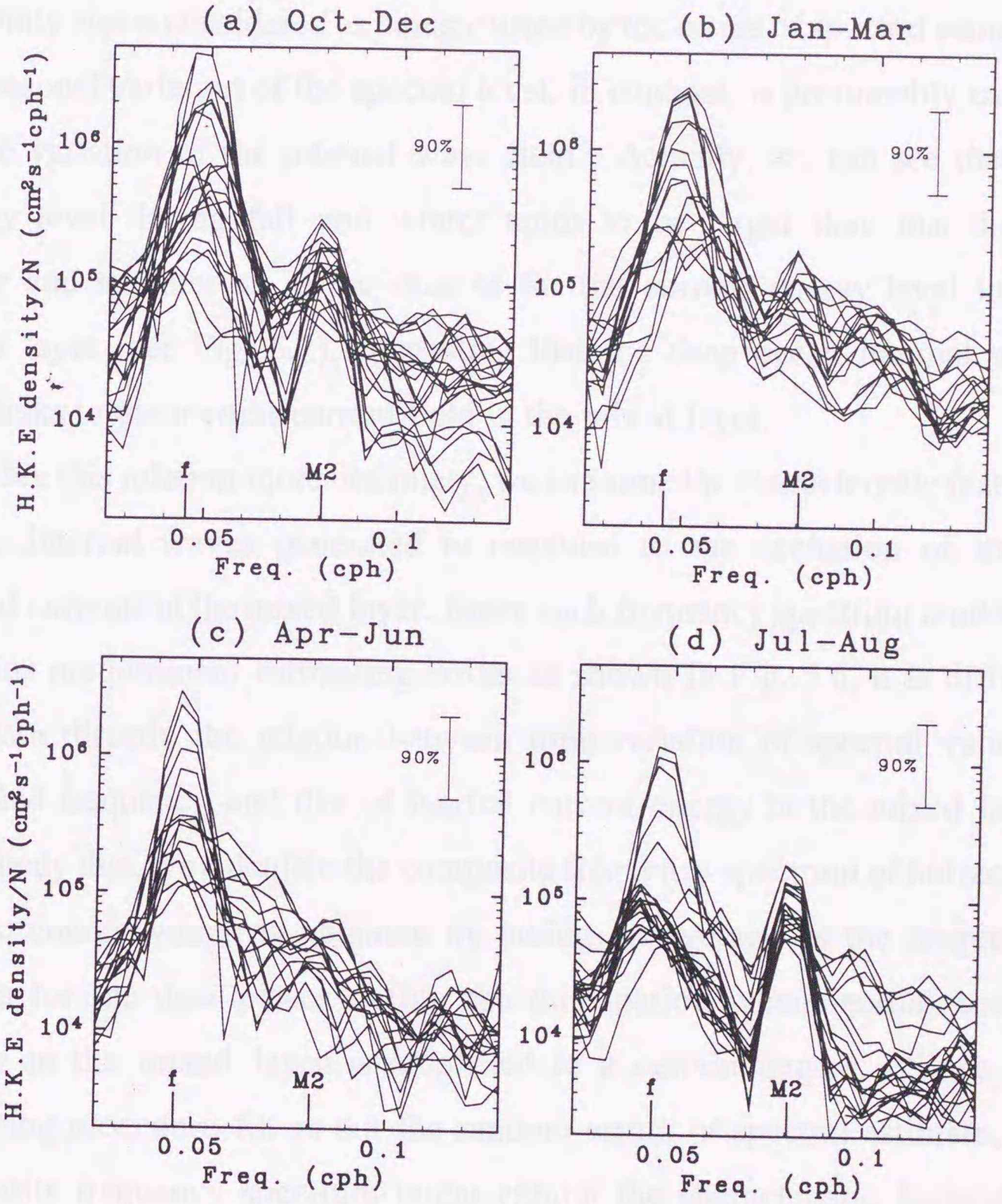

Figure 5.6. All the frequency spectra of horizontal kinetic energy for the divided data pieces of A1 during fall (Oct.-Dec.) (a), winter (Jan.-Mar.) (b), spring (Apr.-Jun.) (c), and summer (Jul.-Sep.) (d). Note that the spectra are divided by the annual mean buoyancy frequency. Vertical bar in the upper right of each figure denotes the 90% confidence range of spectral estimate.

sumably caused by two factors, namely, time variation of the deep ocean internal wave field (physical factor) and estimating errors of spectral values (artificial factor). The spectral diversity in each season seems to occur randomly and is considered as being caused by the errors of spectral estimate; the seasonal variation of the spectral level, in contrast, is presumably caused by the variation of the internal wave field. Actually, we can see that the energy level during fall and winter tends to be larger than that during spring and summer as in the case of inertial current energy level in the mixed layer (see Fig. 5.2), suggesting that the deep ocean internal wave field links to the inertial current field in the mixed layer.

To see this relation more definitely, we examine the characteristic features of the internal waves generated in response to the excitation of strong inertial currents in the mixed layer. Since each frequency spectrum randomly contains predominant estimating errors as shown in Fig. 5.6, it is difficult to obtain directly the relation between time variation of spectral value at specified frequency and that of inertial current energy in the mixed layer. To remedy this, we calculate the composite frequency spectrum of horizontal kinetic energy which is obtained by taking an average of the frequency spectra for the data pieces during the time period when inertial current energy in the mixed layer is amplified to a certain degree. Since this averaging procedure filters out the random errors of spectral estimate, the composite frequency spectrum might exhibit the characteristic features of the internal waves generated in response to the amplification of inertial currents in the mixed layer.

Figure 5.7 shows time variation of inertial energy in the mixed layer within the horizontal distance of 2000 km from the mooring location of A1. Figure 5.8 shows the composite frequency spectra for the time period during which the ratio of the inertial energy in the mixed layer to its annual

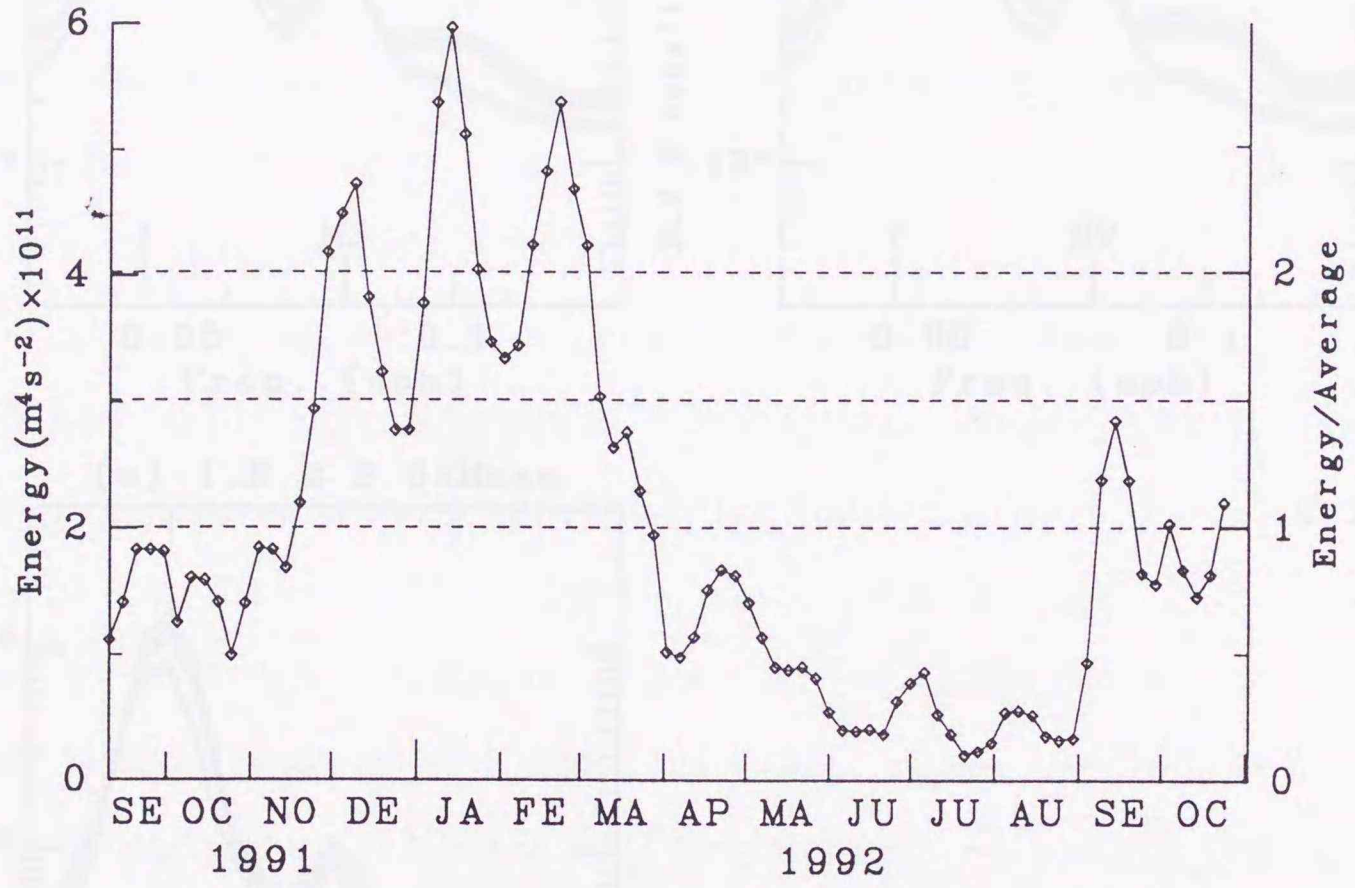

Figure 5.7. The time variation of inertial current energy in the mixed layer within the horizontal distance of 2000 km from the mooring location of A1. Horizontal dotted lines indicate the annual mean energy level, and energy levels 1.5 times and 2.0 times the annual mean, respectively.

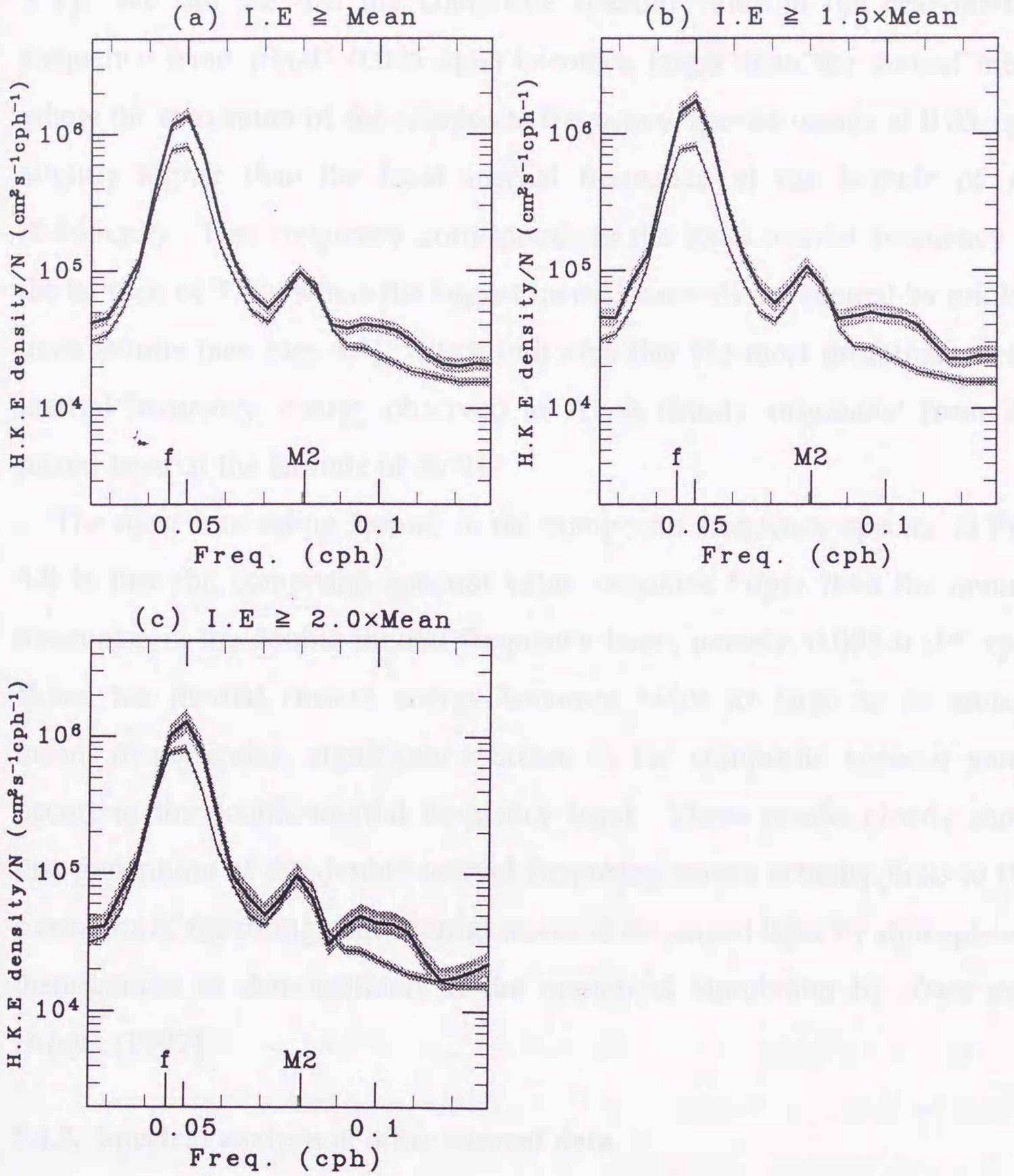

Figure 5.8. The composite frequency spectra of horizontal kinetic energy for A1 during the time period when the ratio of the inertial current energy in the mixed layer to its annual mean value becomes more than 1.0 (a), 1.5 (b) and 2.0 (c). For comparison, the average frequency spectrum of horizontal kinetic energy for A1 (see Fig. 5.5) is also shown by thin solid line. Shading denotes the 90% confidence range of each spectral estimate.

mean value becomes more than 1.0, 1.5 and 2.0, respectively (see Fig. 5.7). We can see that the composite spectral value in the near-inertial frequency band (0.045-0.055 cph) becomes larger than the annual mean where the maximum of the composite frequency spectra occurs at 0.05 cph, slightly higher than the local inertial frequency at the latitude of A1 (0.045cph). This frequency corresponds to the local inertial frequency at the latitude of 37°N where the largest inertial currents are excited by midlatitude storms (see Fig. 5.4), which indicates that the most prominent near-inertial frequency energy observed at A1 is mainly originated from the mixed layer at the latitude of 37°N.

The most interesting feature in the composite frequency spectra in Fig. 5.8 is that the composite spectral value becomes larger than the annual mean also in the double-inertial frequency band, namely, 0.095-0.105 cph. When the inertial current energy becomes twice as large as its annual mean, in particular, significant increase in the composite spectral value occurs in the double-inertial frequency band. These results clearly show that generation of the double-inertial frequency waves actually links to the excitation of the strong near-inertial waves in the mixed layer by atmospheric disturbances as demonstrated in the numerical simulation by *Niwa and Hibiya* [1997].

5.4.2. Spectral analysis of other current data

Figure 5.9 exhibits the composite frequency spectra of horizontal kinetic energy for all the current meter data during the time period when the inertial current energy in the mixed layer within the horizontal distance of 2000 km from each mooring site becomes more than twice the annual mean value.

We can see that each composite spectral value becomes larger than the

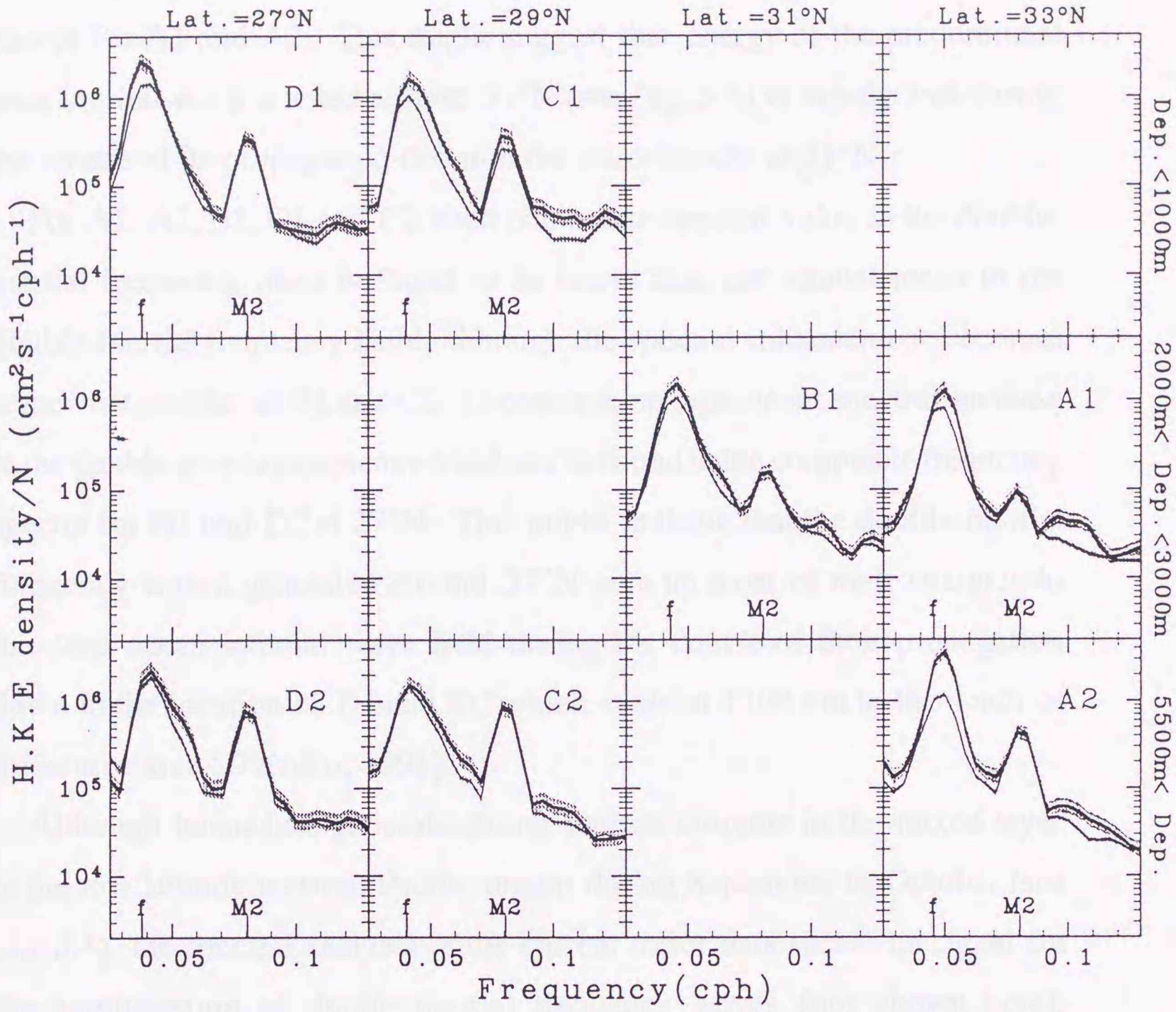

Figure 5.9. The composite frequency spectra of horizontal kinetic energy for all the current meter data (see Fig. 5.1) during the time period when the inertial current energy in the mixed layer within the horizontal distance of 2000 km from each mooring site becomes more than twice the annual mean value. For comparison, the average frequency spectrum of horizontal kinetic energy for each current meter data is shown by thin solid line. Note that each spectrum is divided by the annual mean buoyancy frequency at the depth of each current meter. Shading denotes the 90% confidence range of each spectral estimate.

annual mean in the near-inertial frequency band, although the spectral peak at 0.05 cph can be no more recognized in the composite frequency spectra except for A1 and A2. This might suggest that energy of the predominant near-inertial wave excited around 37°N (see Fig. 5.4) is mostly lost during the course of its propagation down to the mooring site at 31°N.

For A1, A2, B1, C1 and C2, each composite spectral value in the double-inertial frequency band is found to be larger than the annual mean in the double-inertial frequency band, although the spectral enhancement becomes somewhat smaller at B1 and C2. In contrast, no significant spectral increase in the double-inertial frequency band can be found in the composite frequency spectra for D1 and D2 at 27°N. This might indicate that the double-inertial frequency waves generated around 37°N give up most of their energies to the deep ocean internal wave field during the course of their propagation down to the location of D1 and D2 which is about 1100 km to the south of the source area [*D'Asaro*, 1991].

Although hurricanes generate strong inertial currents in the mixed layer in the low latitude western Pacific region during September to October (see Fig. 5.4), the spectral analysis of the current meter data shows no signal for the amplification of double-inertial frequency waves (not shown here). This might be explained in terms of the long horizontal distance between the source region and the mooring locations which exceeds 2000 km as in the cases of D1 and D2.

5.5. Summary and Discussion

In the present study, we have analyzed current meter data from the long term moorings deployed at depth in the Northwest Pacific Basin (see Fig. 5.1) together with sea surface wind data catalogued in the Global Objectively

Analyzed Data to clarify the response of the deep ocean internal wave field to traveling atmospheric disturbances. The major conclusions are summarized as follows.

(1) Inertial currents in the mixed layer are mainly excited by the midlatitude (30°N-50°N) storms traveling eastward during fall and winter (see Figs. 5.2-5.4 and 5.7). In particular, predominant inertial currents are excited around 37°N in the Northwest Pacific Basin (see Fig. 5.4).

(2) In response to the excitation of strong inertial currents in the mixed layer, near-inertial frequency waves in the deep ocean internal wave field are significantly amplified (see Figs. 5.8 and 5.9).

(3) In addition to the near-inertial frequency waves, the double-inertial frequency waves are significantly amplified in the deep ocean internal wave field in response to the excitation of strong inertial currents in the mixed layer (see Figs. 5.8 and 5.9).

The above result (3) validates that the double-inertial frequency waves are actually generated by atmospheric disturbances in the real ocean as demonstrated in the numerical experiment by *Niwa and Hibiya* [1997].

However, the composite spectral level of the double-inertial frequency band relative to that of the near-inertial band (see Figs. 5.8 and 5.9) is much smaller than that predicted in the numerical experiment where the amplitude of the double-inertial frequency waves becomes comparable to that of the near-inertial waves in areas away from the forcing region [see *Niwa and Hibiya*, 1997, Fig. 4]. Several explanations are possible for this difference. Compared to the hurricane model assumed in the numerical experiment, midlatitude storms generally have smaller wind stress amplitude (less than 2.0 N m^{-2}, see Fig. 5.2) and larger traveling speed (about 20 m s^{-1}, see Fig. 5.3) so that nonlinear effects causing the generation of the double-inertial frequency waves [*Niwa and Hibiya*, 1997] become much smaller.

Furthermore, nonlinear interactions of the double-inertial frequency waves with the background internal wave field are not considered in the numerical experiment, which might cause the decay of energy in the double-inertial frequency band by transferring it to small dissipation scales.

The double-inertial frequency waves are believed to provide energy for diapycnal mixing in the deep ocean [*McComas and Müller,* 1981; *Hibiya et al.*, 1997]. The exact parameterization of diapycnal mixing in the world ocean therefore requires the knowledge on the global field of the double-inertial frequency waves which depends on their propagation distance as well as their source distribution. Assuming source region of double-inertial frequency waves is around 165°E and 37°N (see Fig. 5.4), we can estimate that propagation distance of the observed double-inertial frequency waves is of the order of 1000 km because these waves almost vanish at the mooring location of D, namely, 165°E and 27°N (see Fig. 5.9). This propagation distance is consistent with the mean free path of the low-vertical-mode double-inertial frequency waves which is theoretically predicted from the magnitudes of group velocity and nonlinear interaction time [*D'Asaro*, 1991].

We can see that the spectral peak at 0.05 cph (inertial frequency at the latitude of 37°N) vanishes to the south of 33°N (see Fig. 5.9), indicating that propagation distance of the predominant near-inertial waves is much less than that of the double-inertial frequency waves. This might reflect the limitation of the propagation of near-inertial waves through the interactions with mesoscale eddies [*Kunze*, 1985] and bottom topographies [*Müller and Xu*, 1992].

References

Bryan, F., Parameter sensitivity of primitive equation ocean general circulation models, *J. Phys. Oceanogr., 17*, 970-985, 1987.

D'Asaro, E. A., A strategy for investigating and modeling internal wave sources and sinks, in *Dynamics of Oceanic Internal Gravity Waves. Proc. Aha Huliko'a Hawaiian Winter Workshop*, pp. 451-466, edited by P. Müller and D. Henderson, Hawaii Institute of Geophysics, 1991.

D'Asaro, E. A., C. C. Eriksen, M. D. Levine, P. P. Niiler, C. A. Paulson, and P. Van Meurs, Upper-ocean inertial currents forced by a strong storm. Part I: Data and comparisons with linear theory, *J. Phys. Oceanogr., 25*, 2909-2936, 1995.

D'Asaro, E. A., The energy flux from the wind to near-inertial motions in the surface mixed layer, *J. Phys. Oceanogr., 15,* 1043-1059, 1985.

Hibiya, T., Y. Niwa, K. Nakajima, and N. Suginohara, Direct numerical simulation of the roll-off range of internal wave shear spectra in the ocean, *J. Geophys. Res., 101*, 14123-14129, 1996.

Hibiya, T., Y. Niwa, and K. Fujiwara, Numerical experiments of nonlinear energy transfer within the oceanic internal wave spectrum, submitted to *J. Geophys. Res.,* 1997.

Krauss, W., The erosion of a thermocline, *J. Phys. Oceanogr., 11,* 415-433, 1981.

Kunze, E., Near-inertial wave propagation in geostrophic shear, *J. Phys. Oceanogr., 15*, 544-565, 1985.

Large, W. G., and S. Pond, Open ocean momentum flux measurements in moderate to strong winds, *J. Phys. Oceanogr., 11,* 324-336, 1981.

Levitus S., and T. P. Boyer, *World Ocean Atlas 1994,* Vol. 4, *Temper-*

ature: NOAA Atlas NESDIS 4, U. S. Dep. of Commer., Washington, D. C., 1994

Levitus S., and R. Burgett, and T. P. Boyer, *World Ocean Atlas 1994,* Vol. 3, *Salinity: NOAA Atlas NESDIS 3,* U. S. Dep. of Commer., Washington, D. C., 1994

McComas, C. H., and P. Müller, The dynamic balance of internal waves, *J. Phys. Oceanogr., 11,* 970-986, 1981.

Müller, P., and N. Xu, Scattering of oceanic internal gravity waves off random bottom topography, *J. Phys. Oceanogr., 22,* 474-488, 1992.

Munk, W. H., Internal waves and small-scale processes, in Evolution of Physical Oceanography, edited by B. S. Warren and C. Wunsch, pp. 264-291, MIT Press, Cambridge, Mass., 1981.

Niwa, Y., and T. Hibiya, Nonlinear Processes of energy transfer from traveling hurricanes to the deep ocean internal wave field, *J. Geophys. Res., 102,* 12469-12477, 1997.

Pollard, R. T., and R. C. Millard Jr., Comparison between observed and simulated wind-generated inertial oscillations, *Deep-Sea Res., 17,* 813-821, 1970.

Chapter 6

General Conclusion

The pattern and magnitude of the numerically reproduced general ocean circulation strongly depend on the value of eddy diffusivity coefficients, which indicates that the evaluation of the intensity of turbulent mixing at depth is crucial to accurate modeling of the large-scale general circulation [*Bryan*, 1987].

In the present study, we have proposed an approach feasible to clarify the global distribution of turbulent mixing intensity which makes use of the dynamics of the oceanic internal gravity waves. Actually, the main energy for mixing processes in the deep ocean is considered to be originally supplied at large scales by atmospheric forcing and tide-topography interactions, and then transferred across the internal wave spectrum down to small dissipation scales through nonlinear wave-wave interactions. Therefore, once the energy transfer processes within the internal wave spectrum are clarified, we can expect that parameterization of turbulent mixing becomes possible in terms of the distribution of energy sources such as atmospheric disturbances and internal tides.

From this point of view, in Chapter 2, we have reproduced the quasi-equilibrium internal wave field having the actually observed GM-like spectrum with the roll-off at a vertical wavenumber of ~0.1 cpm by calculating the nonlinear interactions among randomly phased linear internal waves, each amplitude of which is determined from the GM model. It has been shown that, when the energy level of high-vertical-wavenumber (0.01-0.04cpm) near-inertial ($f<\omega<2f$) portion of the spectrum is increased (or decreased), the roll-off shifts to lower (or higher) wavenumbers, indicating that the strength of high-vertical-wavenumber near-inertial current shear strongly controls the intensity of turbulent mixing in the deep ocean. At the same time, it has been found that the inverse Richardson numbers

remain subcritical at the roll-off wavenumbers implying that the roll-off is not caused by shear instability or convective instability [*Munk*, 1981]. This result is more consistent with the mechanism suggested by *Gregg et al.* [1993] that the roll-off is caused by Doppler shifting and critical layer interactions associated with high-vertical-wavenumber near-inertial current shear.

In Chapter 3, forcing mechanism of large-scale internal waves has been examined. Three-dimensional multilevel numerical model has been used to investigate the energy supply from a traveling hurricane which is one of major sources for large-scale internal waves. It has been found that a traveling hurricane generates two distinctive kinds of internal waves, namely, near-inertial waves and superinertial waves with frequencies of 2f and 3f which are generated through nonlinear effects. In areas away from the hurricane track, in particular, the amplitude of the double-inertial frequency waves becomes comparable to that of the near-inertial waves. In order to examine generation mechanism of such superinertial waves, bispectral analysis has been carried out to show that the most predominant superinertial wave, namely, first-vertical-mode double-inertial frequency wave is generated efficiently through nonlinear interactions between high-vertical-mode near-inertial waves which are originally excited in the mixed layer.

In Chapter 4, we have examined how the energy thus supplied by external forcing at large scales cascades through the internal wave spectrum down to small dissipation scales. For this purpose, the quasi-equilibrium spectrum obtained in Chapter 2 has been perturbed initially by adding energy bump to different parts of low- wavenumber low-frequency portion of the spectrum, and thereafter time evolution of the perturbed spectrum has been examined. We have found that when the spectral bump is added to low-vertical-wavenumber region within superinertial band ($2f<\omega<3f$), the energy is trans-

ferred efficiently to high vertical wavenumber near-inertial region. In contrast, when the spectral bump is added to low-vertical-wavenumber near-inertial region ($f<\omega<2f$), no significant energy cascade to high wavenumber region occurs. These results indicate that energy transfers to small dissipation scales within the internal wave spectrum are dominated by the resonant interaction mechanism called parametric subharmonic instability (P.S.I) [*McComas and Müller*, 1981].

The above result clearly shows that the superinertial waves reproduced in the numerical experiment in Chapter 3 can be efficient energy sources for the turbulent mixing in the deep ocean. In Chapter 5, therefore, we have analyzed current meter data from long term moorings in the Northwest Pacific Basin together with global sea surface wind data to see whether such superinertial waves are actually excited in the deep ocean under strong atmospheric forcing. By incorporating the wind data into a simple damped slab model, it has been found that predominant inertial currents are excited in the mixed layer by midlatitude storms in the Northwest Pacific Basin during fall and winter. We have calculated the frequency spectra of the horizontal kinetic energy for the deep ocean internal wave field during the time period when the predominant inertial currents are excited in the mixed layer. It has been shown that the spectral level significantly increases in the double-inertial frequency band as well as in the near-inertial frequency band, thus validating that double-inertial frequency waves are indeed excited in the real ocean under strong atmospheric forcing. The superinertial waves thus excited have been found to propagate over horizontal distances of the order of 1000km from their source region. This propagation distance is consistent with the mean free path of the low-vertical mode double-inertial frequency waves theoretically predicted from the magnitudes of group velocity and nonlinear interaction time [*D'Asaro*, 1991].

Putting all the results together, we can propose here one possible scenario for the energy transfer processes from large-scale atmospheric forcing down to small-scale turbulent mixing as follows.

(1) Stong atmospheric disturbances traveling over the ocean excite high-vertical mode near-inertial waves in the mixed layer.
(2) The high-vertical-mode near-inertial waves interact to generate low-vertical-mode superinertial waves with frequencies just over 2f.
(3) The low-vertical-mode superinertial waves propagate over horizontal distances of O(1000km) from their sources, while supplying their energy to the local internal wave spectrum in the deep ocean.
(4) The energy thus supplied by the low-vertical-mode superinertial waves are transferred efficiently across the local internal wave spectrum down to high-vertical-mode near-inertial frequency region under the P.S.I mechanism. As a result, small-vertical-scale near-inertial current shear is enhanced.
(5) As small-vertical-scale near-inertial current shear is enhanced, the roll-off shifts to lower vertical wavenumbers leading to the increase in the rate of energy dissipation and associated turbulent mixing at critical layers.

Schematic diagram illustrating the above scenario is shown in Fig. 6.1. This scenario implies that the exact parameterization of turbulent mixing in the deep ocean requires the knowledge of the global field of low-vertical-mode superinertial internal waves which depends on the distribution of atmospheric forcing and propagation distances of superinertial internal waves. The information of atmospheric forcing field is available from the Global Objectively Analyzed Data provided by the Japan Meteorological

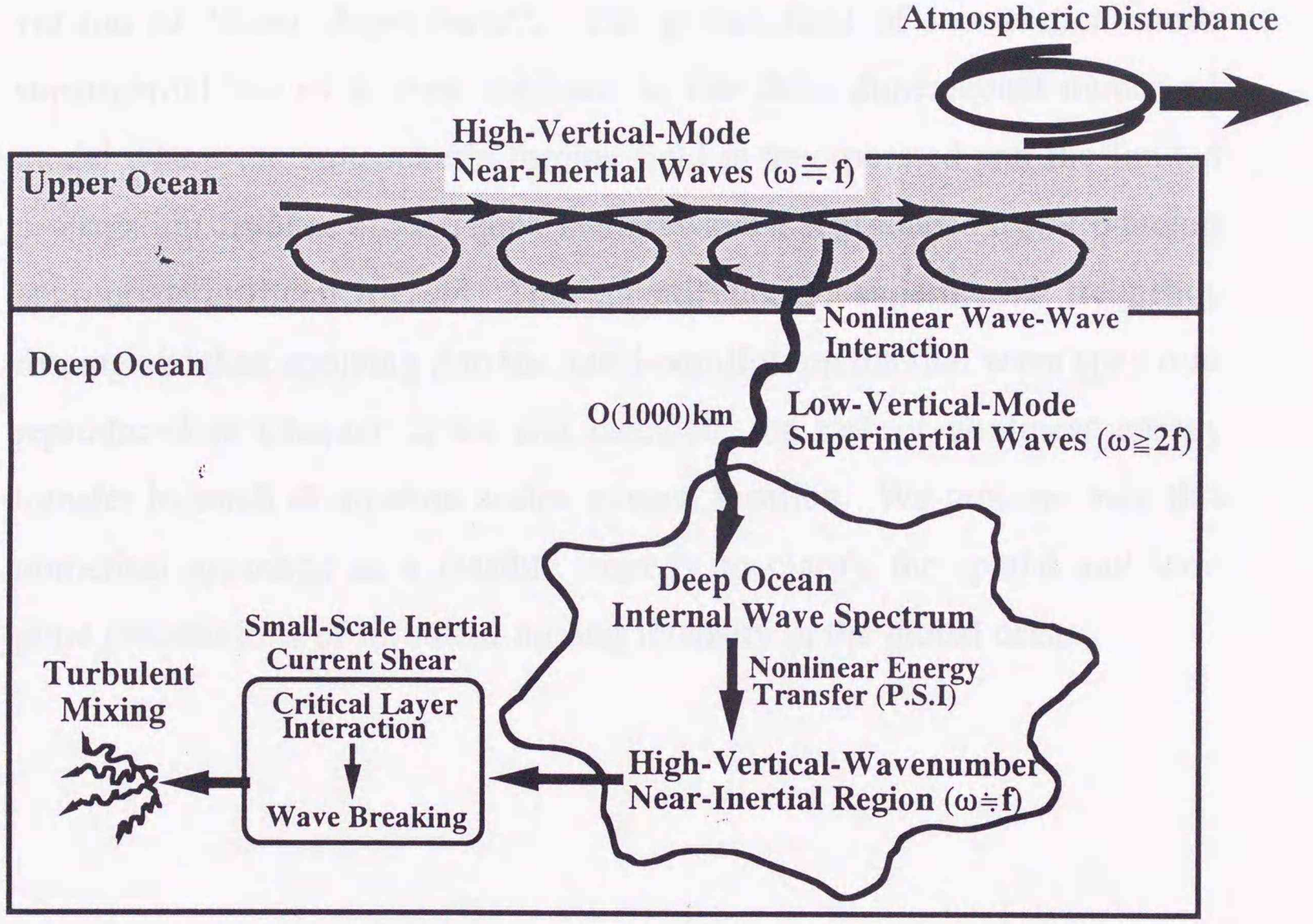

Figure 6.1. Schematic diagram illustrating the energy transfer processes from large-scale atmospheric forcing down to small-scale turbulent mixing across the oceanic internal wave spectrum.

Agency whose spatial and temporal resolutions ($\Delta x \simeq 200$ km, $\Delta t = 6$ hrs) are sufficiently high so that predominant atmospheric disturbances such as midlatitude storms and hurricanes can be tracked. The propagation distance of each superinertial wave is determined by multiplying the group velocity by nonlinear interaction time which can be estimated from the extended version of "*Bump Experiment*". The global field of low-vertical-mode superinertial waves is then obtained in the three-dimensional numerical model where the atmospheric forcing field is incorporated and the limited propagation distance of each superinertial wave is reproduced by introducing appropriate artificial friction. Thus quantifying the superinertial frequency forcing and then applying it to the quasi-equilibrium internal wave spectrum reproduced in Chapter 2, we can calculate the rate of nonlinear energy transfer to small dissipation scales at each location. We propose here this numerical approach as a feasible strategy to clarify the spatial and temporal distributions of turbulent mixing intensity in the global ocean.

References

Bryan, F., Parameter sensitivity of primitive equation ocean general circulation models, *J. Phys. Oceanogr., 17*, 970-985, 1987.

D'Asaro, E. A., A strategy for investigating and modeling internal wave sources and sinks, in *Dynamics of Oceanic Internal Gravity Waves. Proc. Aha Huliko'a Hawaiian Winter Workshop*, pp. 451-466, edited by P. Müller and D. Henderson, Hawaii Institute of Geophysics, 1991.

Gregg, M. C., D. P. Winkel, and T. B. Sanford, Varieties of fully resolved spectra of vertical shear, *J. Phys. Oceanogr., 23*, 124-141, 1993.

McComas, C. H., and P. Müller, The dynamic balance of internal waves, *J. Phys. Oceanogr., 11*, 970-986, 1981.

Munk, W. H., Internal waves and small-scale processes, *in Evolution of Physical Oceanography*, edited by B. S. Warren and C. Wunsch, pp. 264-291, MIT Press, Cambridge, Mass., 1981.

Acknowledgments

I am most indebted to my principal advisor, Prof. T. Hibiya of University of Tokyo. I would like to express my sincere thanks for his many valuable suggestions and discussion throughout this study and refinement of the manuscript. Without his support and encouragement during my entire graduate career, I could not complete the thesis. I greatly thank Prof. S. Kanari and Prof. S. Minobe of Hokkaido University for their helpful suggestions and heartfelt encouragement and critical readings of the manuscript. I would like to thank Prof. K. Taira and Prof. M. Kawabe of University of Tokyo for their continuous support and kindly supplying the current meter data. I am also grateful to Prof. N. Suginohara of University of Tokyo and Dr. K. Nakajima of Kyusyu University for their valuable comments and useful advices on the numerical experiments. I also thank Prof. K. Kikuchi and Prof. T. Harimaya of Hokkaido University for their critical readings of the manuscript.

Numerical calculations in Chapter 3 were carried out on the HITAC S-3800/380 in the Hokkaido University Computing Center and those in Chapters 2 and 4 were on the HITAC S-3800/480 in the University of Tokyo Computing Center. The GFD-DENNOU Library and the NCARG Library were used to produce the major parts of the figures in Chapters 3 and 5 and in Chapters 2 and 4, respectively.

inches 1 2 3 4 5 6 7 8

cm 1 2 3 4 5 6 7 8 9 10 11 12 13 14 15 16 17 18 19

Kodak Color Control Patches

Blue Cyan Green Yellow Red Magenta White 3/Color Black

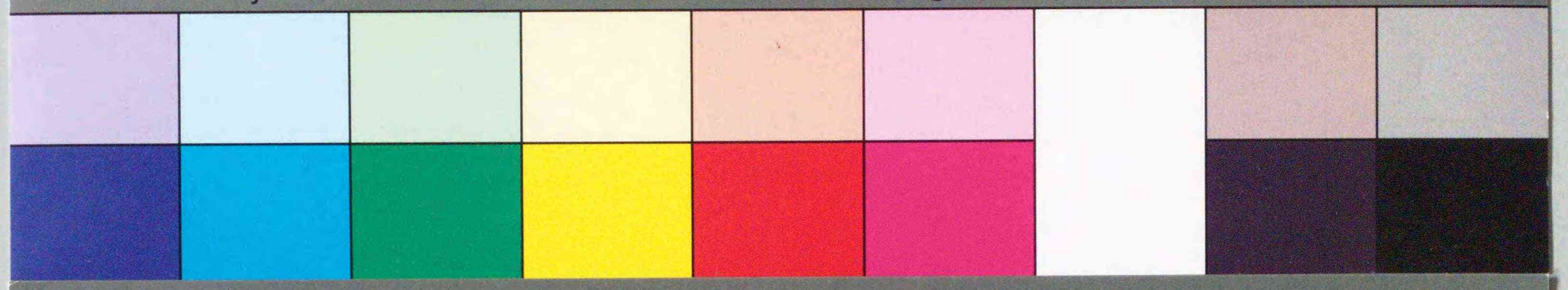

Kodak Gray Scale

C Y M

A 1 2 3 4 5 6 M 8 9 10 11 12 13 14 15 B 17 18 19